



Virginia Commonwealth University
VCU Scholars Compass

Theses and Dissertations


Graduate School

2018

Branched Short Chain Fatty Acid Isovaleric Acid Causes Smooth Muscle Relaxation via cAMP/PKA Pathway, Inhibits Gastrointestinal Motility, and Disrupts Peristaltic Movement

Bryan Adam Blakeney
Virginia Commonwealth University

Follow this and additional works at: <https://scholarscompass.vcu.edu/etd>

 Part of the [Digestive, Oral, and Skin Physiology Commons](#), [Physiological Processes Commons](#), and the [Systems and Integrative Physiology Commons](#)

© Bryan Adam Blakeney

Downloaded from

<https://scholarscompass.vcu.edu/etd/5548>

This Dissertation is brought to you for free and open access by the Graduate School at VCU Scholars Compass. It has been accepted for inclusion in Theses and Dissertations by an authorized administrator of VCU Scholars Compass. For more information, please contact libcompass@vcu.edu.

Branched Short Chain Fatty Acid Isovaleric Acid Causes Smooth Muscle Relaxation via
cAMP/PKA Pathway, Inhibits Gastrointestinal Motility, and Disrupts Peristaltic Movement

A dissertation submitted in partial fulfillment of the requirements for the degree of Doctor of
Philosophy at Virginia Commonwealth University.

Bryan Adam Blakeney

B.S Biomedical Engineering, University of Alabama at Birmingham, 2010

Directors: John R. Grider, Ph.D. and Srinivasa M. Karnam, Ph.D.

Professors

Physiology and Biophysics

Virginia Commonwealth University

Richmond, Virginia

June, 2018

Contents

Table of Figures	vii
Table of Tables	x
Table of Abbreviations	xi
Abstract	xiv
Introduction.....	1
Fatty Acids	1
Definition, Types, and Sources of Fatty Acids	1
Absorption and Metabolism of Fatty Acids.....	3
Isovaleric Acid	4
Fatty Acid Receptors and Signaling	7
Free Fatty Acid Receptor Family.....	7
Olfactory Receptor Family	9
Potassium Channel Activation by Fatty Acids	10
Peristalsis	11
Definition and Basic Mechanism.....	11
Regular Movement and Patterns	13
Smooth Muscle Contraction and Relaxation	14
Ca ²⁺ -Independent Sustained Contraction.....	16

Straight-Chain SCFAs' Effect on Peristalsis	17
Methods of Analysis	17
Materials and Methods.....	20
Materials	20
Animal Preparation	20
Longitudinal Colon Segment Force Measurement	21
Setup	21
Peristalsis and Spatiotemporal Maps	25
Setup	25
Analysis.....	26
Single Cell Contraction and Relaxation.....	36
Immunofluorescence Staining and Imaging	36
Results.....	38
Tracings of Longitudinal Colon Force.....	38
Isovaleric Acid Induces Smooth Muscle Relaxation	52
Dose-Dependent Relaxation of Longitudinal Smooth Muscle Tissue and Dispersed Cells.	52
Gender and Region in Longitudinal Muscle Relaxation.....	62
IVA's Effect on Longitudinal Colon When Creating a Low pH Environment	67
Effects of Neural Inhibition (via Tetrodotoxin).....	74
Effects of Nitric Oxide Inhibition (via L-NNA).....	74

Effects of 2-Ethylhexanoic Acid on IVA Relaxation	79
Comparison of BCFA Isovaleric Acid and Straight Chain Valeric Acid	79
Effects of Adenylate Cyclase & Protein Kinase A inhibition (via SQ22536 and H-89).....	84
Isovaleric Acid Changes Peristaltic Patterns in Whole Colon.....	92
Luminal IVA Changed Mean Diameter along Length of Colon	92
Luminal IVA Disrupts Orad-to-Anal Peristalsis.....	102
Luminal IVA Slows Proximal Colon Peristalsis	114
Colonic Smooth Muscle, Enteroendocrine Cells Possess OLF Receptor	119
Murine Colon, Ileum, and Cultured STC-1 cells, Stain Positive for Olfr558	119
Discussion	124
Direct Signaling of Smooth Muscle by Fatty Acids	124
Response to IVA	124
cAMP/PKA Pathway Signaling.....	126
Presence of IVA Sensitive Receptors	130
SCFA and BCFA Response.....	131
Regionally-Specific Inhibitions of Peristalsis.....	132
Differences in Colon Diameter	132
Differences in Peristaltic Waves.....	133
Conclusions.....	135
Physiological Applications	135

Directions for Further Study	137
References	139
Vita.....	164

Table of Figures

Figure 1) Diagram of vertical force measurement organ bath for colon segments	23
Figure 2) Diagram of custom gastrointestinal motility monitor organ bath	28
Figure 3) Example Frame of Colon Video Color-Coded for Regions	30
Figure 4) Example and Description of ST Map Calculation	32
Figure 5) Explanation of ST Maps of change in diameter and wave velocity	34
Figure 6) Representative tracing of two female mice colons without any treatments	40
Figure 7) Representative tracings of mouse colons treated with 10 μM ACh followed by 50 mM IVA	42
Figure 8) Representative tracings of two male mice colon segments treated with L-NNA ...	44
Figure 9) Representative tracings of two male mice colon segments treated with TTx	46
Figure 10) Representative tracings of two female mice colon sections treated with adenylate cyclase inhibitor SQ22536	48
Figure 11) Representative tracing of a female mouse colon treated with pH-unadjusted IVA, increasing IVA concentration to 10 mM and dropping bath pH from 7.6 to 6.7	50
Figure 12) Dose-response curve of longitudinal smooth muscle maximum relaxation to IVA	54
Figure 13) Dose-response curve of longitudinal smooth muscle 5 minutes out relaxation to IVA	56
Figure 14) Smooth Muscle Cell length after contraction and relaxation by IVA (1 minute)	58
Figure 15) Smooth Muscle Cell length after contraction and relaxation by IVA (5 minute)	60
Figure 16) Male mouse 50 mM IVA Induced Relaxion of Longitudinal Smooth Muscle by Colon Region	63

Figure 17) 50 mM IVA induced relaxation of longitudinal colon smooth muscle by gender	65
Figure 18) IVA induces relaxation in Longitudinal Colon segments, curve shifts to lower concentrations in lower pH conditions compared to pH 7.4	68
Figure 19) 10 mM IVA with pH reduction to 6.7 induced relaxation in longitudinal colon by region	70
Figure 20) 10 mM IVA reducing pH to 6.7 induced relaxation of Longitudinal colon, male vs. female	72
Figure 21) Relaxation induced by 50 mM IVA is not mediated by TTx	75
Figure 22) Relaxation induced by 50 mM IVA is not inhibited by L-NNA	77
Figure 23) BCFA's 2-EHA and IVA affect Colon Segments Similarly, not Affected by TTx	80
Figure 24) 20 mM Valeric acid induces more relaxation than 20 mM IVA	82
Figure 25) 500 μM SQ22536 decreases average 30 mM IVA-induced relaxation of longitudinal colon segments	86
Figure 26) Adenylate Cyclase Inhibitor SQ22536 and PKA Inhibitor H-89 Inhibit Relaxation Induced by IVA at 1 Minute	88
Figure 27) Adenylate Cyclase Inhibitor SQ22536 and PKA Inhibitor H-89 Inhibit Relaxation Induced by IVA at 5 Minutes	90
Figure 28) Still frames of a mouse colon filled with A) Krebs buffer or B) 50 mM IVA in Krebs buffer	94
Figure 29) Spatiotemporal mapping of mouse colons before and after 50 mM Intraluminal IVA	96
Figure 30) Intraluminal IVA has increases proximal colon diameter	98

Figure 31) Mean Diameter of Colon at Different Intraluminal pH	100
Figure 32) DyDt Spatiotemporal mapping of mouse colons before and after 50 mM Intraluminal IVA	104
Figure 33) Example measurement of contractions in ST Map	106
Figure 34) Length and Center of Contractions Along Colon Comparing Krebs Buffer vs 50 mM IVA, or Changes in pH	108
Figure 35) Example ST Wave Velocity Maps showing relative change of velocity of changes in diameter	115
Figure 36) Mean relative contraction wave velocity of contraction along colon over 20 minutes	117
Figure 37) 40x Images of fluorescent staining of mouse Olfr558 (A,C,E) or Control (B,D,F) on 10 μM cryosections of mouse colon (A-D) and ileum (E-F)	120
Figure 38) Cultured STC-1 cells stained with OR51E1 (A-B) or no Primary Antibody (C-D)	122

Table of Tables

Table 1) **All Full Waves of Contraction and/or Relaxation Counted Over 20 Minutes.....** 110

Table 2) **All Proximal-to-Distal Contractile Propagations Counted Over 20 Minutes.....** 112

Table of Abbreviations

AA.....	Arachidonic Acid	DMap	Diameter Map
ACh.....	Acetylcholine	DMSO	Dimethylsulfoxide
AH.....	After-Hyperpolarizing	DyDt.....	Change in the Y-Axis (Diameter of Colon in ST Map) with respect to change in Time.
ATP	Adenosine Triphosphate	ECs.....	Enterochromaffin Cells
BCFA	Branched Chain Fatty Acid	ERK.....	Extracellular signal– regulated kinases
BDNF	Brain Derived Neurotrophic Factor	FA	Fatty Acid
Ca ²⁺	Calcium Ion	FFAR.....	Free Fatty Acid Receptor
CaCl	Calcium Chloride	FFA	FFAR Specific Receptor Prefix
cAMP	Cyclic Adenosine Monphosphate	GI	Gastrointestinal
cGMP	Cyclic Guanosine Mopnphosphate	GIMM	GI Motility Monitor
CGPR	Calcitonin Gene Related Peptide	GLP-1	Glucagon-Like Peptide 1
CMMC	Colonic Migrating Motor Complexes	GPCR	G-Protein Coupled Receptors
CoA.....	Coenzyme A	GPR.....	GPCR Specific Receptor Prefix
CO ₂	Carbon Dioxide	Gα _x	Protein Gα of type X coupled to GPCR
CPI-17	PKC-Potentiated Inhibitor 17	Gβγ.....	Proteins Gβ and Gγ coupled to GPCR
CPG.....	Central Pattern Generator neurons	GEF	Guanine Exchange Factor
cPLA2	Cytosolic phospholipases A2	Gα _{olf}	Gas-like protein coupled to Olfactory GPCR
CT	Computed Tomography	GRKs.....	G-protein Coupled Receptor Kinases
C#.....	Fatty Acid with # number of Carbons	HAPC	High Amplitude Propagating Contractions
DAG	Diacylglycerol		
DAPI	4',6-diamidino-2- phenylindole		

HEPES4-(2-hydroxyethyl)-1-piperazineethanesulfonic acid
 H₂SHydrogen Sulfide
 IDInside Diameter
 ICCInterstitial Cells of Cajal
 IP21,4,-bisphosphate
 IP3Inositol 1,4,5-triphosphate
 IVAIsovaleric Acid
 IUPAC.....International Union of Pure and Applied Chemistry
 K⁺Potassium Ion
 KCl.....Potassium Chloride
 KH₂PO₄Potassium Phosphate
 K2PTwo-Pore Domain Potassium Channel Family
 LCFALong Chain Fatty Acid
 LED.....Light Emitting Diode
 L-NNAL-N-nitroarginine
 MCFAMedium Chain Fatty Acid
 MCTMonocarboxylate Transporter
 MLCMyosin Light-Chain
 MLCKCa²⁺/calmodulin-dependent MLC Kinase
 MgSO₄.....Magnesium Sulfate
 MPOMyenteric Potential Oscillations
 MRIMagnetic Resonance Imaging
 MYPT1Myosin Phosphatase Target Subunit 1
 Na⁺Sodium Ion

NaClSodium Chloride
 NaHCO₃Sodium Bicarbonate
 NH⁴⁺Ammonium Ion
 NONitric Oxide
 NOS.....Nitric Oxide Synthase
 OD.....Outside Diameter
 OR.....Prefix for Olfactory Receptor (Human)
 Olfr.....Prefix for Olfactory Receptor (Rodent)
 PBSPhosphate Buffered Saline Solution
 PACAP.....Pituitary Adenylyl Cyclase Activating Peptide
 PDEPhosphodiesterase
 PIP2.....Phosphatidylinositol 4,5-bisphosphate
 PI3Phosphoinositide 3
 PI3KPhosphoinositide 3-kinase
 PKA.....Protein Kinase A
 PKC.....Protein Kinase C
 PKG.....Protein Kinase G
 PLCPhospholipase C
 PLDPhospholipase D
 PopdcPopeye domain containing family of proteins
 PP1cMLC Phosphatase catalytic subunit
 PTX.....Pertussis Toxin
 PYY.....Peptide YY
 ROCKRho Kinase

SCFA.....Short Chain Fatty Acid

SerAmino Acid Serine

SMCSmooth Muscle Cell

SMMSmooth Muscle Media

ST Map.....Spatiotemporal Map

TREKTWIK-related K⁺ channels

TTX.....Tetrodotoxin

VIPVasoactive Intestinal Protein

ZIPK.....Zipper Interacting Protein
Kinase

2-EHA2-Ethylhexanoic Acid

5-HT5-Hydroxytryptamine
(Serotonin)

Abstract

Isovaleric Acid (IVA) is a 5-carbon branched chain fatty acid present in fermented foods and produced by the fermentation of leucine by colonic bacteria. IVA activates G-protein coupled receptors such as FFAR2, FFAR3, and OR51E1 known to be expressed on enteric neurons and enteroendocrine cells. We previously reported that the shorter, straight chain fatty acids acetate, propionate and butyrate, differentially affect colonic propulsion; however, the effect of branched chain fatty acids on gastrointestinal motility is unknown. We hypothesize that IVA relaxes smooth muscle in a cAMP/PKA dependent manner by direct action on smooth muscle cells. IVA will also decrease peristalsis and encourage retention of luminal contents. This thesis investigates the effect of IVA on smooth muscle tension and peristaltic activity in isolated colon and individual smooth muscle cells.

Colon segments from C57BL/6J mice were placed in a longitudinal orientation in organ baths in Krebs buffer and fastened to force transducers. Segments were contracted with 10 μ M acetylcholine (ACh) and the effects of IVA at several concentrations were measured in the absence and presence of Nitric Oxide Synthase inhibitor L-N-nitroarginine (L-NNA), neuronal action potential inhibitor tetrodotoxin (TTX), and adenylate cyclase inhibitor SQ22536. To study individual live cells, mouse smooth muscle was isolated from colon, suspended in smooth muscle buffer, and after contraction with ACh were relaxed with micromolar concentrations of IVA. For peristalsis studies, whole colonic segments isolated from C57BL/6J were catheterized and placed horizontally in organ baths with circulating Krebs buffer. The colon was clamped on the anal end, and a solution (5 μ L per mm of colon length) of either Krebs buffer or 50 mM IVA was delivered from the oral end to the lumen. Video of the peristalsis was then analyzed for

diameter, changes in diameter, velocity of diameter changes along the length of the colon, normalized to the anatomical changes in the proximal region.

IVA in concentrations of 10 mM to 50 mM relaxed the ACh-induced contraction in a sigmoidal fashion. In separate studies, L-NNA nor TTX affected the ability of IVA to inhibit relaxation. SQ22536 inhibited IVA induced relaxation in longitudinal colon compared to vehicle control. In isolated cells, SQ22536 and PKA inhibitor H-89 inhibited IVA-induced relaxation. In peristalsis studies, 50 mM IVA in Krebs buffer changed the character of the peristaltic action by increasing proximal diameter, inhibiting contractions in the proximal end of the colon, and decreasing overall velocity of peristaltic contractions in the proximal region.

The data indicate that the branched chain fatty acid IVA causes a concentration-dependent relaxation of colonic smooth muscle that is direct to the smooth muscle and independent of neuronal activity. This relaxation is cAMP/PKA dependent. In addition to the direct relaxation of smooth muscle, intraluminal IVA decreased overall colonic propulsive activity and encouraged retention of the luminal contents. We conclude that the ingestion and production of branched chain fatty acids could affect overall GI motility and is an area for study in dietary and therapeutic control of bowel activity.

Introduction

Fatty Acids

Definition, Types, and Sources of Fatty Acids

Fatty acids are carboxylic acids with an alkyl tail. With some variation between sources, the designation “short chain” fatty acid (SCFA) is assigned to fatty acids (FA’s) with 2 to 5 (or 8) carbons. “Medium chain” fatty acids (MCFA) are 6 (or 8) to 12 carbons in length, “long chain” fatty acids (LCFA) are 13 to 21 carbons long. Very long chain fatty acids are longer than 22 carbons.^{1,2} The shorthand for a fatty acid is $C\#_C:\#_D$, where $\#_C$ is the number of carbons and $\#_D$ is the number of double bonds. Much research and popular culture focus has been placed on unsaturated fatty acids, which have double bonds within the carbon chain and may be oriented in a cis or trans position, and their comparison to saturated fats which have no double bonds (“saturated” with hydrogen)². Branched chain fatty acids (BCFA) possess a fork in the carbon chain at least a methyl-group or longer. Less research attention exists for BCFA; however, what research there is focuses on the most common symmetrical methyl group substitutions either at the end of the carbon chain (*iso*- substituted) or a methyl- and ethyl- group fork at the end (*anteiso*- substituted) as opposed to no fork at the end for a normal fatty acid (*n*-FA)³.

The LCFAs are important structural molecules, either directly incorporated into the plasma membranes of cells or forming the building blocks of other molecules such as triglycerides, which serves as the primary long-term energy storage for animals⁴. A fatty acid is catabolized for energy by β -oxidation, which leaves a fatty acid 2 carbons shorter than the original⁵. While *n*-FA are the most common in eukaryotes and most prokaryotes, BCFA do form a significant portion of the cell membrane of species *Bacilli*, *Lactobacilli*, and *Bifidobacterium*.

In humans, long chain BCFA are rare with exceptions: approximately 15% of skin⁶, and 29% of the vernix caseosa⁷ are medium and long BCFA. Because the vernix is consumed by the fetus *in utero*, this is of interest to gastrointestinal development; by comparison, only 500 mg of mean human intake (1/10th a teaspoon) is a BCFA³.

The primary source of dietary SCFA is fermentation by the resident bacteria of the colon of hydrolysis-resistant starches which pass unabsorbed through the small intestine^{8,9}. BCFA are produced when proteins pass through the small intestines unabsorbed, and the branched amino acids valine, isoleucine, and leucine are respectively fermented to isobutyric acid, 2-methylbutyric acid, and isovaleric acid¹⁰. The Stickland reaction is performed by gastrointestinal bacteria, and is the primary metabolic pathways for some members of the genus *Clostridium*¹¹⁻¹³. The Stickland reaction involves the reciprocal oxidation-reduction of two amino acids to produce NH⁴⁺, CO₂, and two fatty acids¹⁴. The oxidized amino acid is the source of CO₂, and thus the fatty acid is one carbon shorter. Glycine, proline, and hydroxyproline are comparatively efficient electron acceptors and are usually reduced; alanine, isoleucine, and leucine are efficient electron donors and are thus usually oxidized¹¹. Acetate is also a reduction partner for valine and leucine¹⁵.

Fermentation of carbohydrates are predominantly in the cecum and proximal colon because substrate has yet to be fermented and absorbed, and water is more available⁹. In pigs, the range of three common SCFA (acetate, propionate, butyrate) in the colon was found to be 70 to 140 mM at the proximal end, falling to 20 to 70 mM at the distal end¹⁶. The quantity of BCFA along the length of the colon is not as well studied. In one study using an *in vitro* model of fermentation of samples from the deceased, SCFA believed to be derived from fermented protein (BCFA) was 38% of the distal colon fermentation products, compared to 17% of SCFA from

proximal colon fermentation products¹⁷. The potential for complex interplay of diet, bacteria, and SCFA and BCFA composition leaves plenty of opportunity for physiological application. Cancer has been associated with changes to the microbiome^{18,19} and to the fatty acid composition of stool¹⁹, and changes to high protein diets^{20,21}. Changes to diet also affect changes to the microbiome^{22–25} and to SCFA composition²¹, which begs the question of whether one event comes first, or if it is a cascade that can be started by a drastic change of any origin.

Absorption and Metabolism of Fatty Acids

There are questions whether absorption of short, medium and long chain fatty acids into the body is either through active transport or passive diffusion, with conflicting sources as to the degree each mechanism contributes^{2,26}. The pKAs of SCFAs are close to 4.7²⁷; in an intestinal lumen with a pH of from 5.5 to 6.5, the SCFA will be over 99% in ionic form^{28,29}. The charge would inhibit diffusion across a non-polar membrane and necessitate the use of a Na⁺ exchange pump to get into the cell. Known transporters of SCFA include member of the monocarboxylate transporter family MCT1 (SLC16A1)³⁰ and SLC5A8³¹, and the presence of fatty acids appear to upregulate at least some MCT family transporters³². The presence of a basolateral transporter, with the potential of moving SCFA from the mucosa to the submucosa is also reported³³. Other sources say the primary mechanism of absorption appears to be diffusion; in rat colon, the removal of Na⁺ or the use of ouabain to inhibit ion exchange did not inhibit SCFA transport³⁴. Some early papers making the argument for a primarily ion exchange mechanism of transport acknowledged some diffusion³⁵. For the last step crossing a cellular membrane, desorption, there is a logarithmic increase in the desorption rate constant of a fatty acid for every 2 carbons removed or 2 double bonds removed from a long or medium chain fatty acid³⁶, which implies a quicker transit for smaller fatty acids.

Cells in the colonic mucosa rapidly metabolize the SCFA for energy, with butyrate as the preferred source and sparing other such as acetate and propionate^{9,37}. Branched chain fatty acids are not as well studied in colonocyte oxidation, but some organ systems tested showed decreased oxygen consumption when the BCFA isovaleric acid was used as the energy source³⁸ and inhibition of mitochondrial metabolic function^{39,40}. If BCFAs do delay metabolism, increased time for cross-membrane transport to the submucosa and to the blood stream adds relevance to BCFA's potential role as a signaling molecule. While larger fatty acids often make it into the lymphatic system while in transit through the small intestines, over 90% of short chain fatty acids entering the stomach are absorbed to the portal vein^{41,42}.

Isovaleric Acid

For many foods, beverages, and even body odors, fatty acids provide part of the characteristic smell; for example, butyric acid (C4:0) has a rancid-butter smell and valeric acid (C5:0) has a cheesy smell. Fatty acids are frequently produced by bacterial fermentation of carbohydrates and proteins during the production of foods such as cheeses⁴³ and alcoholic beverages⁴⁴.

Isovaleric acid (IVA; IUPAC: 3-methylbutanoic acid) is a 5-carbon branched saturated fatty acid with two symmetrical methyl groups forking off the third carbon. Its odor is described as “cheesy” or “stinky feet” which lingers^{†45}. The production of IVA has been described in cheeses by *Propionibacterium freudenreichii*⁴³ and *Lactococcus Lactis*⁴⁶, and in beers and wines by yeast of the *Brettanomyces* family⁴⁴.

[†] According to “The Good Scents Company” website, IVA’s “substantivity” is described to last for 400 hours. For comparison, DL-menthol (IUPAC: 5-methyl-2-propan-2-ylcyclohexan-1-ol) has a substantivity of 32 hours. While not tested directly, this author and records of complaints to the VCU Office of Environmental Health and Safety can attest to the longevity of the pungency.

IVA is produced in the metabolism of, both fermentation and non-fermentation, the amino acid L-leucine, a branched amino acid with an isobutyl R-group (leucine is one carbon longer than IVA). Amino acids not used for anabolic protein building can be catabolized for use in the citric acid cycle. In a eukaryotic reaction, after leucine is converted to an α -keto acid by an amino transferase, a branched chain α -keto acid dehydrogenase enzyme complex converts it to a isovaleryl-CoA complex. A key step is converting the isovaleryl-CoA complex by isovaleryl-CoA dehydrogenase to 3-methylcrotonyl-CoA.⁴⁷ Genetic conditions are known to divert the normal leucine metabolism pathway to the production of isovaleric acid. In isovaleric acidemia, the gene for isovaleryl-CoA dehydrogenase produces either a reduced efficiency or ineffective enzyme, leading to a buildup of isovaleryl-CoA, which is then converted to isovaleric acid by removal of the CoA (likely by a reversible CoA transferase). A symptom of isovaleric acidemia, in addition to aversion to foods, seizures, and eventual brain damage, is the characteristic stinky feet smell emanating from the person. Treatment is limiting leucine in the diet.⁴⁸

Even without a genetic disorder of metabolism, IVA is one of the most prominent fatty acids in human blood. Most analysis of SCFA in blood ignore the branched fatty acids, and there appears to be drastic differences in measured concentrations potentially based on the methods, time period and the location of the measurements. In fasting patients in Denmark, *Jakobsdottir et al.* found that IVA in venous blood ranked second at 40 μ M, behind C2:0 acetic acid (245 μ M), and ahead of C3:0 propionic acid and the other prevalent BCFA isobutyric acid (13 μ M)^{49‡}. That study did not see increases with microscopic colitis or celiac disease. A study in Armenia found much lower concentrations (of all SCFA compared to the Denmark study), but also showed a 5 to

‡ In Arthur and Hommes' 1995 paper in the Journal of Chromatography, a method measuring just IVA and propionic acid in plasma found IVA at 0.89 μ M and propionic acid at 0.54 μ M¹⁷³. This paper lacks the perspective of having other SCFA's, but demonstrated that IVA is still more prevalent in blood than a prototypical SCFA.

20 fold increase of venous SCFA after bowel inflammation by either salmonella or Familial Mediterranean Fever⁵⁰. In isovaleric acidemia, a case study in Japan found up to 8 µg/mL (78 µM) IVA in a stable patient and up to 813 µg/mL (7960 µM) during a patient crisis (compared to below 0.6 µg/mL or 5.9 µM IVA in their controls)^{51§}. IVA is present in feces in significant amounts, approximately 5% of SCFA in feces¹⁹ and by another measurement 3.2 mmol/kg (wet weight)⁵², but is behind most straight SCFA in concentration.

Because other fatty acids are preferred for metabolism^{9,37}, and the potential to slow down metabolic activity^{38–40}, branched chain fatty acids like IVA are attractive to study as a signaling molecule. Known effects of BCFA such as IVA on physiological systems is scattered. IVA has been shown to inhibit cAMP-mediated lipolysis and inhibit new lipogenesis stimulated by insulin.⁵³ IVA in diet has been associated with changes in gestation time and birth weight.⁵⁴ High IVA in stool is associated with depression⁵⁵, which may be mediated crossing the blood-brain barrier and causing the inhibition of Na⁺/K⁺ ATP pumps.⁵⁶ There are even musings that chewing plants of the *Valeriana* family and consuming IVA may have been an early anticonvulsant.⁵⁷ The stool levels of IVA and isobutyric acid (as well as the amino acid precursors leucine and valine) were found higher in colorectal cancer patients¹⁹. With changes in the colonic microbiome with cancer patients^{18,19}, how the changing bacterially-produced metabolites effect cancer progression is a natural question being studied. The branched chain amino acids leucine and valine were also found in circulation at higher levels in pancreatic ductal adenocarcinoma patients⁵⁸, which begs the question whether circulating branched chain amino acids affect circulating BCFA levels.

§ Certain fish have normal blood level of IVA at 4.4 mM¹⁷⁴

Fatty Acid Receptors and Signaling

Free Fatty Acid Receptor Family

There are at least four known members of the Free Fatty Acid Receptor (FFAR or FFA in some literature) family, labeled FFAR 1 through 4 (or in older literature, referred to as their pre-characterization generic GPR number). They are all G-protein coupled receptors (GPCR), of which FFARs 1,2, and 4 couple to $G\alpha_q$, while FFARs 2 and 3 couple to $G\alpha_i$. FFAR2 (GPR43) and FFAR3 (GPR41) have SCFA as their natural ligands, while FFAR1 (GPR40) and FFAR4 (GPR120) are activated by longer fatty acids. FFAR1,2, and 3 (and GPR42, closely related to FFAR3 and once considered a pseudogene⁵⁹) are all located on human chromosome 19q13; FFAR4 is located on 10q23⁶⁰.

FFAR4 is the least similar by amino acid of the group (10%) but shares a similar LCFA ligand profile as FFAR1, preferring LCFA⁶⁰. FFAR4 is expressed in the intestines, and induces Glucagon-Like Peptide-1 (GLP-1) secretion by enteroendocrine cells⁶¹.

The FFAR1 gene is expressed comparatively high in the brain, pancreas, and monocytes; FFAR1 is coupled to $G\alpha_{q/11}$ and in humans identified ligands include both unsaturated fatty acids such as linoleic and oleic acid and saturated fatty acids from C6 to C23 while ruling out Formic acid (C1)⁶². Most literature does not investigate its activation with shorter fatty acids; however, at least one paper identifies butyric acid (C4) as a ligand of exogenously expressed murine FFAR1 while ruling out acetic (C2) and propionic (C3) acids⁶³ and leaves open the question of whether short BCFA activate FFAR1. The availability of specific agonists and antagonists of FFAR1 allow for easier investigation of the physiological effects⁶⁴. FFAR1 has been shown to promote contractility in trachea-derived smooth muscle⁶⁵, as well as promote smooth muscle cell (SMC) proliferation via ERK and PI3K pathways⁶⁶.

FFAR2 is highly expressed in cells of the immune system, including lymphocytes, neutrophils, and monocytes.⁶⁷ One example of FFAR2 function includes neutrophil chemotaxis with concentration-dependent increase in activity.⁶⁸ This lends itself to suspecting a role of FFAR2 in inflammation; however, there are multiple examples of contradictory results with FFAR2/GPR43 gene knockout mice. This is further complicated by examples of differences in mouse and human responses to GPR43 agonists in β -islet cells and adipocytes.⁶⁹ In the colon, FFAR2 is present in enteroendocrine cells positive for GLP-1, but not 5-HT⁷⁰. FFAR2 is preferentially activated by the shortest chain fatty acids, such as C1 formate and C2 acetate, while still showing some affinity for all SCFA including some BCFA.⁷¹ Among the four FFAR's, FFAR2 is unique in being characterized as coupling to both pertussis toxin (PTX)-sensitive $G\alpha_i$ and PTX-insensitive $G\alpha_q$ ^{67,72}. There is one known antagonist of FFAR2, GLP0974, which has been in human safety trials for ulcerative colitis patients⁷³; however, a downside for investigative purposes is that a single amino acid polymorphism common in wildtype rodents negates the effectiveness of this drug⁷⁴.

FFAR3 is closely related to FFAR2, with which substitutions of specific amino acid residues can change the selectivity of either receptor for specific fatty acids to be more like its sibling receptor.⁷⁵ FFAR3 also has another closely related receptor, GPR42, which was once believed to be an unexpressed “pseudogene”, has some evidence of transcription and differs from FFAR3 by as few as one amino acid in certain haplotypes.⁷⁶ FFAR3 is more selective for SCFA C3 to C5 and for BCFA such as isovaleric acid and 2-methylbutyrate.⁷¹

FFAR3 tissue expression is varied, with very prominent expression in adipose, but also standout in the pancreas, spleen, placenta, and other organs.⁶² FFAR3 is expressed on the neurons and enteroendocrine cells of the gut. In rats, nerve fiber endings of the myenteric and

submucosal plexus of the proximal colon stained positive for FFAR3. Some cell bodies of the myenteric plexus were also positive for FFAR3.⁷⁷ In proximal colon, FFA3-specific agonists inhibit circular muscle contraction induced by high dose nicotine, as well as inhibit the loss of circular muscle rhythm caused by low dose nicotine or 5-HT, but does not inhibit contraction caused by non-neuronal muscarinic receptor 3 agonist bethanechol.⁷⁸ This implies that FFAR3 mediated effects on circular smooth muscle are neuronal, not direct to the smooth muscle. FFAR3 was expressed in enteroendocrine L cells positive for peptide YY (which induces relaxation), but not positive for 5-HT or FFAR2.⁷⁹

FFAR2 and FFAR3 have the ability to heterodimerize, changing the degree of its Ca^{2+} and cAMP signaling.⁸⁰ While this is important to consider, this may not be relevant in gastrointestinal motility physiology outside immune systems effect on motility because of the segregation of FFAR2 and FFAR3 positivity among enteroendocrine cells.

Olfactory Receptor Family

SCFA are volatile and often associated with a characteristic smell. It is no surprise that olfactory receptors would be sensitive to fatty acids. Olfactory receptors are GPCRs which interact with the $\text{G}\alpha_s$ -like $\text{G}\alpha_{\text{olf}}$. Adenylate Cyclase III is essential for smell, and once activated by $\text{G}\alpha_{\text{olf}}$ produces the second messenger cAMP.^{81,82} This smell can vary from person to person, as exemplified by an allele of OR11H7P, which is associated with a stronger sensation for isovaleric acid.⁸³ The olfactory receptor family is large and diverse. The complex interplay of a multitude of receptors for a wide diversity of volatile ligands to produce the sense of smell is beyond the scope of this writing; however, olfactory receptors sensitive to the BCFA isovaleric acid have been found outside the olfactory organs and recycled as chemical sensors for a multitude of organs such as heart⁸⁴, kidneys⁸⁵, colon⁸⁶, and even the eye⁸⁷.

The olfactory receptor OR51E1 (Olf558 in mice) is sensitive to a number of medium and short chain fatty acids, and reportedly fatty acid agonism is antagonized by one BCFA, 2-Ethylhexanoic acid.⁸⁴ Isovaleric acid induces a Ca^{2+} current in enterochromaffin cells to release 5-HT, is more potent than isobutyric acid or straight chain fatty acids, and the effect is ablated by the knock-out of Olf558.⁸⁸

Potassium Channel Activation by Fatty Acids

TWIK-related K^+ channels (TREK) are part of the two-pore domain potassium channel family (K2P) and when activated TREK-1 creates an outward rectifying K^+ current. TREK-1 is activated by stretch, and by the unsaturated LCFA arachidonic acid (AA). AA activation of TREK-1 is mediated by the internal carboxy terminus of the channel, as determined by deletion of that domain and patch-clamp experiments exposing the intracellular portion to TREK-1.⁸⁹ AA is produced by hydrolysis of phosphatidylcholine by cPLA2, and induces an increase in Ca^{2+} in longitudinal smooth muscle to cause contraction, and low doses of exogenous AA induces membrane depolarization to cause contraction.⁹⁰ TREK-1 is also inhibited through cAMP/PKA-dependent pathways⁹¹ and cAMP/PKA-independent Popdc-domain containing proteins⁹².

TREK-1 is located throughout the smooth muscle in mouse ileum and colon. TREK-1 activators Riluzole and BL-1249 induced relaxation in longitudinally-oriented mouse ileum and colon, and this effect was inhibited by K^+ -channel blocker Barium, and resistant to TTX treatment implying that neurons were not the effector.⁹³ TREK-1 has been studied as a target of drugs of psychology, and the mood stabilizer drug and short BCFA valproic acid (trade name Depakote) activates TREK-1 currents (while antipsychotics and anti-depressants such as fluoxetine and citalopram inhibit TREK-1).⁹⁴ Like other short BCFA, valproic acid has been seldom studied in smooth muscle with only one study; this study found contraction at low

concentrations and relaxation at higher concentrations in rat and guinea pig stomach and taenia coli.⁹⁵

Peristalsis

Definition and Basic Mechanism

Peristalsis is a contraction which moves in a wave down a tube to push the contents of the tube's lumen in a direction. In the context of physiology, peristalsis is the organized muscular contraction around a segment of a tube-like organ which propagates like a wave forward with further contraction, often while relaxing tension ahead of the wave-like contraction, to push the contents of the organ in the direction the wave of contraction is moving. Propagating contractions move contents, in contrast to stationary contractions which churn the contents in place. While normal peristaltic contractions move contents from the oral to the aboral/anal end, anti-peristaltic contractions move contents in the opposite direction. The combination of normal contractility patterns in the small intestines which maintain homeostasis are called the migrating motor complex; a three-phase process beginning with relative calmness, followed by low amplitude contractions, and ending with larger propagating contractions. In the colon, more stationary churning patterns and anti-peristaltic movements occur, fitting its role as storing food before defecation and providing the last opportunity for digestion and absorption of the contents.⁹⁶

The mechanism for peristalsis in the intestine has numerous complexities, but there are some basic concepts. An intrinsic neuron, such as a multipolar Dogiel type II AH (after-hyperpolarizing) neuron with projections from the myenteric plexus to the mucosa, detects stretching in the region it covers^{97,98}. These cells project to inter-neurons behind and ahead of the region of stretch, which in turn project to circular smooth muscle⁹⁹. The adjacent smooth muscle

are connected by gap junctions, allowing an electrochemical signal to travel from muscle cell to muscle cell to work together as a single unit¹⁰⁰. Projections to neurons towards the oral end are usually excitatory, and release neurotransmitters acetylcholine or tachykinin in the synapse with the circular smooth muscle to induce contraction¹⁰¹. Projections to neurons towards the anal end are usually inhibitory (to open up the lumen) and release neurotransmitters such as ATP, vasoactive intestinal peptide (VIP), and pituitary adenylyl cyclase activating peptide (PACAP)^{102,103}. Gaseous messengers such as nitric oxide (NO)¹⁰⁴ and hydrogen sulfide (H₂S) are also produced to cause relaxation^{105,106}.

Longitudinal muscle is less understood, but there appears to be coordinated excitation and relaxation. While one group claims that the longitudinal and circular muscle contractions and relaxations are roughly the same response in the same region^{107,108}, Grider showed that longitudinal smooth muscle is relaxed when the circular muscle is contracting and vice-versa¹⁰⁹. Maintaining the integrity of the tissue is essential for these types of studies; improvements in techniques to measure these physiological phenomena are necessary to improve our understanding of peristalsis physiology.

Enteroendocrine cells are specialized epithelial cells along the gastrointestinal tract secrete signaling molecules of various types, and are categorized by what is released such as K cells (secrete gastric inhibitory peptide), L cells (secrete GLP-1 or PYY), or Enterochromaffin cells (ECs).⁹⁶ ECs are relatively rare sensory cells in the mucosa, which also have sub-populations of specifically secreting cells with different signaling molecules and distributions that differ between large and small intestine^{110,111}. EC's signal to neurons via the signaling molecule 5-hydroxytryptamine (5-HT, serotonin) and are important for sensing changes within the lumen. ECs are chemosensors which respond to glucose¹¹², fatty acids^{88,113}, nicotine¹¹⁴, and

more¹¹⁵. EC's respond to mechanical stimulation of the mucosa by releasing 5-HT, which excites sensory neurons to release calcitonin gene related peptide (CGRP) to excite interneurons to begin peristaltic activity.^{116–118}

To test effects of neuronal activity on peristalsis, inhibitors are useful. The use of tetrodotoxin (TTX), which inhibits sodium channels, prevents action potential conduction along axons; TTX exposes latent or hidden pacemaker activity in colon tissue^{119,120}. L-N-nitroarginine (L-NNA), prevents Nitric Oxide Synthase (NOS) from producing NO; L-NNA causes CMMC amplitude and frequency to increase¹²¹. The use of either on colon induces smooth muscle activity. This implies a tonic inhibition of smooth muscle activity by neurons or an endocrine inhibitor.

Regular Movement and Patterns

Outside of mechanical or chemical stimulation, regular, rhythmic waves of contraction, colonic migrating motor complexes (CMMCs), called high amplitude propagating contractions (HAPCs) in humans, ensure the eventual movement of colonic contents to make room for new sustenance. Human HAPC's and murine CMMC's appear to have similar frequencies *ex vivo*, approximately every 3 to 4 minutes. *In vivo*, Human mass waves of peristalsis appear to be much rarer; HAPC's happen 7 to 10 times a day.^{120,122}

These regular waves appear to be regulated by myenteric neurons and are inhibited by muscarinic antagonists^{98,123,124}. A set of central pattern generator (CPG) neurons in the myenteric plexus which signal via 5-HT through at least 7 types 5-HT receptors with more subtypes^{120,125,126} are most likely responsible for the timing of the waves^{127,128}. The network of Interstitial Cells of Cajal (ICC) include these pacemaker cells. The ICC run along the myenteric plexus (ICC-MY) which generate fast electrical waves called myenteric potential oscillations

(MPOs) and run along submucosal border (ICC-SM) which generate slow electrical waves. The ICC-MY generated MPO's and the ICC-SM generated slow waves, together with release of tonic inhibition of contraction provided by neurons¹²⁹, combine to form the contractile patterns of the colon^{97,122}.

Smooth Muscle Contraction and Relaxation

There is a diversity of ligands and target receptors for smooth muscle action, and multiple pathways to achieve contraction or relaxation. Understanding a few possibilities for how nutrients could signal smooth muscle requires some basic knowledge of the major players in smooth muscle contraction and relaxation.

In circular smooth muscle of the colon, the most abundant receptor to induce smooth muscle contraction is the muscarinic cholinergic receptor M3^{130,131}. M3 is coupled to $G\alpha_q$, which binds the carboxy terminus of PLC- β 1 to activate the enzyme¹³². This enzyme hydrolyzes phosphatidylinositol 4,5-bisphosphate (PIP2) to diacylglycerol (DAG) and inositol 1,4,5-triphosphate (IP3)¹³³. An activated IP3 receptor (IP3R-I) on the sarcoplasmic reticulum causes the release of stored Ca^{2+} ^{134,135}. Ca^{2+} /calmodulin-dependent myosin light-chain kinase (MLCK) is phosphorylated and activated, which then phosphorylates 20-KDa myosin light chain (MLC₂₀). MLC₂₀ Ser19-P then forms a crossbridge with actin, and myosin ATPase (on the head of the myosin filament) induces the increased overlap of myosin and actin to cause contraction¹⁰⁰.

There are some differences with colonic longitudinal smooth muscle. In longitudinal smooth muscle, PLC- β 1 primarily hydrolyzes phosphatidylinositol 4-phosphate (PIP), creating 1,4-bisphosphate (IP2)¹³³, which does not cause the release Ca^{2+} with the same efficiency¹³⁶. Longitudinal muscle requires calcium influx from outside the cell^{135,137}, and uses the enzyme

cPLA2 to produce arachidonic acid which activates membrane Ca^{2+} channels^{137,138}. Longitudinal muscle may also have a different receptor make-up compared to circular muscle, as such demonstrated by its comparative non-response to somatostatin-14¹³⁹.

Alternative receptor/ligand pairs incorporate other G-protein coupled receptors such as using $\text{G}\alpha_i$ via natriuretic peptide clearance receptor¹⁴⁰, and/or take advantage of the $\text{G}\beta\gamma$ subunit activating PLC- $\beta 3$ to achieve contraction¹⁴¹. Caveolae (small inwardly-directed cell membrane pouches) created primarily in smooth muscle by the protein caveolin-1, when activated can block the muscarinic receptors¹⁴², but have also been shown to facilitate enhanced contraction through $\text{G}\alpha_q$ -coupled Muscarinic receptor M3 (but not $\text{G}\alpha_{i3}$ -coupled M2)¹⁴³. Eventually, G-protein coupled receptors are desensitized to the ligands, and G-protein Coupled Receptor Kinases (GRKs) or other protein kinases inhibit the receptors^{90,144}.

Well characterized mechanisms for smooth muscle relaxation are through the receptors for the homologous ligands VIP and PACAP, and through the gaseous signaling molecules NO and H_2S . VIP/PACAP signal through $\text{G}\alpha_s$ coupled receptors, which activate adenylate cyclase V and VI, to generate cAMP, which activates Protein Kinase A (PKA), which inhibit Rho-Kinase mediated contraction¹⁴⁵. PKA also inhibits Ca^{2+} mediated contractions by decreasing intracellular Ca^{2+} levels in the cytosol by inhibiting either the formation of IP3 or IP3 mediated Ca^{2+} release mechanisms, and by inhibiting influx of extracellular Ca^{2+} .^{90,134,141} NO, which can be generated by the neuron or by the smooth muscle in response to VIP/PACAP $\text{G}\alpha_{i1/2}$ coupled natriuretic peptide clearance receptors by activating Nitric Oxide Synthase (NOS) III, activates soluble guanylate cyclase, creating cGMP, which activates PKG, which activates myosin phosphatase, which deactivates myosin cross-linking¹⁴⁰. H_2S induces relaxation by inhibiting

phosphodiesterase (PDE) 5, thereby slowing cGMP breakdown¹⁰⁵, and inhibits RhoA activity by sulfhydrating it¹⁰⁶.

Less-well characterized mechanisms for smooth muscle add to the complexity of peristaltic activity. The descriptively named “Exchange protein directly activated by cAMP”, or Epac, activates Rac1 and decreases RhoA activation, leading to MLC kinase inhibition^{146,147}. Independent of cAMP, potassium-channels have been shown to act as mediators of smooth muscle contraction¹⁴⁸; opening K⁺ channels hyperpolarize the membrane to cause the closure of Ca²⁺ channels¹⁴⁹. In the trachea, fundus, and duodenum, Gs-coupled β 3-adrenoreceptor mediated relaxation independent of cAMP via voltage-gated potassium channels have been observed^{150,151}.

These differences allow for differential signaling between longitudinal and circular smooth muscle. Activation or inhibition of a pathway in one group of smooth muscle that is not as pertinent in the other can allow for different responses to the same ligand.

Ca²⁺-Independent Sustained Contraction

After the initial smooth muscle contraction, which is regulated by Ca²⁺, contraction independent of Ca²⁺ signaling takes over to sustain the contraction in a “latch state”¹⁵² with less than 30% of the phosphorylated cross-bridges, thus using less ATP¹⁰⁰. Activation of Gq/G13 coupled receptors leads to the activation of RhoGEF, which exchanges a GDP with a GTP to activate RhoA. RhoA activates Rho Kinase (ROCK) and Phospholipase D (PLD). Ca²⁺-independent sustaining of contraction now has at least two paths. Activated ROCK phosphorylates Myosin phosphatase target subunit 1 (MYPT1) at T696, which causes the disassociation of MLC phosphatase catalytic subunit (PP1c), which normally would have caused MLC dephosphorylation and relaxation.⁹⁰ ROCK also phosphorylates Zipper Interacting Protein

Kinase (ZIPK), which maintains MYPT1-T696 phosphorylation¹⁵³. In parallel, PLD hydrolyzes phosphatidylcholine to phosphatidic acid, which activates diacylglycerol, leading to activation of protein kinase C (PKC). PKC phosphorylates PKC-potentiated inhibitor 17 (CPI-17), which also inhibits PP1c. Another pathway for Ca^{2+} -independent sustained contraction is $\text{G}\beta\gamma/\text{PI3K}$ activation of Integrin-Linked Kinase which phosphorylates MLC and CPI-17.¹⁵⁴

Straight-Chain SCFAs' Effect on Peristalsis

In flat preparations of rat colon stimulated by stroking the mucosa with a brush where the colon was compartmentalized into oral, central, and anal compartments, addition of acetate (C2), propionate (C3), and butyrate (C4) to the central compartment increased the ascending contraction and descending relaxation in a dose-dependent fashion approaching 100 mM. 5-HT and CGRP (but not BDNF) release was increased by the fatty acid, and 5-HT₄ receptor antagonism decreased the release of CGRP and the contraction and relaxation responses.¹¹³

Differential effects have been observed with acetate and propionate versus butyrate in peristalsis. Spatiotemporal maps generated from videos of proximal guinea pig colons infused with propionate or acetate have shown a decrease in propagating contractions, while infusion with butyrate increased the number of propagating contractions. In particular, butyrate increased the number of full-length propagations, while all three fatty acids decreased the number of short-length propagations.¹⁵⁵

Methods of Analysis

There are both advantages and hurdles to understanding an internal organ that is not only biologically and biochemically dynamic, but also has mechanical activity. While maintaining proper physiological and anatomical context can be more complicated when studying a dynamic

organ, measuring the mechanical changes themselves provide another assay by which physiological effects can be studied.

Imaging of the internal shape and organization of live small intestines and colon has been possible since the use of x-ray imaging. Computed tomography (CT) and magnetic resonance imaging (MRI) provide 3-dimensional information about bowel shape¹⁵⁶; however, MRI is the modality of choice for imaging humans *in vivo* because of the lack of ionizing radiation allows for more long-term study and longer sessions allowing for temporal resolution in the range of 2 frames per second¹⁵⁷. For current medical practice, motility is often pharmacologically inhibited before MRI because movement introduces artifacts when a static image is the current standard¹⁵⁸. Live video of the movement is improving *in vivo*. Video fluoroscopy and lower radiation requirements for imaging enhances x-ray technology. Cameras can be swallowed¹⁵⁹ or inserted (endoscopy). Specialized manometers can measure pressure with improving resolution as manometers become smaller and more can be fit into a device¹⁶⁰. While these techniques are great at determining anatomical normal and detecting abnormalities for patients, their use as a tool to study peristalsis may require more invasiveness than practical. Removing sections of digestive organs and studying them *ex vivo* is more practical.

One of the earliest, and still relevant, measurements of gastrointestinal response is the measurement of tension generated by the organ, either as strips of organ, or measured along the length of the organ¹⁶¹. This allowed for real-time measurement by “enterograph” (or less specific term polygraph) which could be easily quantified. As video became more practical, measured diameters were reported. The diameter map (DMap) or also called spatiotemporal maps (ST Map), was an accident of using images to store diameter data, which then became an easy way to visualize changes in *ex vivo* intestine diameter along the length of the organ. With information

about time and distance, other information such as change in diameter, velocity, and frequency can be calculated, much of this automated by image analysis techniques.¹⁶² Overlaying increasingly higher resolution manometry data allows for better understanding of the dynamics in the lumen¹⁶³. While a very useful tool, this has to be balanced against artifacts caused by the actual measuring instrument. The future is likely in completely automated analysis of 3D imagery, maintaining the spatial position information as well as the temporal and length information.

Materials and Methods

Materials

Chemicals not specified were acquired from Sigma-Aldrich (St. Louis, MO). Aqueous solutions were made with ultrapure water produced by Millipore Milli-Q Reference (Burlington, MA). Krebs buffer was prepared as follows: 118 mM NaCl, 4.75 mM KCl, 1.19 mM KH₂PO₄, 1.2mM MgSO₄, 2.54 CaCl; a 10x concentration of the preceding was diluted to 1x and the following solutes added to make the concentrations: 25 mM NaHCO₃, 11 mM Glucose. Unless otherwise specified, bubbled Krebs buffer is with 95% O₂ and 5% CO₂ and is adjusted to pH 7.4 before use as a control solution or as a solution to maintain the whole organ.

HEPES-buffered smooth muscle media (SMM) contains 25 mM HEPES, 120 mM NaCl, 4 mM KCl, 2.6 mM KH₂PO₄, 0.6 mM MgCl₂, 14 mM glucose and 2.1% Eagle's essential amino acid mixture (ThermoFisher).

Fatty acids tested include Isovaleric Acid (IVA), Valeric Acid, and 2-Ethylhexanoic Acid (2-EHA) in Krebs buffer both unadjusted and adjusted to pH 7.2 in stock solution. Other chemicals used were Acetylcholine (ACh), Tetrodotoxin (TTX; Tocris Bio-Techne, Minneapolis, Minnesota), L-N-nitroarginine (L-NNA; Tocris Bio-Techne), SQ22536 (Tocris Bio-Techne), and H-89 (Tocris Bio-Techne).

Animal Preparation

Mus muscularis C58Bl/6 were purchased from Charles River Laboratories (Wilmington, MA) and housed in the Division of Animal Resources facility, Virginia Commonwealth University. Mice were euthanized by CO₂ asphyxiation under protocols approved by VCU Institutional Animal Care and Use Committee. The colon was dissected out and placed in a

silicone bottom petri dish with bubbled Krebs buffer warmed to 37°C. Extraneous mesenteric tissue was carefully removed while avoiding unnecessary tearing or stretching of the colon.

Longitudinal Colon Segment Force Measurement

Setup

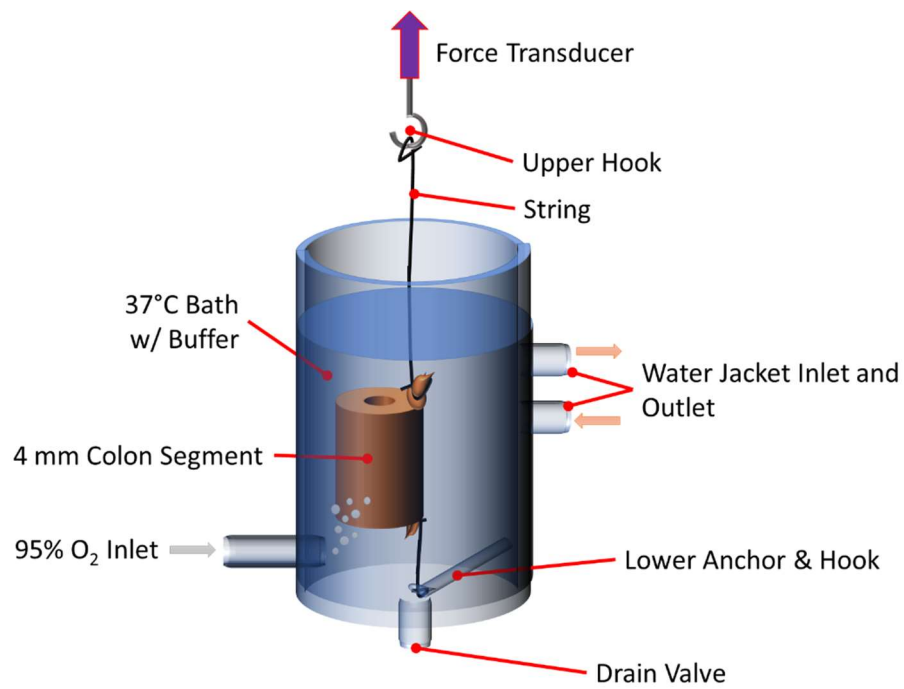
Colon segments approximately 4 mm were cut from the colon, and tied at both ends with surgical silk string, while not occluding the lumen. One end of string was tied in a loop and placed around a glass hook, and the other end was tied to a ring. The glass hook was submerged in bubbled Krebs buffer in an organ bath of volume 3 to 6 mL (Radnoti, Monrovia, CA) with water jacket attached to circulator (Julabo MC-12; Seelbach, Baden-Württemberg, Germany) set to 40°C (Figure 1). Krebs buffer was removed through a turn valve at the bottom and replaced by pipette from above opening. The ring was hooked to a model FT03C Force Transducer (Grass Technologies, Quincy, MA), which was attached to a Powerlabs 8/35 with Octal Bridge Amp (ADInstruments, Colorado Springs, CO). Continuous data was collected with LabChart 8 (ADInstruments) software.

The colon tension was adjusted by moving the force transducer with a mounting rack and pinion, and oscillating tension kept between 0.5 g and 1.1 g for the initial setup. After tension adjustment, the Krebs buffer was replaced at 15 minute intervals 3 times before initial experiment. Volume of treatment was calculated based off volume of buffer in the organ bath and treatment added by pipette to reach target concentration in bath. Between treatments with fatty acids, the bath was rinsed with at least 3 bath volumes of Krebs buffer, and left for 15 minutes before drug treatment. Dose response curve was created from the initial fatty acid treatments and before subsequent treatment with drugs or their vehicle controls.

The following treatments and concentrations were tested: ACh at 10 μ M at least 10 minutes before dosing with IVA in Krebs buffer at concentrations of 0.1 mM to 50 mM at pH 6.8 and pH 7.4, 10 μ M TTX in citrate buffer pH 4.8, 100 μ M L-NNA in ultrapure water, 10 μ M and 500 μ M SQ22536 (Tocris Bio-Techne) in DMSO, 10 mM pH 6.8 and 20 mM pH 7.4 Valeric Acid in Krebs buffer, 10 mM pH 6.8 2-EHA and 25 mM 2-EHA + 25 mM IVA pH 7.4 in Krebs buffer.

LabChart data files were converted by LabChart 8 to individual MATLAB data files per channel and analyzed by a custom-created MATAB (Version R2018a; Mathworks; Natick MA) script (see Appendix 1). The script analyzed maximum and minimum points of tension averaged over 15 seconds within the first 300 seconds after addition of the dose, and a 30 second average after 300 seconds, and compared it to a 60 second baseline average ending 1 second before dosing. Relaxation and contraction data, as well as relative relaxation compared to contraction caused by preceding 10 μ M ACh dose, were compared. Statistical analysis was performed in Microsoft Excel 2016 and MATLAB R2018a.

Figure 1) **Diagram of vertical force measurement organ bath for colon segments.**



Peristalsis and Spatiotemporal Maps

Setup

Colon was placed in a water jacketed glass petri dish (Radnoti) with silicone bottom filled with bubbled Krebs Buffer and heated by water circulator. Approximately 10 mm of polyethylene tube 1.7 mm OD 1.19 mm ID (Becton Dickinson) was placed in each end of the colon and tied with surgical silk. The open end of the tube was then inserted into Tygon 5/32 inch OD 3/32 inch ID tubing (Fisher Scientific) which was threaded into a custom designed and printed organ bath. The bath was designed using OpenSCAD 2017.01.20 (Figure 2 - See Appendix 2) and printed using Formlabs (Somerville, MA) Form 2 with Clear Resin GPCL04 with the assistance of the Virginia Commonwealth University Innovative Media department. Bubbled Krebs buffer was circulated with a peristaltic pump at 10 mL/min through a glass jacketed coiled condenser with 46 °C water before entering the organ bath at approximately 35 °C and actively bubbled in bath when not recording. Vacuum suction maintained organ bath volume during continuous circulation. Baths were back-lit with adjustable blue LED surface (GIMM-100; Catamount Research and Development, St. Albans, Vermont), and cameras were operated with GI Motility Monitor (GIMM Ver. 2.0.2.14; Catamount Research and Development). Washout before each infusion before imaging was with at least 15 mL of bubbled Krebs buffer. The colons and viewing dimensions were measured using the GIMM software. Before imaging, colons were flushed of the previous contents with the control or experimental solution and allowed to relax to a baseline. Solutions were Krebs buffer pH 7.4 (control), Krebs buffer pH 4.8, 10 mM IVA in Krebs buffer pH 6.8, 50 mM IVA in Krebs buffer pH 4.8. The distal end was clamped, and then a pipette containing the same solution as just flushed into the colon was adjusted to 5 μ L per mm length of the colon and tip placed in the tube leading to the

proximal end. The pipette plunger was pressed, pushing the contents into the colon inflating the colon, and the proximal end immediately clamped. Video was recorded for at least 25 minutes.

Analysis

The cameras (Med Associates Inc; St. Albans, Vermont; Lenses: FA Mega Pixel M084-MP f=8mm F1.; Computar, Cary, NC) filmed at 320 pixel width by 240 pixel height and were saved by GIMM in WMV format. The video files, dimensions of the field of view measured in mm, and identifying information were entered into custom scripts (see Appendix 3) designed in MATLAB R2018a. Briefly, frames were analyzed for pixels containing colon or background by thresholding a value as background, and changing the background value to 1 and the colon value to 0. Pixels inside the colon which were erroneously set to background due to camera lighting and contrast issues were detected and changed by MATLAB's "imfill(...,'holes')" function (Figure 3)

Spatiotemporal Maps (ST Maps) were created as follows: The diameter along the length of the colon per frame was determined by counting the number of pixels in the Y-axis direction along the colon in an area set to contain only colon or background and using the view area dimension to calculate the mm per pixel (Diameter ST Map). Change in diameter (Dy/Dt ST Map) was calculated by setting a threshold time (10 seconds) and calculating the difference between the calculated diameter then and threshold time prior. The wave velocity was calculated by taking the Dy/Dt ST Map and applying the MATLAB gradient function, which takes the partial derivative with respect to the X and Y axis of a 2D matrix to find the vector in the direction of greatest change (normal to the direction of the peristalsis). The x and y value signs of the gradient vector values generated were used to determine if relaxations or contractions were

moving in directions which showed peristalsis or anti-peristalsis, and the magnitude of the vectors determined relative velocity (Figure 4 and Figure 5).

Figure 2) **Diagram of custom gastrointestinal motility monitor organ bath.**

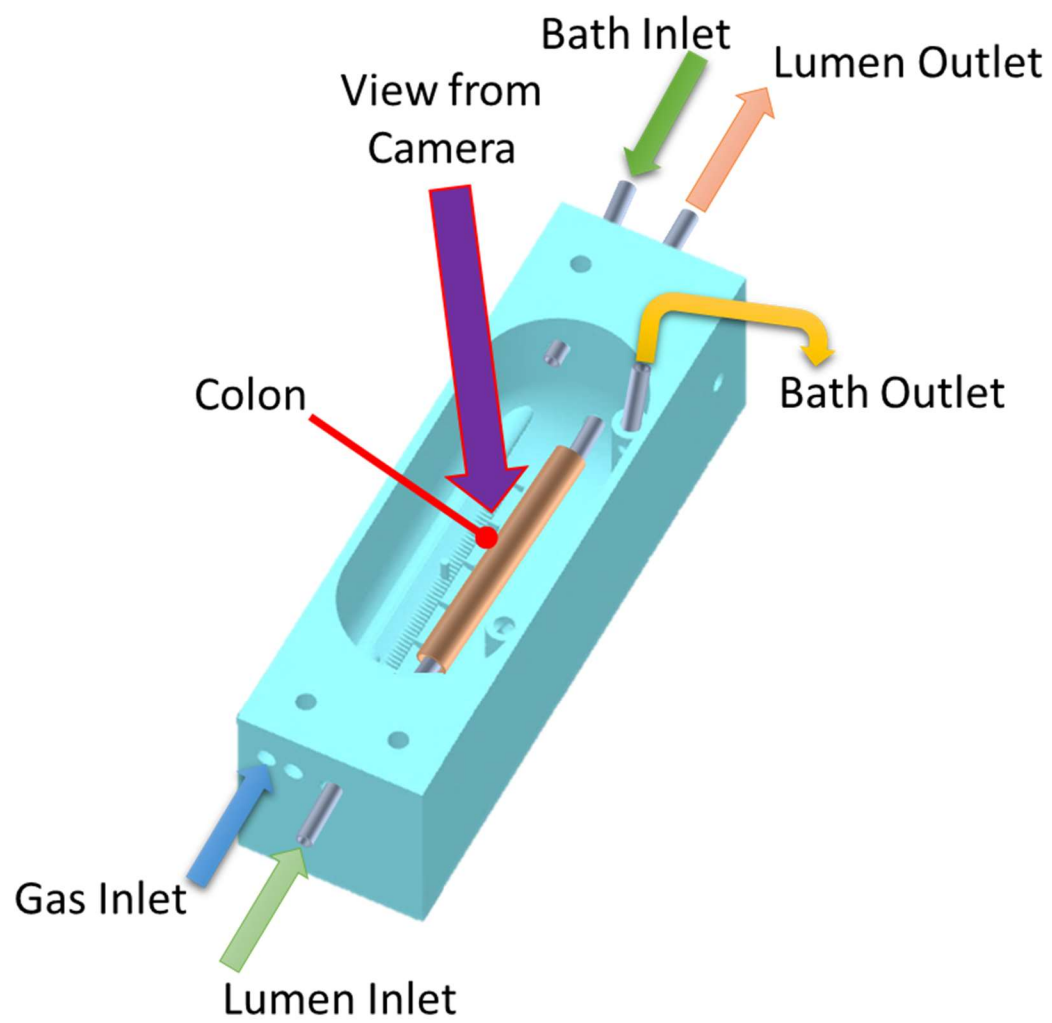
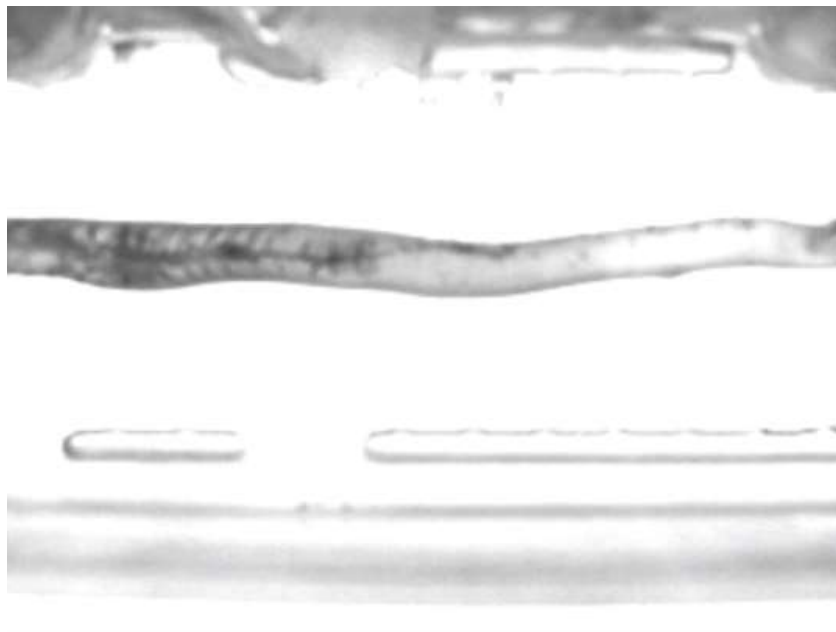


Figure 3) **Example Frame of Colon Video Color-Coded for Regions.** A) Individual frame of video of a colon. B) Frame after analysis by ST Map software. The area inside the blue box is the part of the video to be analyzed. The area in green is detected as background. The area in purple is originally detected as colon. The area is red was initially detected as background based on color but determined to be colon based on its location completely surrounded by colon. The purple regions outside the box are parts of the organ bath.

A)



B)

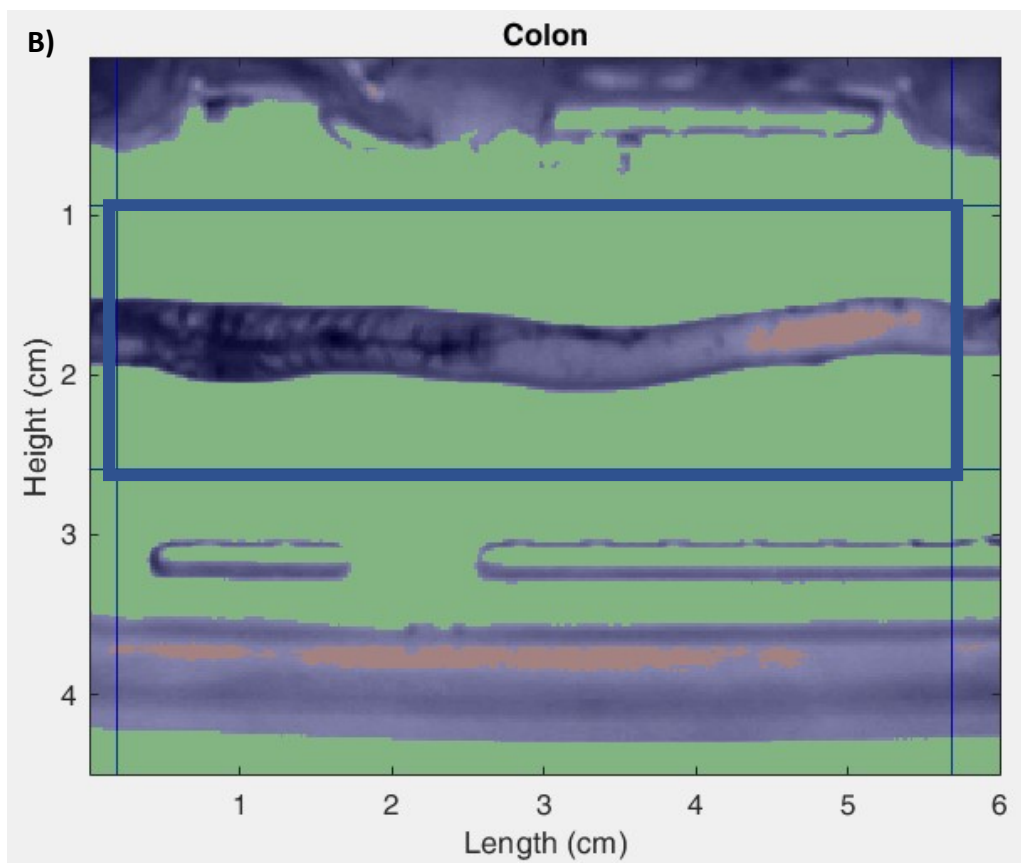


Figure 4) **Example and Description of ST Map Calculation.** A) The first column shows a frame (a) with an analysis region selection the width of the eventual ST Map. The frame is converted to black-and-white by detecting background and colon and compressed from top to bottom of the analysis region into a single line of the ST Map. The derivative of the diameter with respect to time creates the change in diameter ST Map. The partial derivative of the change ST Map in both the X (length) and Y (time) axis creates the Wave Velocity ST Map. B). The partial derivative of an ST Map in both directions creates an X and Y value of a vector indicating the direction of maximum change of diameter. A right angle to that is the lack of change of diameter. Lack of changes of diameter with a negative value slope are peristaltic waves, and lack of changes of diameter with a positive value are anti-peristaltic.

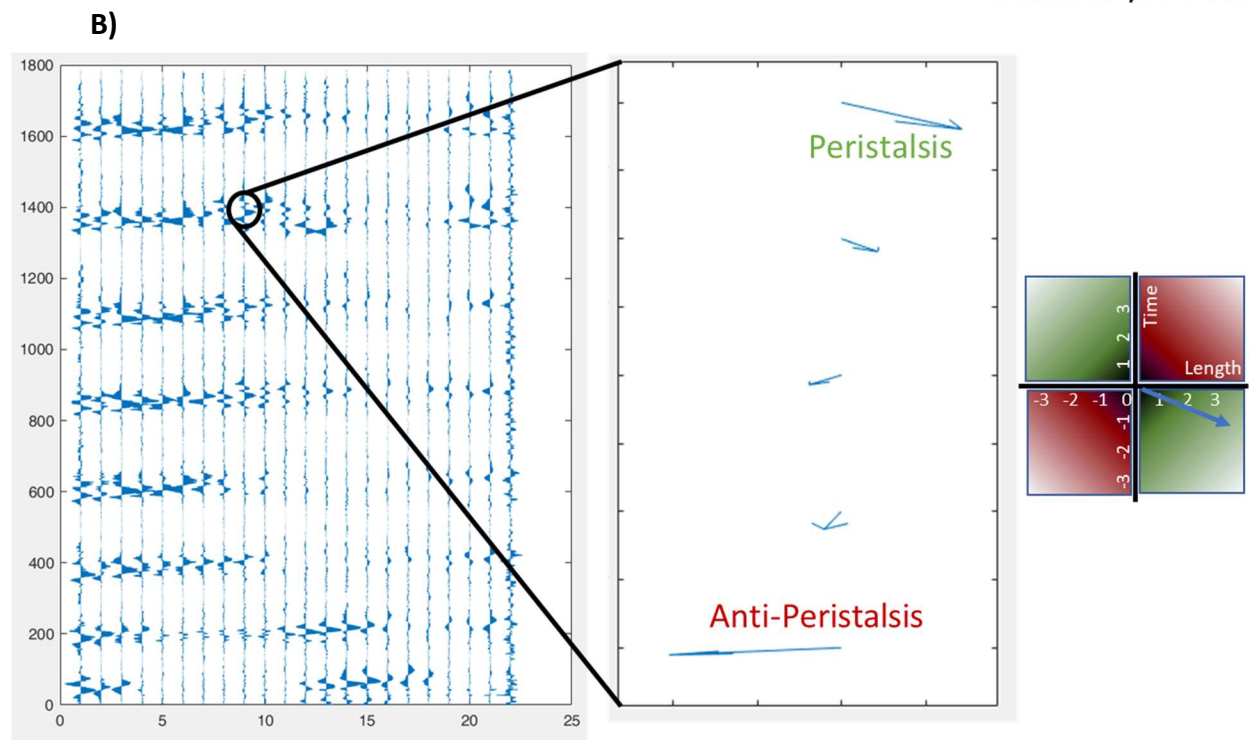
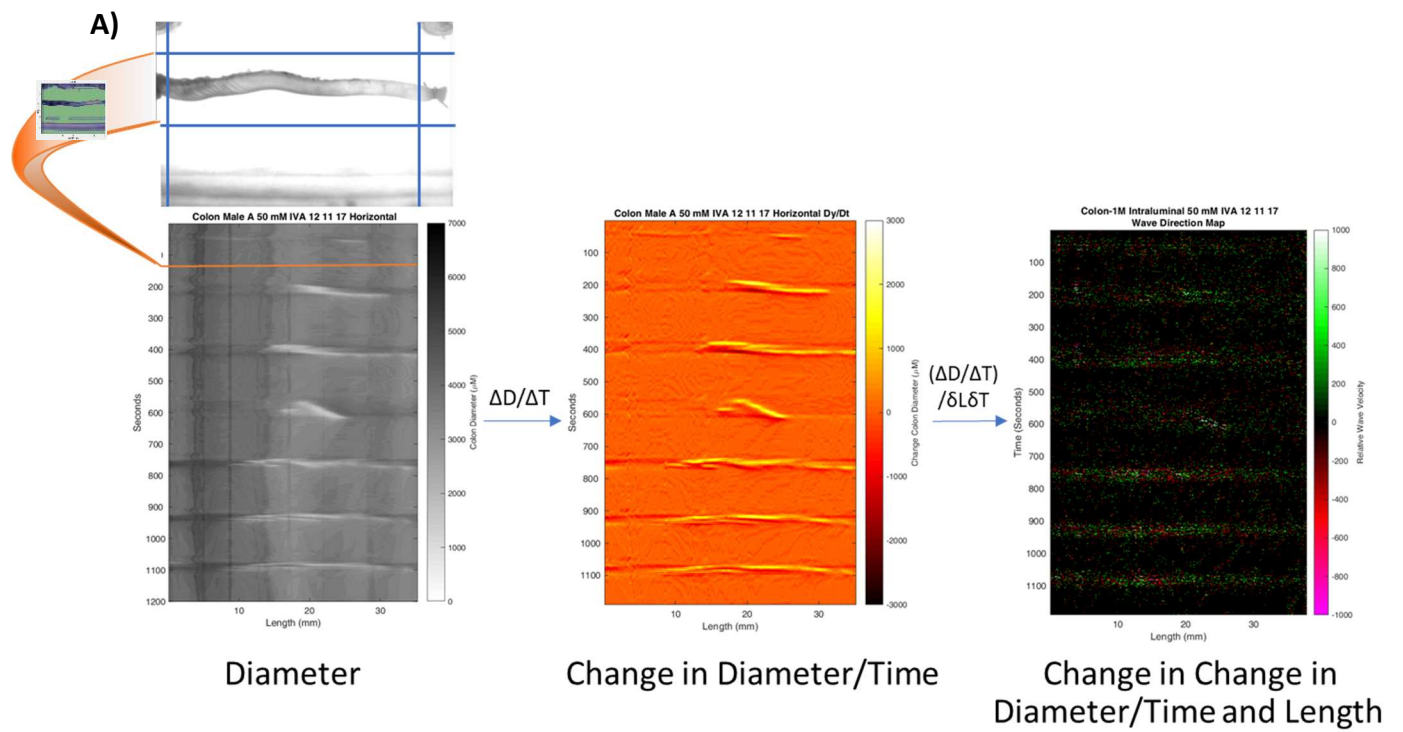
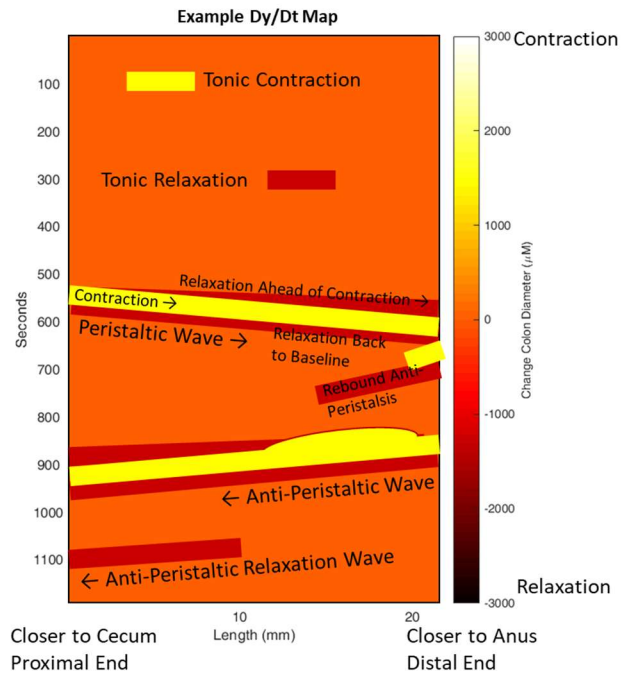
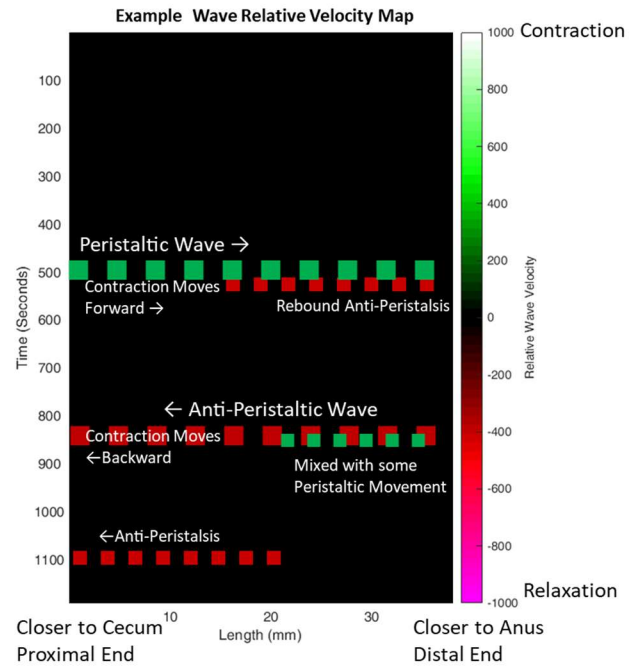


Figure 5) Explanation of ST Maps of change in diameter and wave velocity. A) In a change of diameter ST map, orange indicates no change in the diameter of the colon between then and 10 seconds later, yellow a contraction, and red a relaxation. The x axis is the length of the colon and the y axis is time. A change in contraction that moves along both the x and y axis is a peristaltic wave. A peristaltic wave frequently starts with a contraction, and frequently ahead of the contraction is a relaxation. A tonic contraction or relaxation is a change in diameter that does not move along the x axis. B) In a wave relative velocity ST map, Black indicates no change, and green (peristaltic) or red (anti-peristaltic) indicates the slope of the wave. Along the length of the wave at any there is usually a mixture of both detected, but a predominant pattern is usually apparent.

A)



B)



Single Cell Contraction and Relaxation

Smooth muscle cells were isolated from colon after dissection by gently scraping off the mucosa and placing strips of colon in SMM. After washing the strips with SMM, strips were incubated for 30 minutes at 31 °C in 10 mL 0.1% collagenase II and 0.1% soybean trypsin inhibitor in SMM. Cell solution was filtered through 500 µM Nitex mesh to harvest cells and centrifuged twice at 350 g for 10 minutes to remove debris.

A cell suspension containing 10^4 muscle cells/mL was dosed with 1 µM ACh to induce contractions for 1 minute and 5 minutes. Along with ACh, experimental groups were treated with the following: 1 µM ACh; 1 µM, 10 µM, and 100 µM IVA; 1 and 10 µM SQ22536 (Tocris Bio-Techne), 1 and 10 µM H-89 (Tocris Bio-Techne).

After the timepoint was finished, cells were fixed with 1% acrolein. Cell lengths were measured with a micrometer (Lasico Digital Filar Eyepiece 1602N-10, and M2 Processor; Los Angeles, CA) on a Nikon Optiphot microscope.

Immunofluorescence Staining and Imaging

To fix samples, colon and ileum were placed in 4% paraformaldehyde in PBS for 2 hours, then for antigen retrieval were submerged in a solution of 10 mM sodium citrate and 0.05% Tween 20 at pH 6.0 overnight at 4 °C before a 3 minute boil under gentle stirring before submersion in 30% sucrose in PBS overnight at 4 °C. Tissue was embedded in OCT compound (Tissue-Tek) and frozen at -80 °C before 10 µm sections created with a cryo-microtome. Sections were dried for 1.5 hours at room temperature before keeping at 4 °C. Sections were washed 4 times with PBS-Tween 0.5%, twice with PBS, then 30 minute incubation with 5% normal goat serum (Jackson ImmunoResearch, West Grove, PA) in PBS. Sections were then

incubated overnight with 1:200 Thermo PA5-35298 OR51E1 Antibody in 5% normal goat serum (or no-antibody control) at 4 °C. Slides were washed again 4 times with PBS-Tween 0.5%, twice with PBS, then incubated 1 hour at room temperature with Goat anti-Rabbit Alexafluor 594 1:100 in 2.5% normal goat serum in PBS, washed 4 times with PBS-Tween 0.5% and twice with PBS before covering with Fluoroshield DAPI (Abcam).

STC-1 cells cultured on glass slides in DMEM with 1.0 g/L and 4.5 g/L glucose were rinsed with PBS and fixed with 4% formaldehyde 15 minutes, and left overnight 4 °C in 10 mM sodium citrate and 0.05% Tween 20 at pH 6.0. Cells were then left in 5% normal goat serum at 4 °C overnight. Cells were incubated overnight with 1:200 Thermo PA5-35298 OR51E1 Antibody in 5% normal goat serum (or no-antibody control) at 4 °C. Cells were washed 3 times with PBS, then incubated 1 hour with Goat anti-Rabbit Alexafluor 594 1:300 in 5% normal goat serum in PBS. Cells were rinsed 3 times with PBS before addition of Fluoroshield DAPI before imaging.

Slides were imaged with a Zeiss Imager Z1 controlled with ZEN software and using an EXFO X-Cite Series 120 fluorescence illumination source. Whole organs and STC-1 cells were imaged with 400 ms exposure for rhodamine filter, 200 ms for DAPI filter. Channels were combined using ImageJ¹⁶⁴ (NIH) with FIJI¹⁶⁵, and contrast and brightness kept constant between images with command “setMinAndMax(70, 150)”.

Results

Tracings of Longitudinal Colon Force

Each preparation of colon had some variances in degree of response and frequency of some rhythmic activity, but generally followed the same response pattern to the treatments. Other than the maximal and minimal responses to ACh and fatty acids, descriptions of the qualities and characteristics of the tracings of force generated by longitudinal colon in response to drugs are informational observations not quantified. In general, before an agonist there was usually either a smooth rhythmic contraction and relaxation period of seconds, or a pattern of abrupt spikes of contraction (usually less than a gram) which relaxed either immediately or after several seconds (Figure 6). Once ACh was added, there was an initial spike in tension (usually over 1 gram force), sometimes followed by a quick relaxation to a baseline higher than pre-ACh which gradually relaxed more, but frequently the transition from rise in tension to the new baseline was closer to a 90° angle than a spike. The patterns of relaxation and contraction might sometimes change amplitude when ACh was added, but usually would not stop (Figure 7). Addition of the nitric oxide synthase inhibitor L-NNA, after a rise in tension of a few tenths of a gram, would either accentuate a pre-existing pattern, induce a smooth rhythmic pattern, or induce rhythmic spikes of tension in the longitudinal colon preparations when it was not there before (Figure 8). TTx would usually induce a short rise in tension (unlike the vehicle control) but would only mildly change the basal pattern in frequency or amplitude, if at all (Figure 9). Both the adenylate cyclase inhibitor SQ22536 and the vehicle DMSO would induce a slow relaxation in tension. SQ22536, for several minutes at 10 μ M and longer for 500 μ M, would inhibit amplitude of rhythmic contractions either somewhat or completely (Figure 10).

Isovaleric acid consistently produces a relaxation of contracted smooth muscle. Frequently, there would be a spike in tension of a few tenths of a gram immediately after the addition of IVA, or sometimes in the seconds following and during the relaxation phase. The relaxation phase would begin seconds after the addition of IVA, and peak relaxation would occur within a minute. Over a period of 20 minutes, tension would recover somewhat, usually to a new baseline lower than pre-IVA but not always (Figure 7). If the IVA was not pH buffered, there usually is no contraction (Figure 11), and the relaxation curve shifts to a lower concentration (compare Figure 12 to Figure 18).

Figure 6) **Representative tracing of two female mice colons without any treatments.** Colons exhibit varying amplitudes, frequency, and character of contraction patterns.

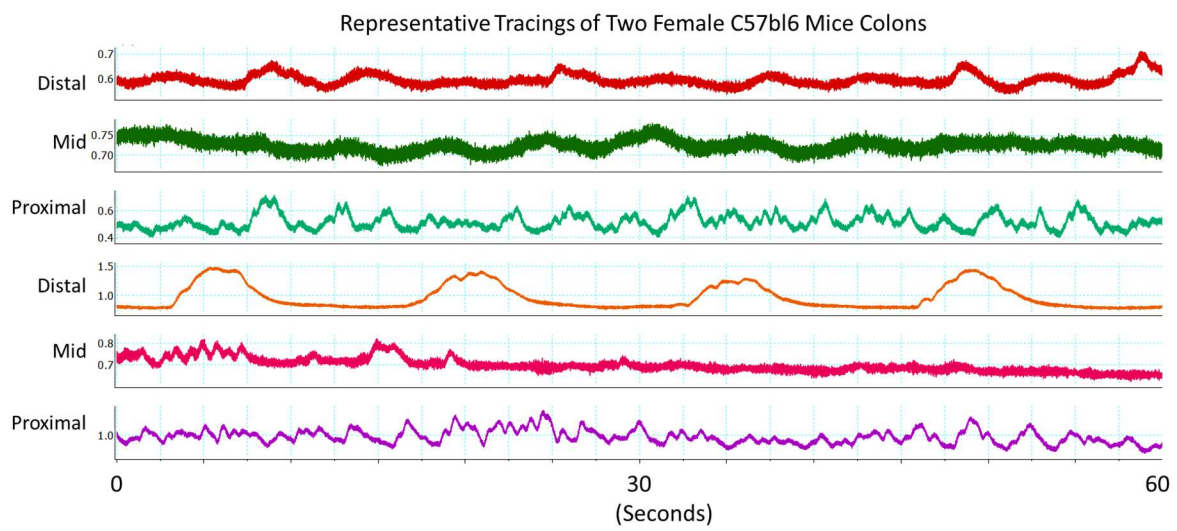


Figure 7) **Representative tracings of mouse colons treated with 10 μ M ACh followed by 50 mM IVA.** While the general response is the same, some differences between colon segment preparations include how pre-ACh treatment patterns change (or don't change) after treatment. All IVA treatments here demonstrated some increase in tension before or during the relaxation phase before reaching a low point in tension. Some preparations demonstrated a slow recovery of some tension.

Representative Tracings of Two Male C57bl6 Mice Colons Treated with ACh and IVA

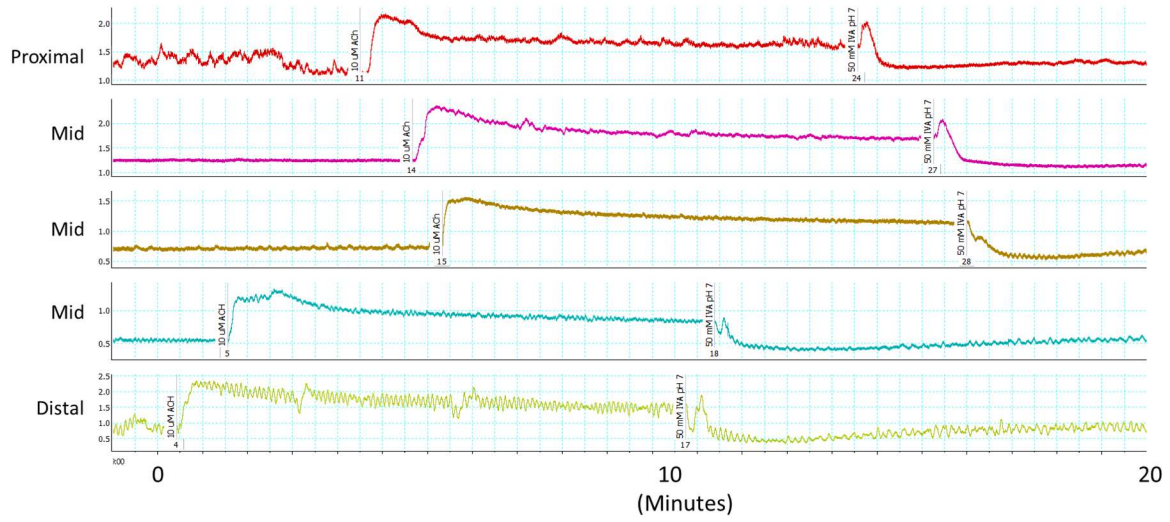


Figure 8) **Representative tracings of two male mice colon segments treated with L-NNA.**

Treatment with L-NNA usually induces a rise in tension of a few tenths of a gram. The L-NNA would either accentuate a pre-existing pattern, induce a smooth rhythmic pattern, or induce rhythmic spikes of tension in the longitudinal colon preparations where not present beforehand.

Representative Tracings of Two Male C57bl6 Mice Colons Treated with LNNA

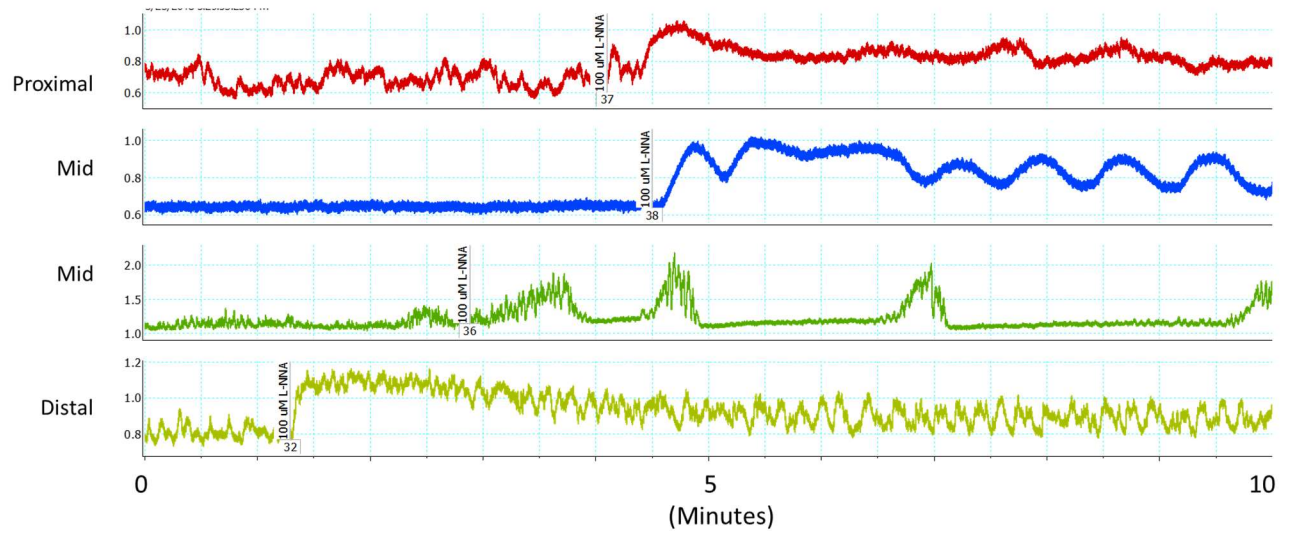


Figure 9) **Representative tracings of two male mice colon segments treated with TTx.** Most colon segments responded to TTx with a rise of tension of a few tenths of a gram. Change in amplitude or frequency of pre-existing patterns of contraction and relaxation were present but usually not a strongly distinguishing feature.

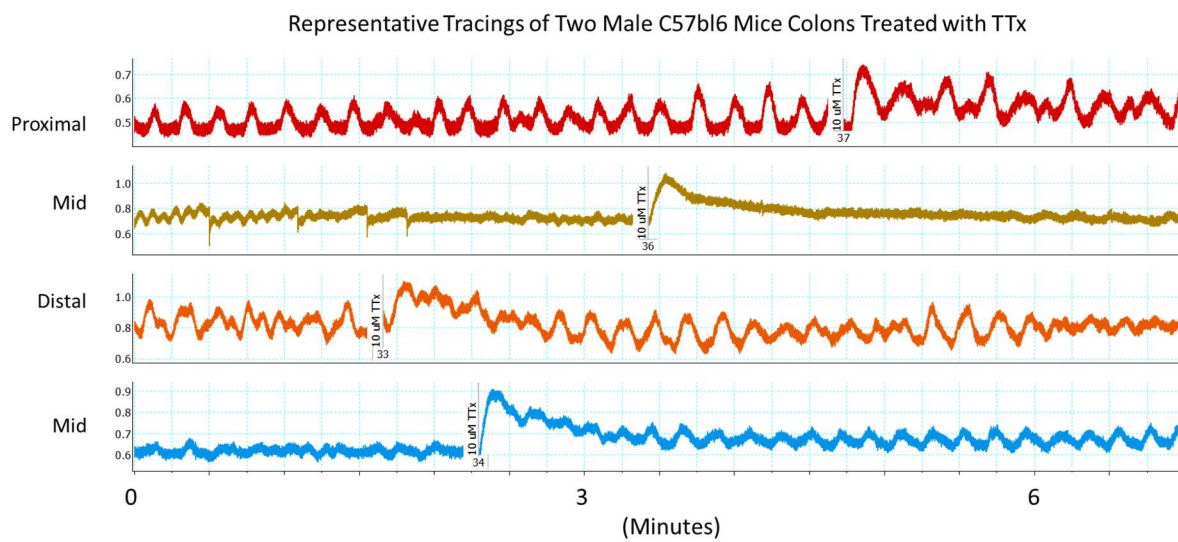


Figure 10) **Representative tracings of two female mice colon sections treated with adenylate cyclase inhibitor SQ22536.** In addition to a slight relaxation of tension, the amplitude of rhythmic contractions decreases before recovering over time.

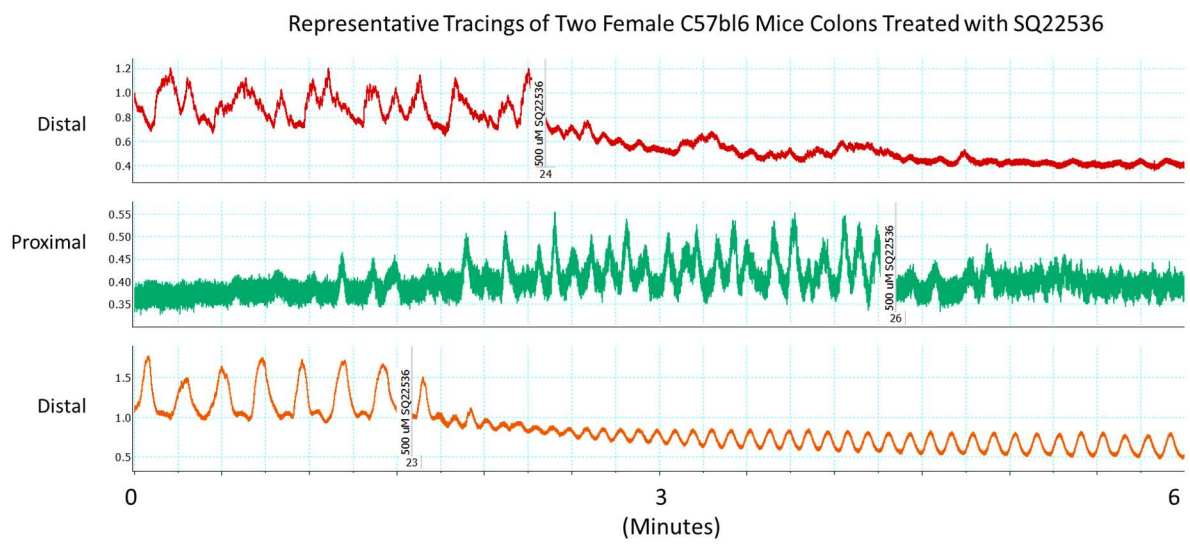
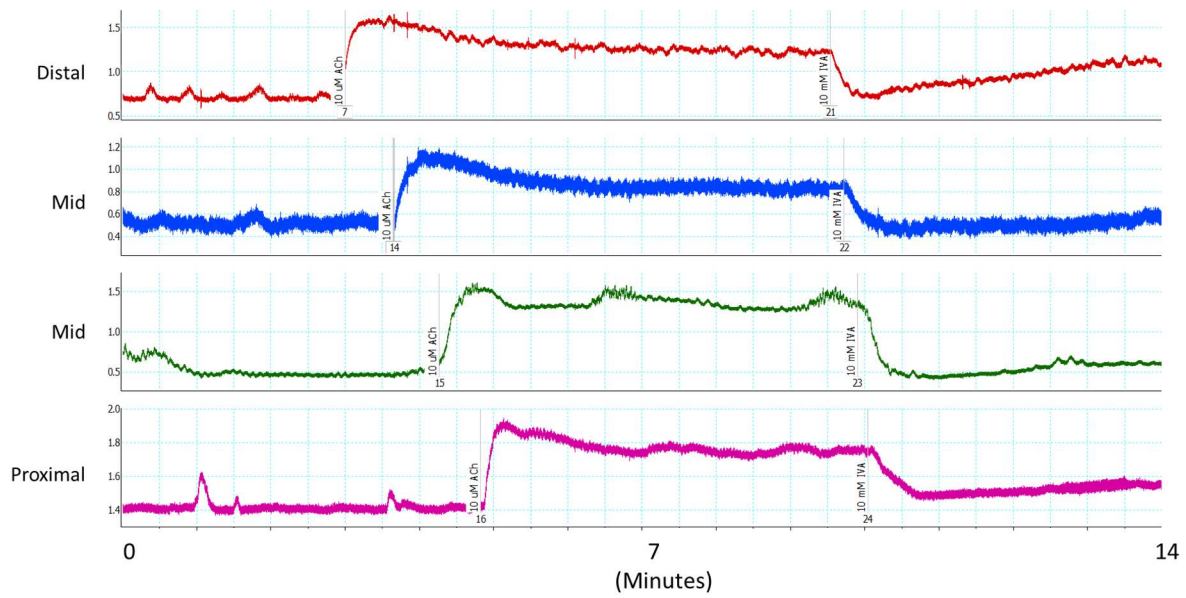


Figure 11) **Representative tracing of a female mouse colon treated with pH-unadjusted IVA, increasing IVA concentration to 10 mM and dropping bath pH from 7.6 to 6.7.** The biggest differences between the pH adjusted and unadjusted IVA is that the response curve is shifted leftward (lower concentration produces a stronger result) and there is rarely an increase in tension before or during the drop in tension.

Representative Tracings of A Female C57bl6 Mice Colons Treated with 10 mM IVA, drop from pH 7.6 to pH 6.7 in Bath



Isovaleric Acid Induces Smooth Muscle Relaxation

Dose-Dependent Relaxation of Longitudinal Smooth Muscle Tissue and Dispersed Cells

Mice colon segments with force measured longitudinally demonstrate a sigmoid dose-response or relaxation to IVA (minimum point of relaxation normalized to the maximum contraction by ACh). Standard deviation indicated by '±'. The linear response is for concentrations under 30 mM, with means of 22%±3% for 10 mM IVA and 49%±10% for 30 mM IVA (***) $p < 0.001$, maximum IVA relaxation compared to the max ACh contraction). From 30 mM to 50 mM, the amount of relaxation increases on average only slightly and the standard deviation is also increases (Figure 12).

The values for experiments using 20 mM IVA were not included with the calculation for the standard curve because this data was acquired at a different timepoint during the experiments. The predicted average relaxation for 20 mM IVA is 37% (Figure 12), and experiments using 20 mM IVA averaged 40%±10% relaxation $n=6$.

At 5 minutes out, the relaxation generally sustains itself. A 30 second average of force 5 minutes from application of IVA (normalized to a 30 second average of ACh-induced contraction) shows a linear response to IVA dosing (Figure 13).

Individual smooth muscle cells respond at μM concentrations in a logarithmic relationship with measurements at both 1 minute after treatment (Figure 14) and 5 minutes after treatment (Figure 15), with increasing concentrations of IVA increasingly reversing ACh-induced contraction (or put another way, increasingly relaxing the ACh-contracted cells). While the average percent length (of untreated smooth muscle cells) decreases slightly from 1 minute to

5 minutes (i.e. a slight increase in contraction from 1 to 5 minutes), there is no statistical difference between the lengths at 1 minute and 5 minutes.

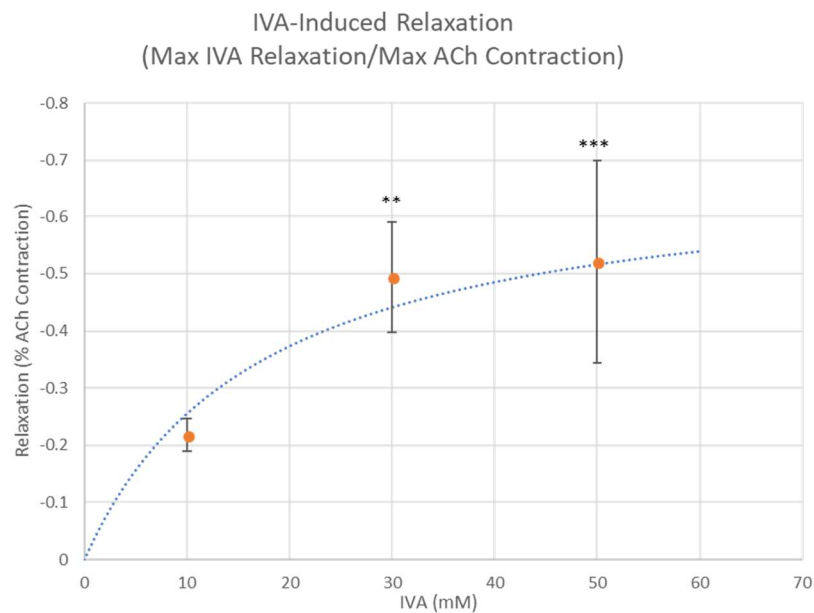
While different in concentration and the type of linear dose relationship, the general pattern remains for both cell response and tissue response to IVA: increasing concentration of IVA increasingly relaxes colon smooth muscle, and this relaxation is sustained.

Figure 12) **Dose-response curve of longitudinal smooth muscle maximum relaxation to IVA.**

Points indicate the mean of several sections of colon ($n = 5, 7, 32$ and for 10 mM, 30 mM and 50 mM respectively). The linear portion is below 30 mM, and above 30 mM the response becomes more erratic (as evidenced by the increase in standard deviation). One-Way ANOVA

$F(2,43)=7.7$; $p < 0.01$. Post-Hoc Fisher's least significant difference ** $p < 0.01$, *** $p < 0.001$.

Bars indicate standard deviation.



General model:

$$f(x) = \frac{(a \cdot x)}{(1 + \text{abs}(b \cdot x))}$$

Coefficients (with 95% confidence bounds):

a = -0.04049 (-0.07947, -0.001505)

b = 0.05843 (-0.01946, 0.1363)

Goodness of fit:

SSE: 1.008

R-square: 0.2524

Adjusted R-square: 0.2346

RMSE: 0.1549

Figure 13) **Dose-response curve of longitudinal smooth muscle 5 minutes out relaxation to IVA.** Average IVA relaxation 5 minutes from application of IVA normalized to ACh contraction (30 second average force for each). Dose response is linear, but with increasing standard deviation as dose increases. One-Way ANOVA $F(2,43)=9.81$; $p < 0.001$. Post-Hoc Fisher's least significant difference # $p < 0.05$ vs 30 mM IVA, *** $p < 0.001$ vs control. Bars indicate standard deviation.

IVA-Induced Relaxation (5 Minutes)

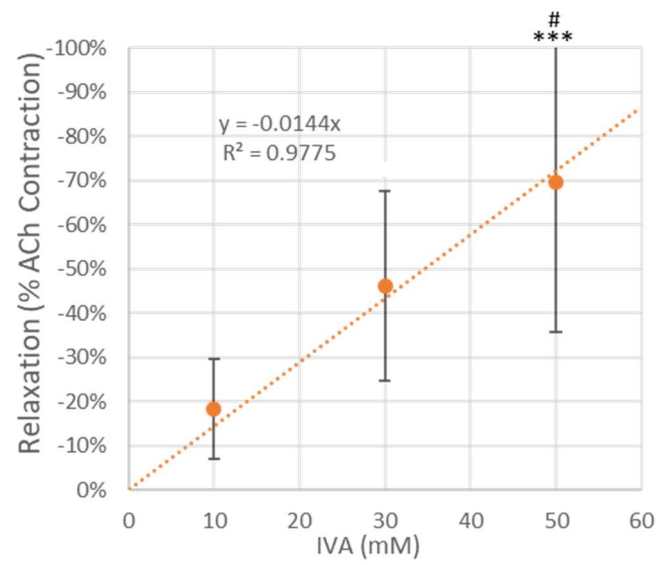
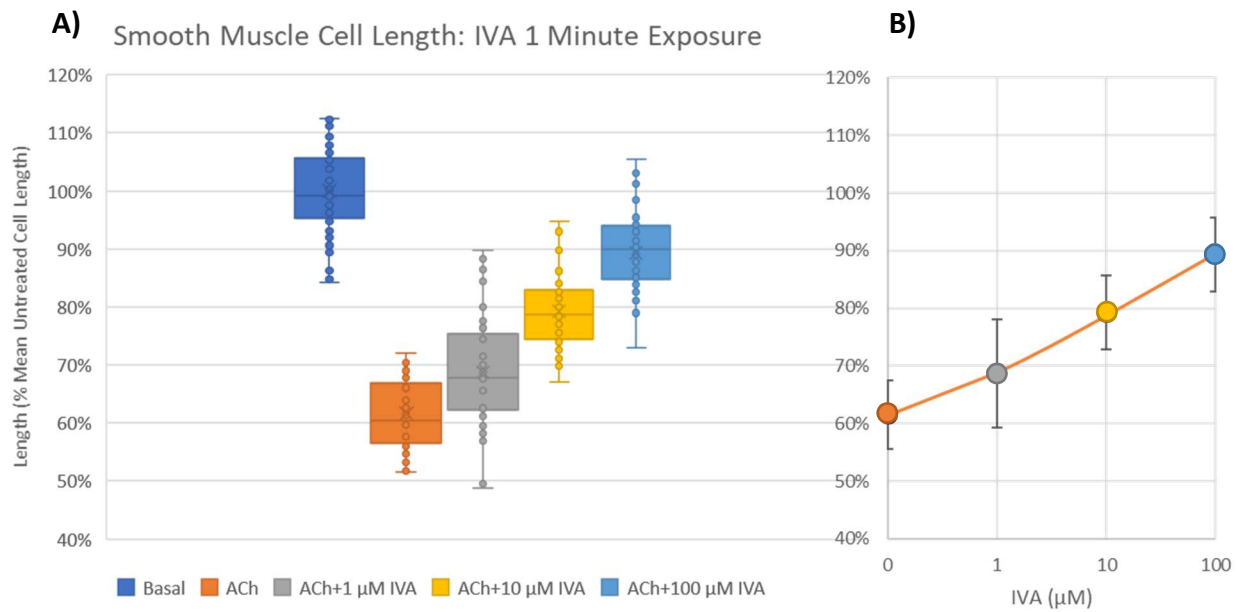


Figure 14) **Smooth Muscle Cell length after contraction and relaxation by IVA (1 minute).**

Values are a percentage of the basal (untreated) cell length. Dose response fits a logarithmic curve $f(x) = a(\log_{10}(bx+1))+c$ where $a = 0.108$, $b = 3.86$, $c = 0.615$. One-Way ANOVA of ACh treated groups $F(3,240)=188.62$, $p < 0.0001$. Post-Hoc analysis of all groups Tukey's HSD $p < 0.001$ between all groups.



General model:

$$f(x) = a \cdot \log_{10}(b \cdot x + 1) + c$$

Coefficients (with 95% confidence bounds):

$$a = 0.1079 \text{ (0.08935, 0.1265)}$$

$$b = 3.86 \text{ (0.1747, 7.544)}$$

$$c = 0.6152 \text{ (0.5952, 0.6353)}$$

Goodness of fit:

SSE: 0.9772

R-square: 0.6914

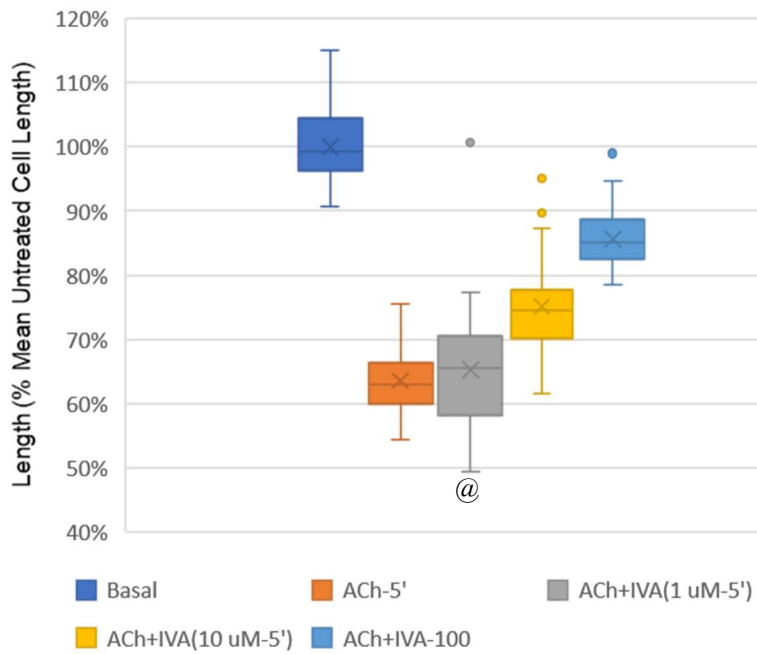
Adjusted R-square: 0.6881

Figure 15) **Smooth Muscle Cell length after contraction and relaxation by IVA (5 minute).**

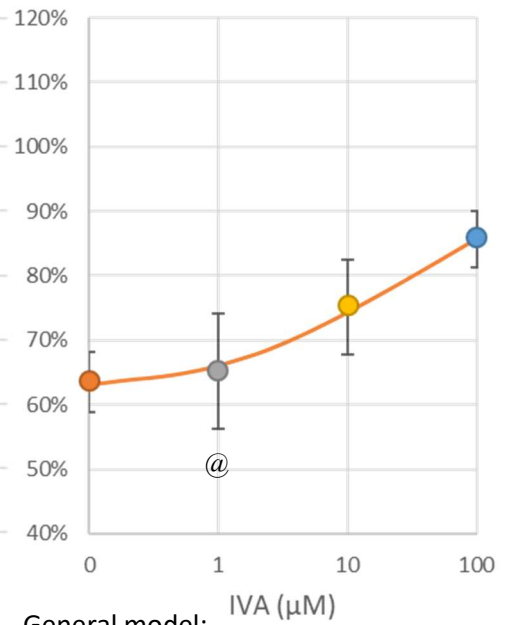
Values are a percentage of the basal (untreated) cell length. Dose response fits a logarithmic curve $f(x) = a(\log_{10}(bx+1))+c$ where $a = 0.121$, $b = 0.763$, $c = 0.631$. One-Way ANOVA of ACh treated groups $F(3,299)=9.81$, $p < 0.0001$. @ Post-Hoc Tukey's HSD analysis vs ACh $p < 0.05$; comparison of all other groups $p < 0.0001$.

A)

Smooth Muscle Cell Length: IVA 5 Minute Exposure



B)



General model:

$$f(x) = a \cdot \log_{10}(b \cdot x + 1) + c$$

Coefficients (with 95% confidence bounds):

$$a = 0.1205 \text{ (0.09049, 0.1505)}$$

$$b = 0.7634 \text{ (-0.09023, 1.617)}$$

$$c = 0.6306 \text{ (0.6112, 0.6501)}$$

Goodness of fit:

$$\text{SSE: } 0.7978$$

$$\text{R-square: } 0.6474$$

$$\text{Adjusted R-square: } 0.6434$$

$$\text{RMSE: } 0.06714$$

Gender and Region in Longitudinal Muscle Relaxation

Each colon segment was marked as the proximal end, the distal end, a middle portion or a piece between the middle and proximal or distal side. At 50 mM IVA, segments not on ends relaxed on average $51\% \pm 18\%$ of the max ACh contraction. In male mice, the most proximal segment of colon (mean $30\% \pm 8\%$ relaxation) was statistically less sensitive to IVA at 50 mM compared to other segments ($53\% \pm 18\%$ to $49\% \pm 17\%$ in middle segments, $68\% \pm 8\%$ in the distal segment, Figure 16) by Student's t-test.

In IVA strips where pH was controlled for, there was no evidence that female mice shared this difference between proximal colon segments and other segments. In aggregate of all segments tested at 50 mM IVA, there was no statistical difference between male and female colon relaxation at 50 mM, although the female colons did respond to 50 mM IVA more on average ($49\% \pm 17\%$ vs $60\% \pm 19\%$).

Figure 16) **Male mouse 50 mM IVA Induced Relaxation of Longitudinal Smooth Muscle by Colon Region.** In male mice, the proximal colon was on average relaxed 30% from max ACh contraction, statistically significantly less than most other regions which relaxed average $53\% \pm 18\%$ to $49\% \pm 17\%$ in mid-regions and $68\% \pm 8\%$ on average in the most distal segment. One-Way ANOVA $F(4,22)=3.28$, $p < 0.05$. Post-Hoc Fisher's least significant difference analysis vs Proximal segment $*p < 0.05$, $**p < 0.01$.

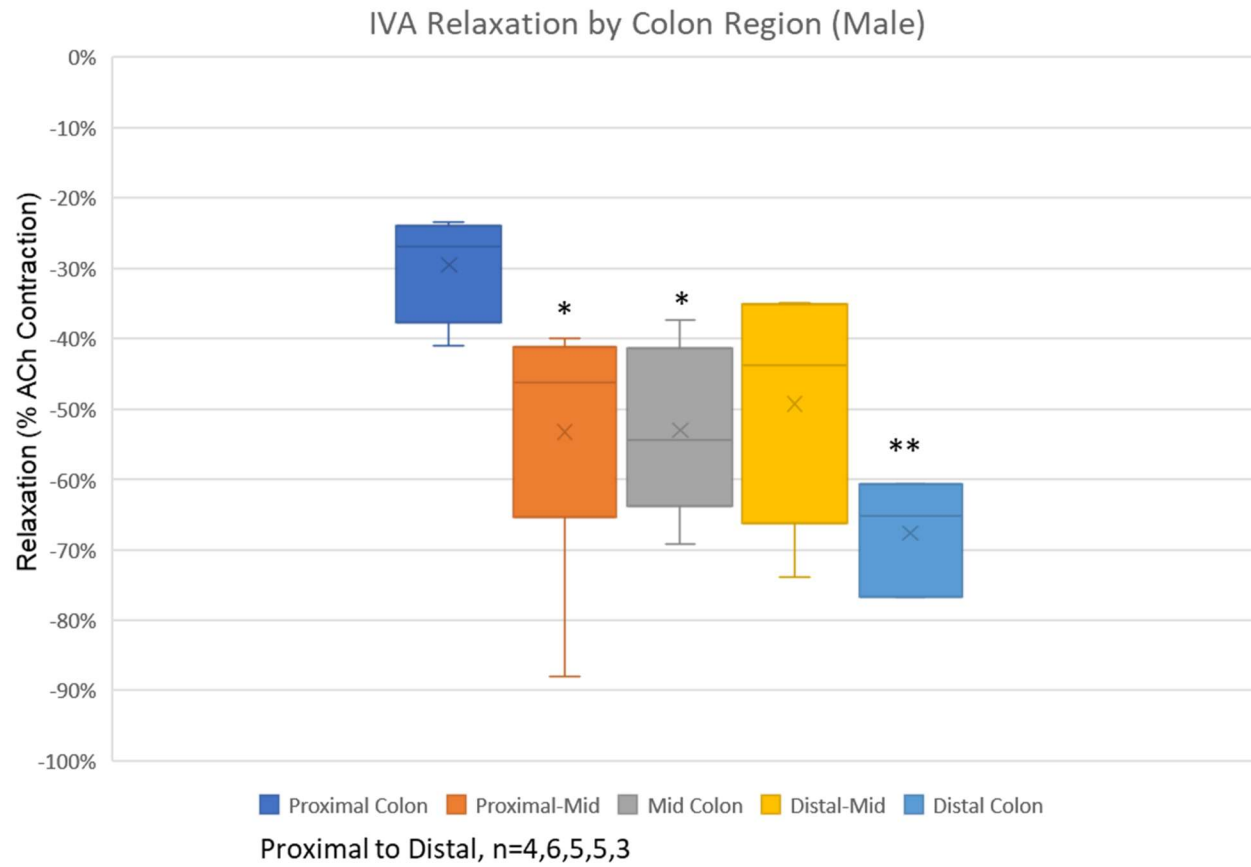
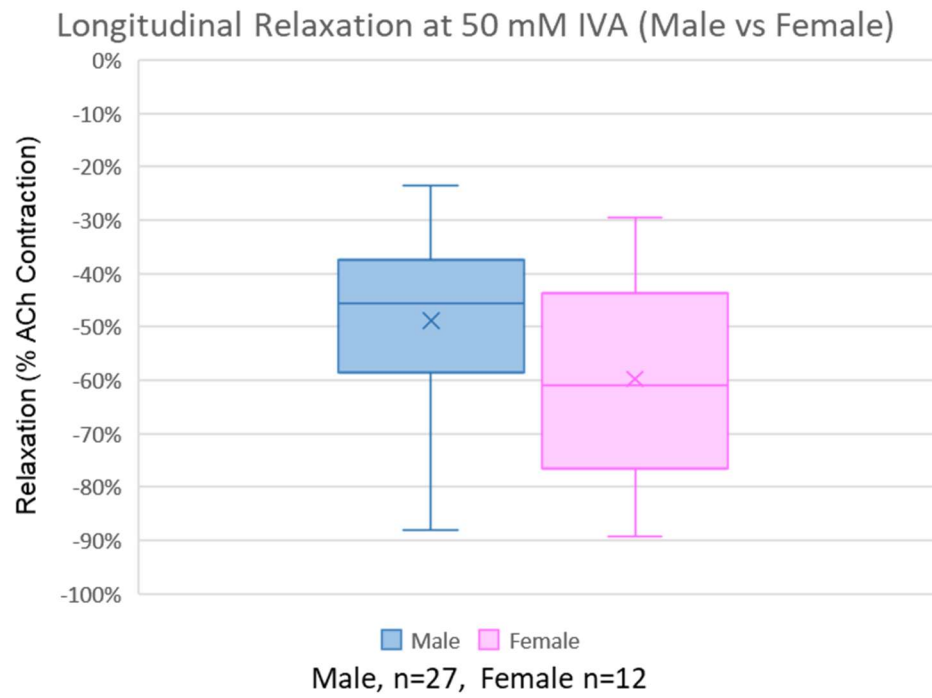


Figure 17) **50 mM IVA induced relaxation of longitudinal colon smooth muscle by gender.**

Average relaxation was $49\% \pm 17\%$ for female mice (n=12) vs $60\% \pm 19\%$ for male mice (n=27).

Comparison of group samples did not meet the threshold $p < 0.05$ by Student's T-test.

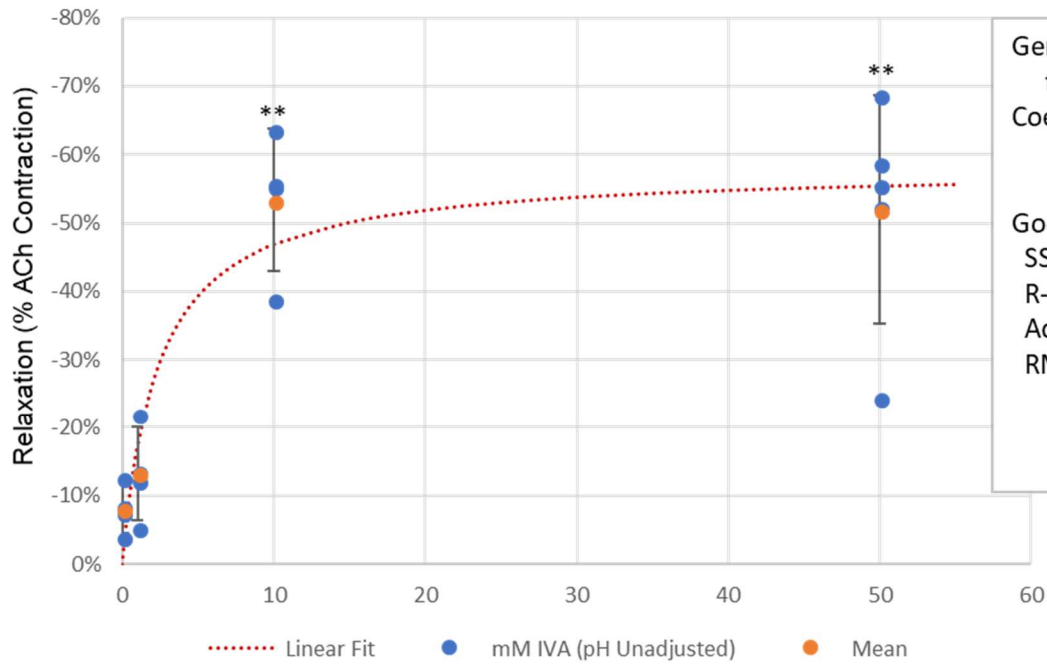


IVA's Effect on Longitudinal Colon When Creating a Low pH Environment

When not adjusted to a neutral pH, 10 mM in Krebs buffer IVA temporarily decreases the pH of CO₂-bubbled Krebs buffer to 6.7 in bath with the colon segment. When not controlling for pH, the relaxation curve of longitudinal colon for IVA shifts to increase the muscle's sensitivity to the more-acidic IVA solution (Figure 18). The regional differences in colon segment response to IVA is not nearly as pronounced; averaging $52\% \pm 7\%$, $54\% \pm 16\%$, and $58\% \pm 2\%$ relaxation from ACh contraction maximum for proximal, middle, and distal segments, respectively (Figure 19). The differences in gender for the aggregate of segments is more pronounced with male mice averaging $51\% \pm 10\%$ relaxation and female mice averaging $66\% \pm 17\%$ relaxation (Figure 20).

Figure 18) **IVA induces relaxation in Longitudinal Colon segments, curve shifts to lower concentrations in lower pH conditions compared to pH 7.4.** n=4 for 0,1, 10 mM. n=5 for 50 mM. (**) $p < 0.01$ compared to 10 mM IVA. One-Way ANOVA $F(3,16)=20.19$, $p \ll 0.0001$. Post-Hoc Fisher's least significant difference analysis vs 1 mM IVA $**p<0.001$. Bars indicate standard deviation.

IVA-Induced Reaxation in Longitudinal Colon (pH Not Controlled)



General model:

$$f(x) = \frac{(a \cdot x)}{(1 + \text{abs}(b \cdot x))}$$

Coefficients (with 95% confidence bound)

a = -0.244 (-0.4834, -0.004683)

b = 0.4207 (-0.04558, 0.8869)

Goodness of fit:

SSE: 0.2158

R-square: 0.7626

Adjusted R-square: 0.7468

RMSE: 0.1199

Figure 19) **10 mM IVA with pH reduction to 6.7 induced relaxation in longitudinal colon by region.** Samples of colon regions did not reach threshold of significance. Average relaxation from ACh contraction maximum: proximal $52\% \pm 7\%$ $n=3$, middle segments $54\% \pm 16\%$ $n=12\#$, and distal $58\% \pm 2\%$ $n=3$. # One outlier segment (relaxation greater than mean – $1.5 \times$ Inter-quartile Range) was removed.

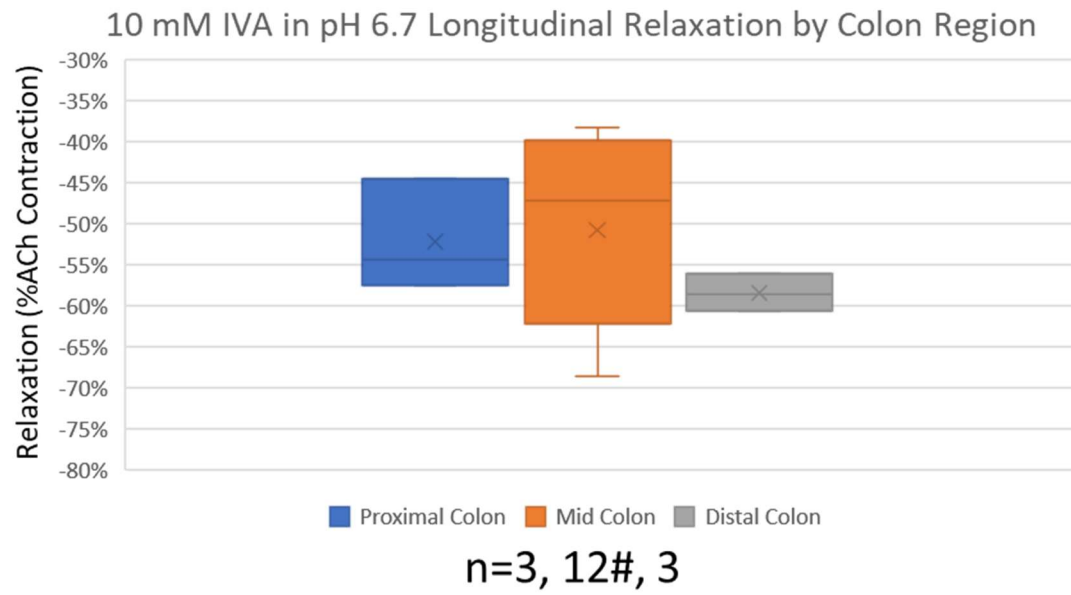
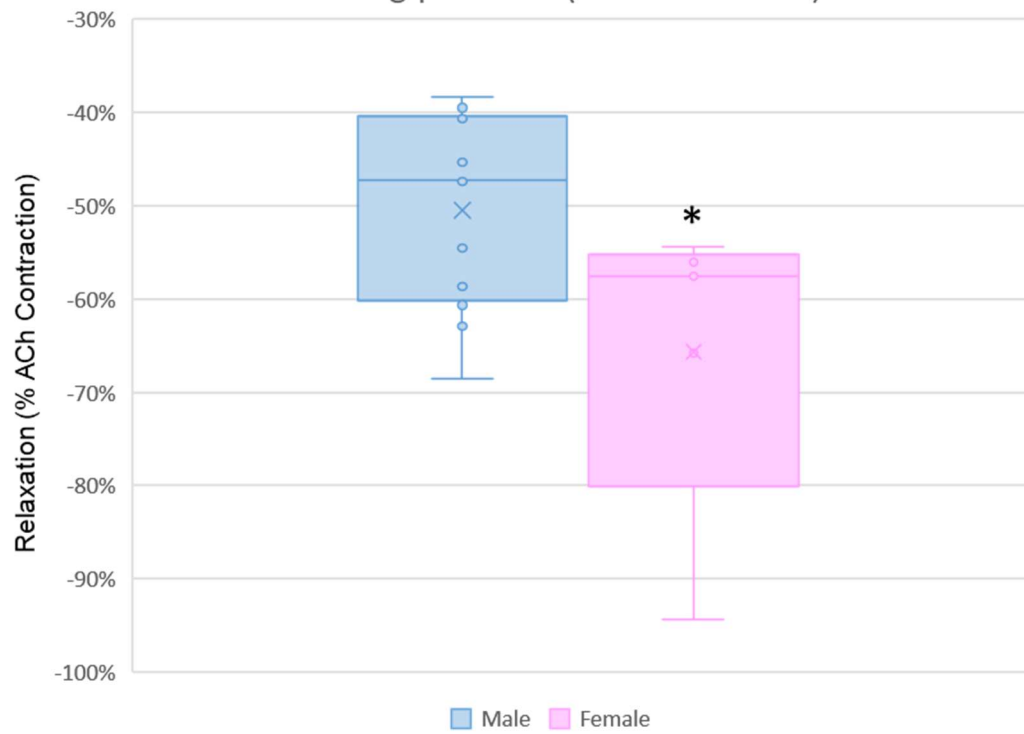


Figure 20) **10 mM IVA reducing pH to 6.7 induced relaxation of Longitudinal colon, male vs. female.** Differences in relaxation of colon segments is more pronounced with male mice when pH is reduced by IVA. Males $51\% \pm 10\%$ $n=14$ vs. female $66\% \pm 17\%$ $n=5$. (*) $p < 0.05$ by Student's T test.

Longitudinal Colon Relaxation of 10 mM IVA
Reducing pH to 6.7 (Male vs Female)



Effects of Neural Inhibition (via Tetrodotoxin)

To determine the effect of neuronal activity on mediating the effects of IVA, colon segments were pre-treated with the fast-gated Na^{2+} channel blocker 10 μM TTx. for at least 30 minutes prior to the addition of 50 mM IVA. All TTx-treated tissues responded to the addition of TTx (Figure 9). The TTx treated groups did not threshold for statistical difference by Student's T test from the citric acid control (average IVA relaxation $57\% \pm 17\%$ for TTx $n=5$ vs $55\% \pm 29\%$ $n=6$ for citric acid buffer). The same strips before TTx relaxed $41\% \pm 13\%$ vs $57\% \pm 17\%$ after TTx (Figure 21); however, this is due mostly to changes in ACh contraction (0.905 ± 0.315 g before TTx vs 0.583 ± 0.192 g after TTx, $p < 0.05$) as opposed to changes in relaxation (0.369 ± 0.147 g vs 0.343 ± 0.152 g).

Effects of Nitric Oxide Inhibition (via L-NNA)

To determine whether Nitric Oxide mediates the relaxant effects of IVA, colon segments were pre-treated with the L-Arginine analogue and NOS inhibitor 100 μM L-NNA. for at least 25 minutes prior to the addition of IVA. All L-NNA-treated tissues responded to the addition of L-NNA (Figure 8). The L-NNA treated groups did not meet statistical threshold for difference from the untreated control (50 mM IVA relaxation post-L-NNA $70\% \pm 21\%$ $n=6$ vs. $43\% \pm 22\%$ $n=3$ for no treatment, $53\% \pm 13\%$ before L-NNA treatment) and in fact the average relaxation as a percentage of ACh increased (Figure 22). Average quantity of relaxation was similar for before, after, and untreated groups (0.478 ± 0.321 g, 0.409 ± 0.163 g, 0.365 ± 0.169 g. respectively), but maximum ACh contraction was significantly less after L-NNA (0.835 ± 0.351 g before, 0.614 ± 0.208 g after, Student's T-test $p < 0.05$).

Figure 21) **Relaxation induced by 50 mM IVA is not mediated by TTx.** Colon segments treated with axonal action potential inhibitor 10 μ M TTx relaxed similarly to 50 mM IVA ($57\% \pm 17\%$, $n=5$) compared to segments treated with just the citric acid buffer vehicle ($55\% \pm 29\%$, $n=6$). Pairwise, before and after treatments were not statistically different ($41\% \pm 13\%$ vs $57\% \pm 17\%$, $n=5$). Bars indicate standard deviation.

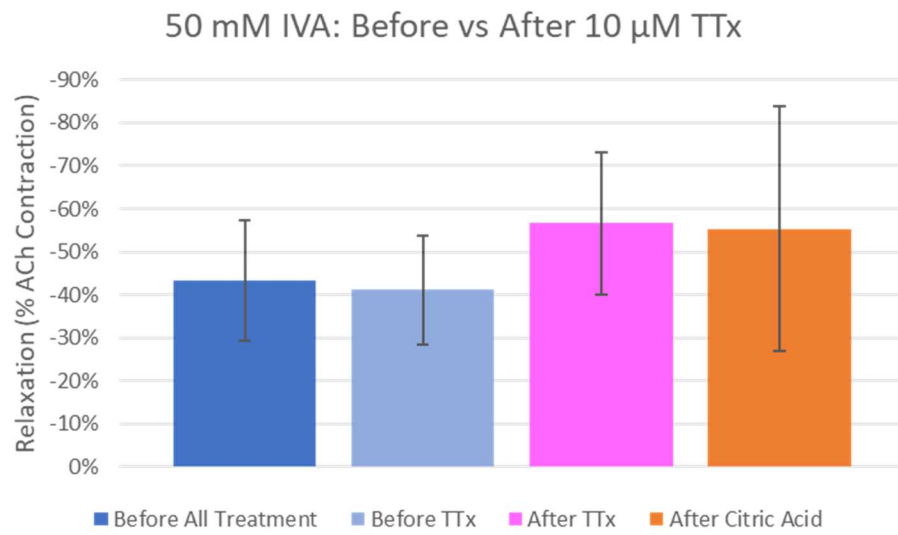
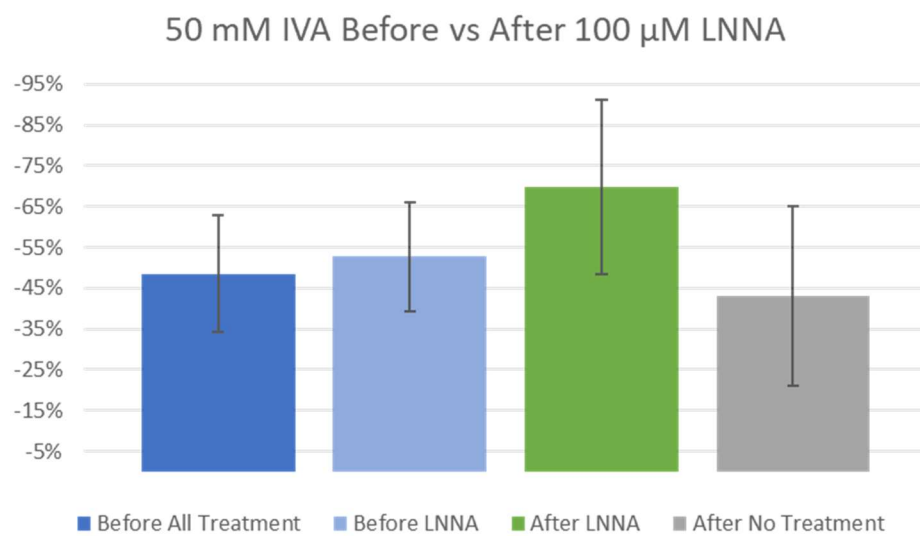


Figure 22) **Relaxation induced by 50 mM IVA is not inhibited by L-NNA.** Colon segments treated with NO synthase inhibitor 100 μ M L-NNA relaxed $70\% \pm 21\%$ as opposed to $53\% \pm 13\%$ before treatment, n=6 colon segments. No treatment relaxed $43\% \pm 22\%$ n=3 colon segments. Bars indicate standard deviation.



Effects of 2-Ethylhexanoic Acid on IVA Relaxation

2-EHA is a purported inhibitor of OR51E1, a known receptor for IVA. 2-EHA is also a BCFA. In colon segments, on average 25 mM IVA plus 25 mM 2-EHA was nearly identical to 50 mM IVA (51% vs 49%, n=8) as a percentage of ACh contraction; and the addition of 10 μ M TTx (52% \pm 16%) did not affect the relaxation as a percent of ACh contraction (Figure 23A). As a percentage of each colon segment's 50 mM IVA response, the means did not significantly differ from no change (Figure 23B).

Comparison of BCFA Isovaleric Acid and Straight Chain Valeric Acid

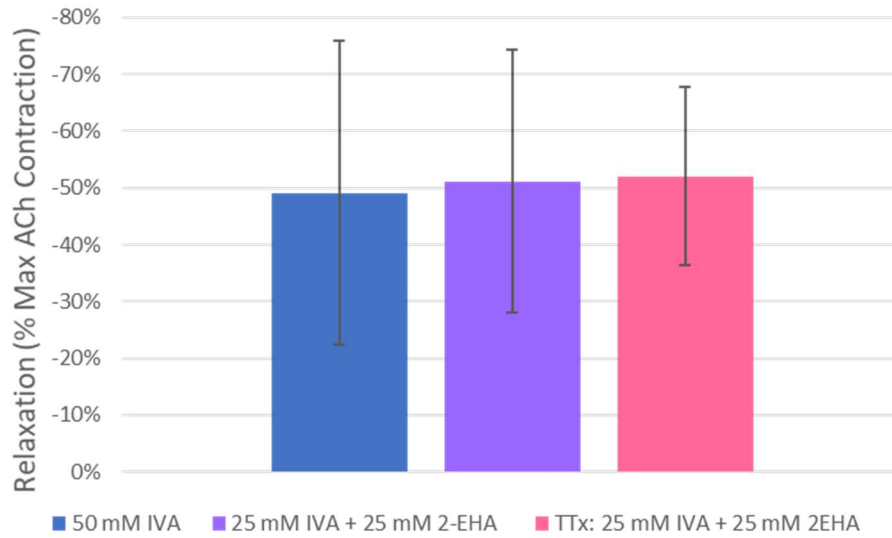
The C5:0 SCFA Valeric Acid was compared to IVA in the same colon strips after washing out the IVA. Colon segments treated with 20 mM Valeric Acid on average relaxed 15% more than 20 mM IVA (45% \pm 3% vs 60% \pm 7%, n=5 paired Student's t-test $p < 0.01$) (Figure 24).

Figure 23) **BCFA's 2-EHA and IVA affect Colon Segments Similarly, not Affected by TTx.**

A) 50 mM IVA relaxation was $49\% \pm 27\%$ vs. 25 mM IVA+25mM 2-EHA $51\% \pm 23\%$ n=8.

Relaxation for TTx-pretreated 25 mM IVA + 25 mM 2-EHA was $52\% \pm 16\%$ n=5. B) As a percentage of each segment's respective 50 mM IVA relaxation response, the without TTx-response was $103\% \pm 13\%$ n=6 and with 10 μ M TTx was $91\% \pm 8\%$ n=5. Bars indicate standard deviation.

A) 50 mM IVA vs 25 mM IVA + 25 mM 2-EHA



B) 25 mM IVA+25 mM 2-EHA
with or without 10 μ M TTx

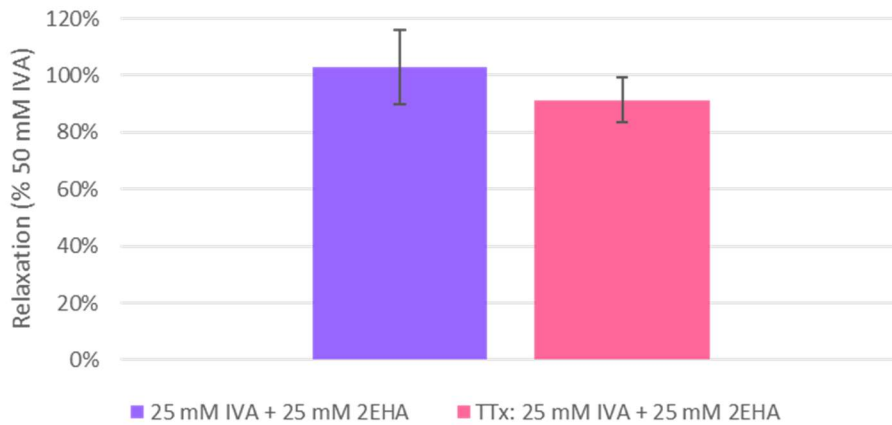
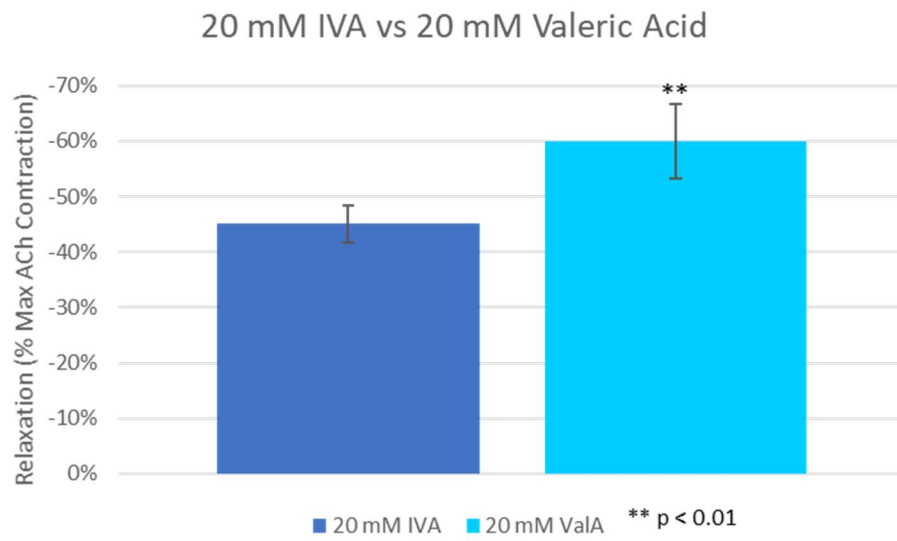


Figure 24) **20 mM Valeric acid induces more relaxation than 20 mM IVA.** As a percentage of maximum % ACh contraction, 20 mM IVA $45\% \pm 3\%$ relaxation vs $60\% \pm 7\%$ for 20 mM Valeric Acid. $n=5$ (**) $p < 0.01$ by Student' T-test. Bars indicate standard deviation.



Effects of Adenylate Cyclase & Protein Kinase A inhibition (via SQ22536 and H-89)

Relaxation through cAMP-mediated pathways can be inhibited through various means. Inhibition of adenylate cyclase with SQ22536 prevents the production of cAMP, inhibiting all cAMP-pathways. With the addition of 500 μ M SQ22536 to colon segments, average relaxation as a percentage of max ACh contraction decreased before and after by 11% ($48\% \pm 9\%$ to $37\% \pm 6\%$ $n=4$), but did not reach statistical significance. Comparing SQ22536 treated strips to DMSO vehicle-only controls, there was a 17% difference in average relaxation ($53\% \pm 6\%$ to $37\% \pm 6\%$, $n = 3$ and 4 respectively, unpaired Student's T-test $p < 0.05$) (

Figure 25). Average ACh contraction also decreased 22% after SQ22536 treatment (compared to a 3% increase after DMSO), while average grams of tension relaxation dropped 35% after SQ22536 (compared to an 8% increase for DMSO).

Relaxation induced by IVA in ACh contracted dispersed smooth muscle cells was considerably inhibited by SQ22536 and by the PKA inhibitor H-89 at both 1 minute and 5 minutes of incubation. At 1 minute, while 100 μ M IVA-treated ACh-contracted cells were on average only $89\% \pm 6\%$ of control length compared to $62\% \pm 6\%$ for ACh-only treated cells, ACh+100 μ M IVA-treated cells pre-treated with 10 μ M H-89 were $67\% \pm 7\%$ and pre-treatment with 10 μ M SQ22536 were $63\% \pm 6\%$ of the basal cell length (Figure 26). There is a dose response to SQ22536; for 100 μ M IVA treated cells, the length was $77\% \pm 7\%$ of control for 1 μ M SQ22536.

At the 5 minute timepoint, the same groups as 1 minute timepoint trend similarly, with the largest difference in means between the same group at 1 minute and 5 minute being 5% (Figure 27).

Figure 25) **500 μ M SQ22536 decreases average 30 mM IVA-induced relaxation of longitudinal colon segments.** The average 30 mM IVA relaxation before SQ22536 was $49\% \pm 10\%$ $n=7$ for all segments ($48\% \pm 9\%$ for pre-SQ22536 segments). Post-SQ22536 treated segments relaxed by 30 mM IVA $37\% \pm 6\%$ $n=4$, and DMSO-vehicle-only treated segments relaxed $53\% \pm 6\%$ $n=3$. One-Way ANOVA $F(2,1)=4.09$, $p < 0.05$. Post-hoc Fisher's least significant difference * $p < 0.05$ vs. before treatment, + $p < 0.05$ vs. SQ22536. Bars indicate standard deviation.

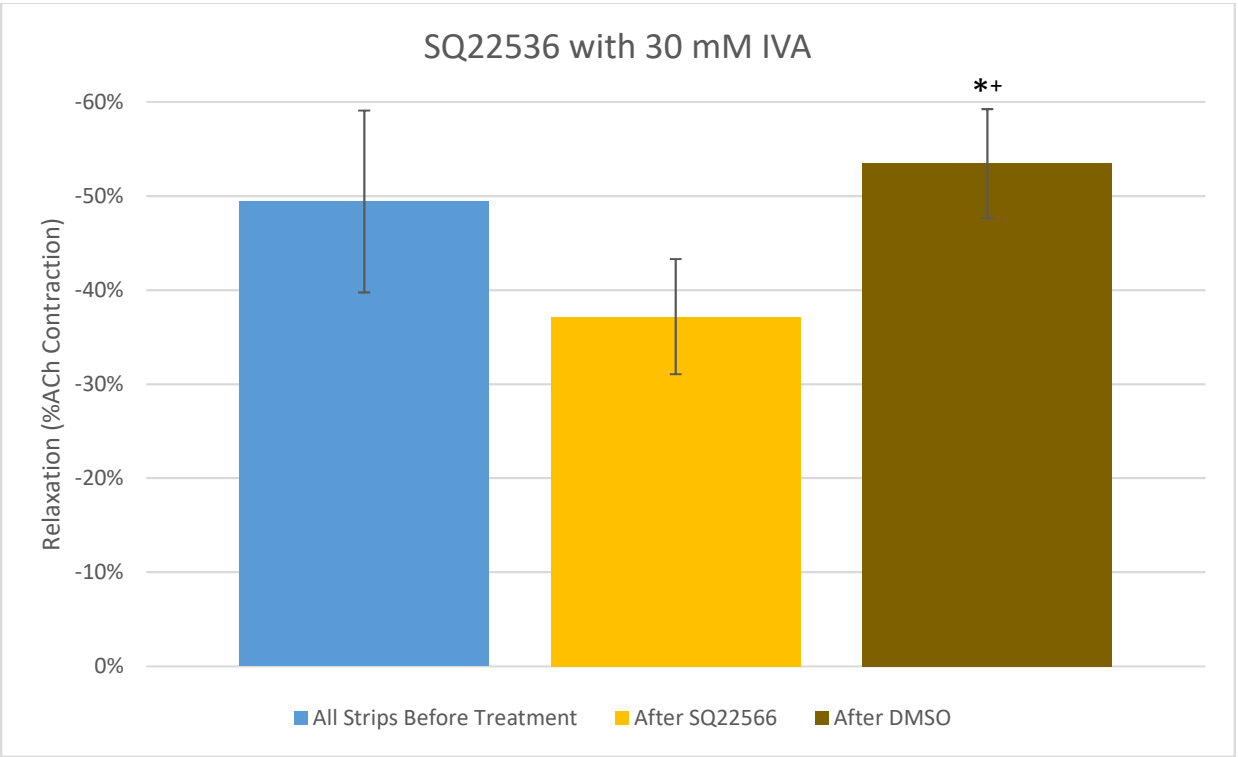


Figure 26) Adenylate Cyclase Inhibitor SQ22536 and PKA Inhibitor H-89 Inhibit

Relaxation Induced by IVA at 1 Minute. Cells respond in a dose-dependent fashion to 10 μ M and 100 μ M IVA (increasing relaxation), and responds to 10 μ M H-89 and to 1 μ M and 10 μ M SQ22536 (inhibiting relaxation). Multi-way ANOVA of SQ22536 treated and untreated groups $F(2,380)=152.98$, $p < 0.0001$, and of H-89 treated and untreated groups $F(2,578)=103.14$. Post-Hoc Tukey's HSD $p < 0.0001$ for all IVA treated groups compared to equivalent SQ22536 or H-89 treated groups. Groups marked @ $p > 0.05$ not statistically different from 1 μ M ACh-only group.

SQ22536 and H-89 Inhibit 100 μ M IVA-Induced Relaxation of Smooth Muscle Cells (1 minute)

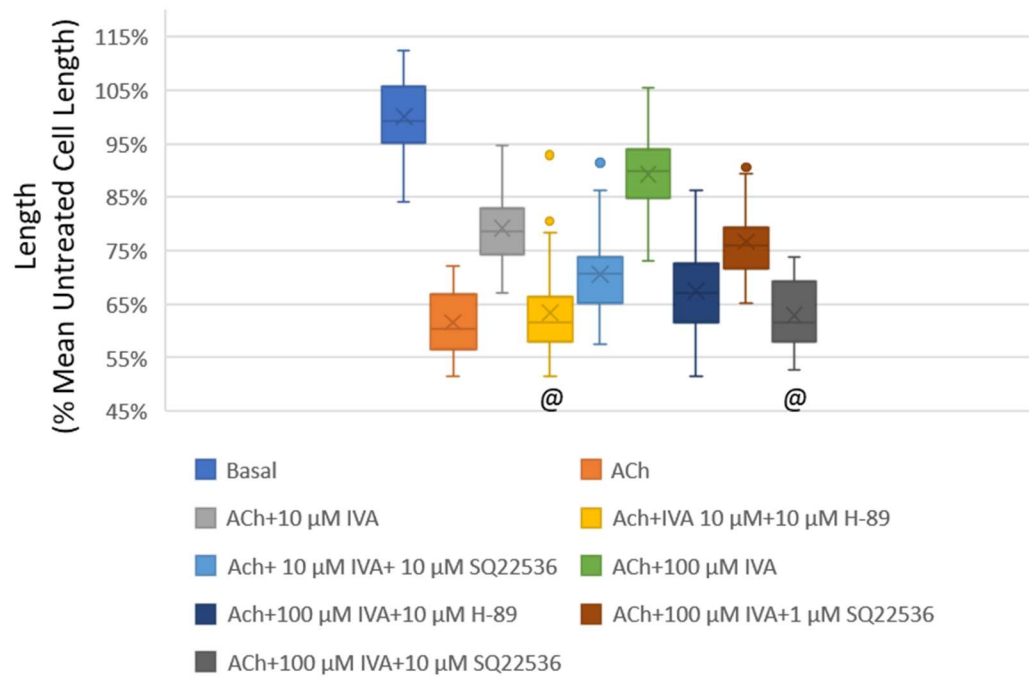
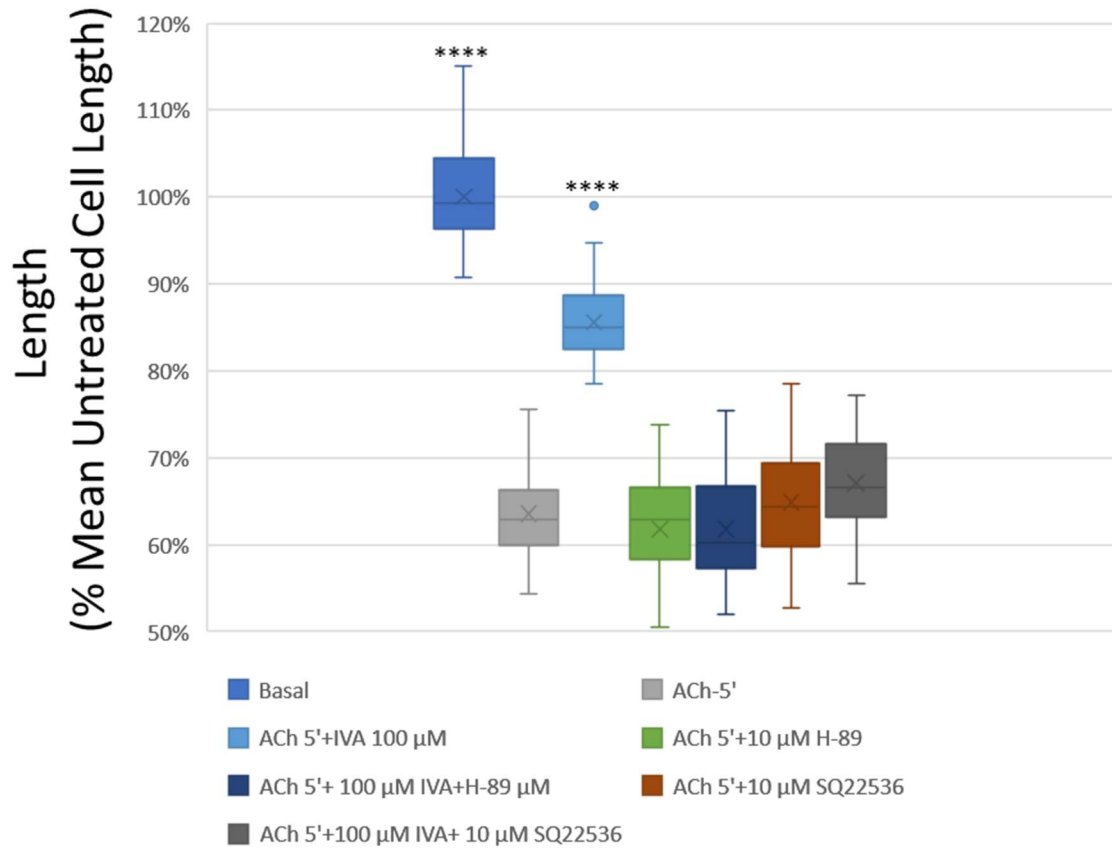


Figure 27) **Adenylate Cyclase Inhibitor SQ22536 and PKA Inhibitor H-89 Inhibit Relaxation Induced by IVA at 5 Minutes.** One-Way ANOVA of all groups (all groups not shown) $F(22,1068)=152.75$, $p \ll 0.0001$. Post-Hoc Tukey's HSD **** $p \ll 0.0001$ compared to all other groups.

SQ22536 and H-89 Inhibit 100 μ M IVA-Induced Relaxation of Smooth Muscle Cells (5 minutes)



Isovaleric Acid Changes Peristaltic Patterns in Whole Colon

Luminal IVA Changed Mean Diameter along Length of Colon

The physiological relevance of smooth muscle relaxation in the colon can go in opposite directions (metaphorically and literally). Relaxation anally-ahead of a bolus of nutrients opens the path for the bolus to move forward, while relaxation at the site of or behind the bolus would encourage stasis or even reversed direction. Observation of actual colonic peristalsis provides medically relevant information about how molecular mechanism plays into physiological function.

In a still photo of a mouse colon filled with Krebs Buffer (Figure 28A) or with Krebs buffer with 50 mM IVA (Figure 28B), we can see the regional differences in the colon, with cross-hatched striations of muscle at the proximal end giving way to the more uniform appearance distally. Looking for differences between Krebs buffer alone and Krebs plus 50 mM IVA, there is a widening of the proximal end where the striations are in the IVA colon.

Diameter over time can be demonstrated in spatiotemporal maps (ST maps) where the darker color indicates a wider diameter of the colon, and the lighter color indicates a narrowing of the colon (Figure 29). Here we can see demonstrated the change in colors at the proximal and distal ends when going from Krebs buffer, to 50 mM IVA, and back to Krebs buffer. Also apparent are the periodic changes in diameter running along the colon, which indicate peristalsis. Usually in the ST maps with Krebs buffer, the highest point (earliest point in time) in the change of diameter is at the proximal end, and the change in diameter travels distally (towards the anus) over time (Figure 29 A1 and B1). In the 50 mM IVA group (Figure 29 A2 and B2), the high points can be seen in the middle of the colon, and changes in diameter propagate in both

directions. Also, instead of contractions (darker to lighter) propagating, relaxations (lighter to darker) appear to propagate middle-to-proximal in the IVA groups. Just after the striation mark, an anomaly caused by the transitioning muscle anatomy sometimes occurs, where during the traveling contractions the colon twists perpendicular to the direction of the colon, causing the reported value to be wider than true (See Figure 29 B1 and B3).

These findings are quantified as averages of diameter at specific points along the colon. When each point on the colon in intervals of 0.2 mm distance from the striations is compared, the colon with 50 mM IVA intraluminally is wider at the striations (Figure 30). At the distal/anal end, there may be a slight narrowing caused by IVA, but this finding is not as consistent as the proximal widening. Comparing pH 7.4 Krebs buffer to pH 4.8 Krebs buffer (without IVA), there was no consistent change in diameter (Figure 31).

Figure 28) **Still frames of a mouse colon filled with A) Krebs buffer or B) 50 mM IVA in Krebs buffer.** In both frames the colon was filled with 5 μ L per mm length. The striations of smooth muscle on the proximal end (near the cecum) were used as a marker to align the position of the colon to other colons in comparison.

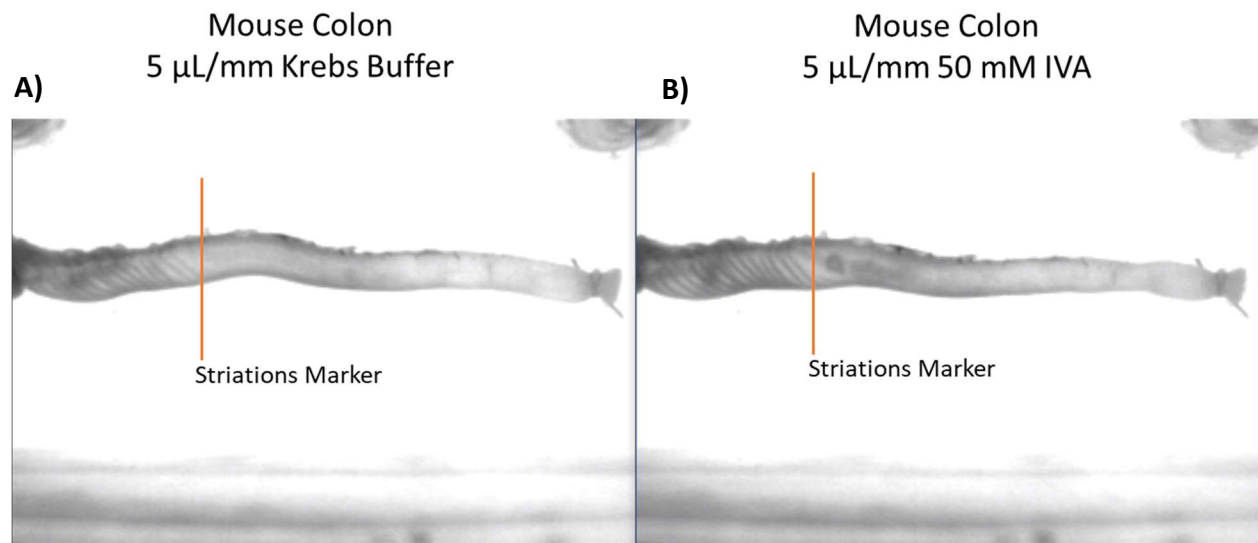


Figure 29) **Spatiotemporal mapping of mouse colons before and after 50 mM Intraluminal IVA**. Orange line indicates the end of the striations in the colon. Orange arrows indicate approximately whether the contractions begin near the oral end (in the Krebs buffer groups) or in the middle (in 50 mM IVA). Arrows correlate to the same features in other ST Maps.

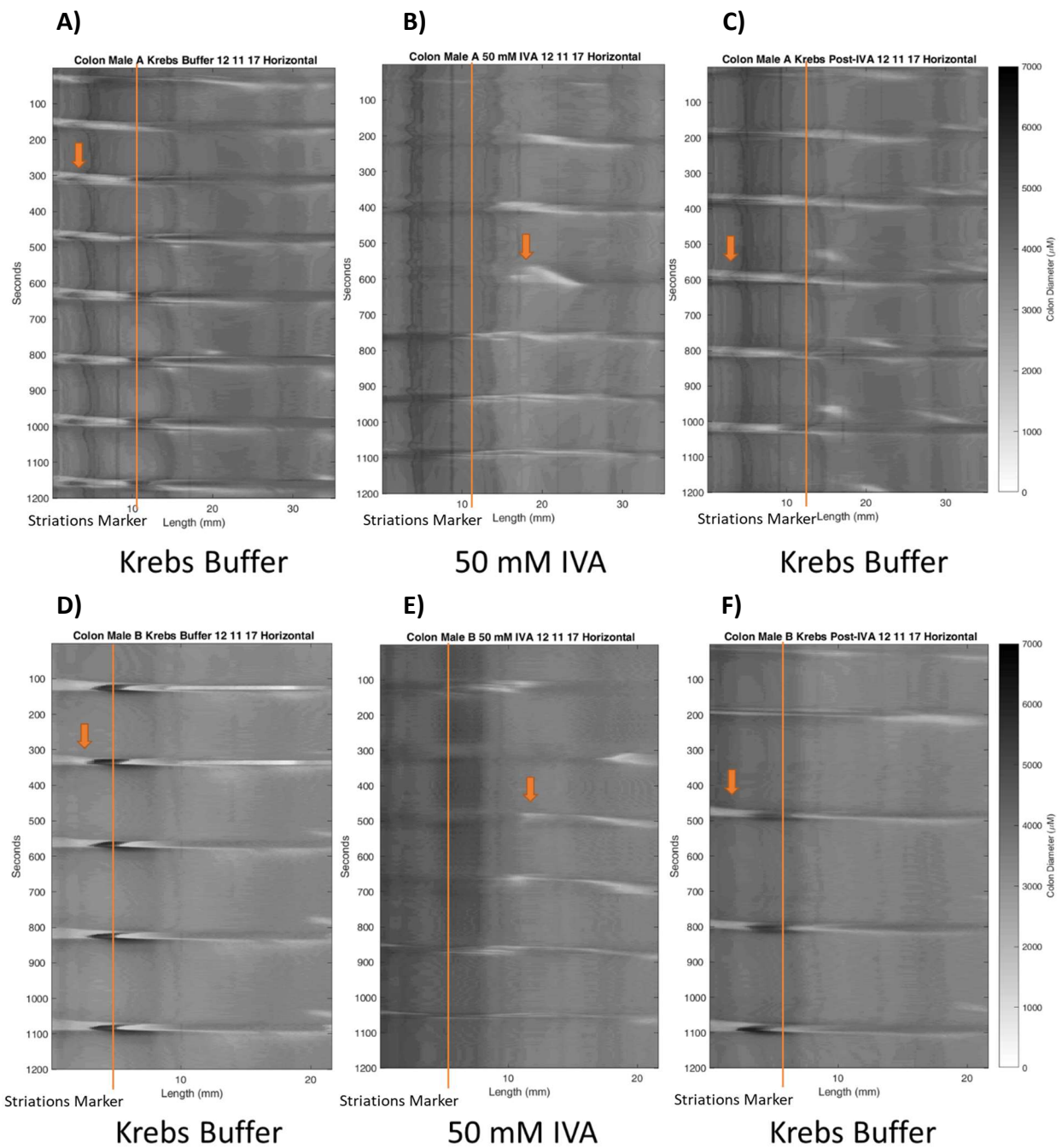


Figure 30) **Intraluminal IVA has increases proximal colon diameter.** n=6 colons, A) paired Student's T test compares diameters at that particular point in the colon as a distance in intervals of 0.2 mm from the approximate end of the striations. Colons varied in length and extremes without n=6 were not compared. B) Mean and 95% confidence interval of the difference between Krebs Buffer and 50 mM IVA.

Colon Mean Diameter Along Length

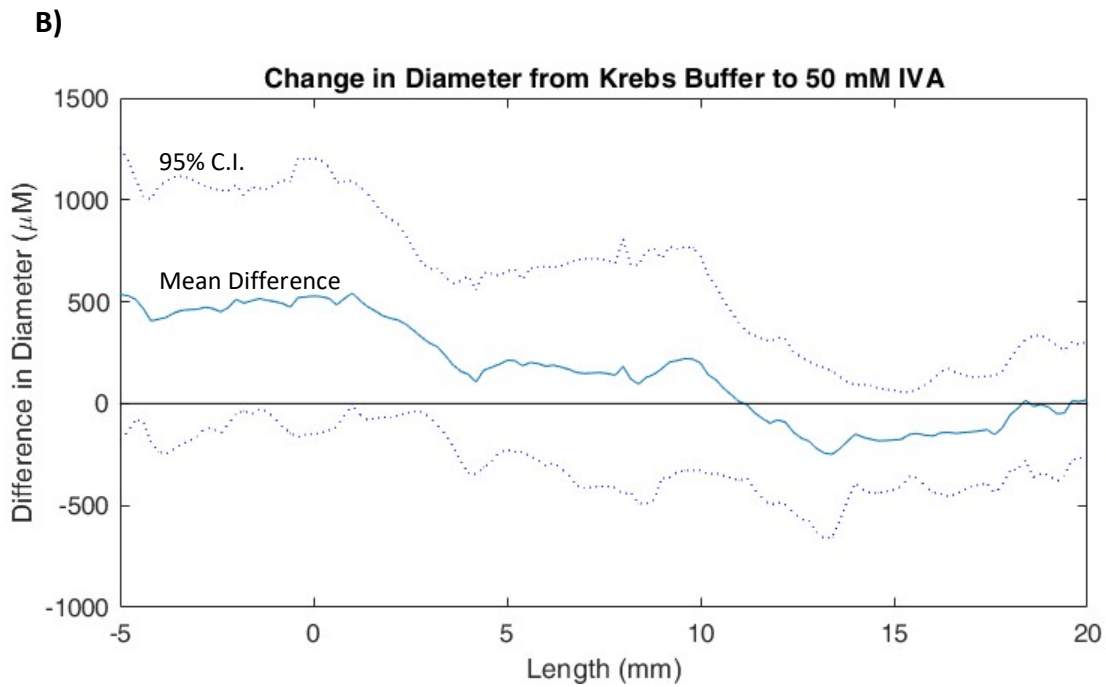
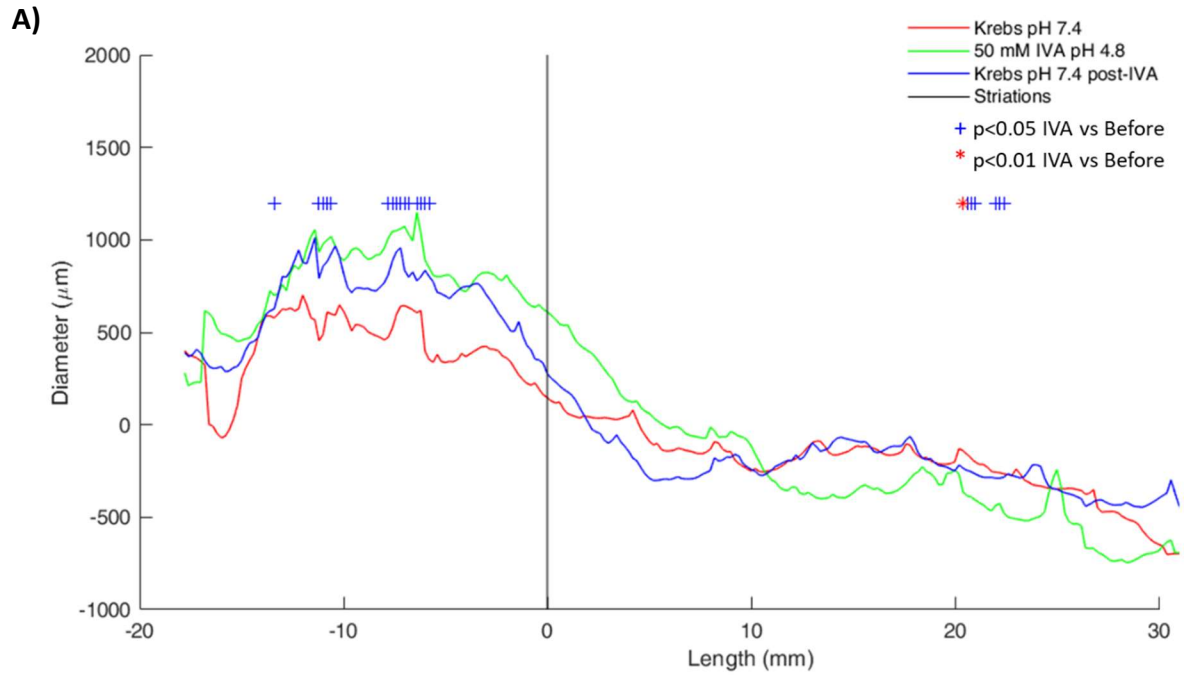
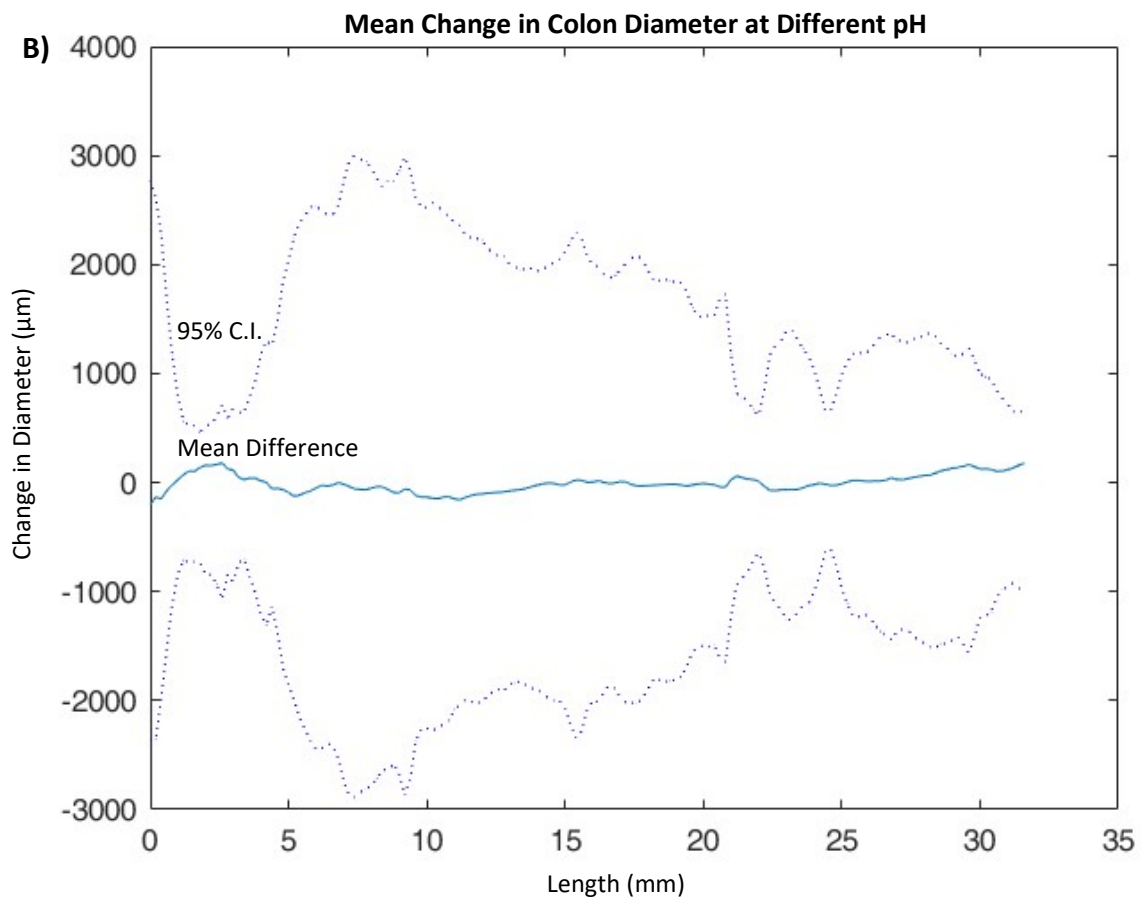
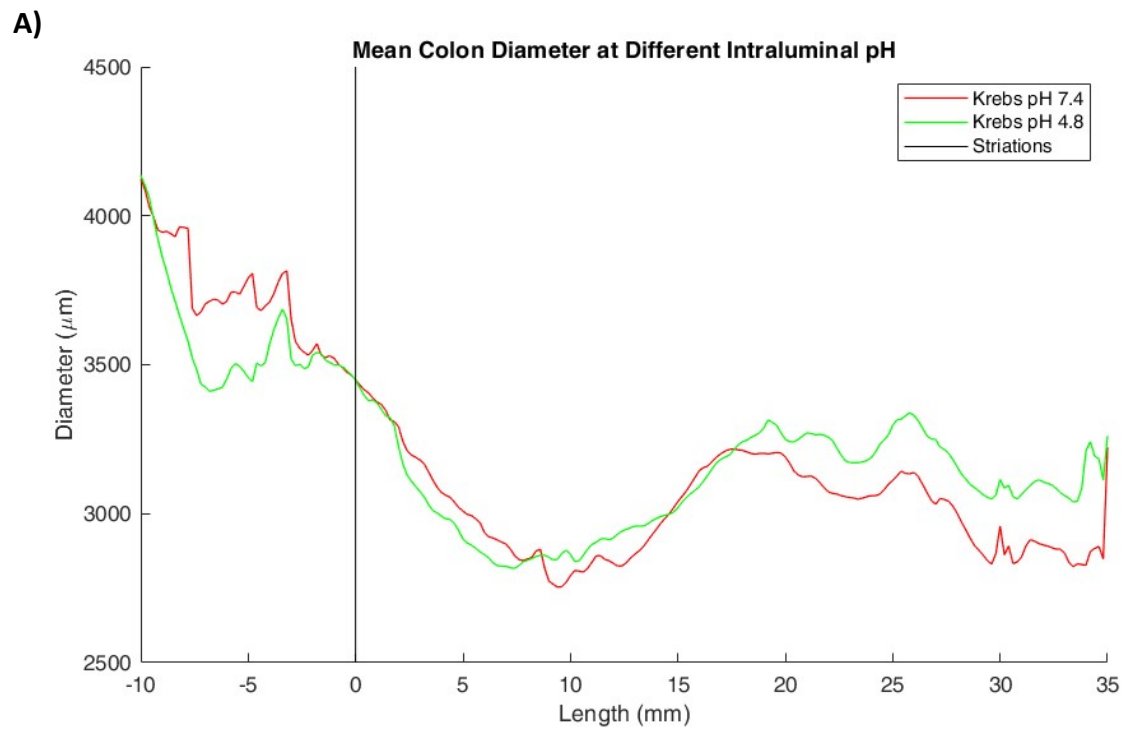


Figure 31) **Mean Diameter of Colon at Different Intraluminal pH.** Average diameter of the colon was found along the length of the colon over 20 minutes, n=3. There was no discernable change in diameter when changing from pH 7.4 to pH 4.8 intraluminally.



To analyze the peristalsis itself without regard for differences in diameter, the change in diameter over a period of 10 seconds was calculated and mapped just like the ST map of diameter-alone (Figure 32). The decreases in diameter (in yellow) demonstrate the propulsive action of radially contracting segments of colon, which can be seen to travel from proximal to distal end in colons with intraluminal Krebs. A widening of the colon (red and black) can be seen ahead of the contractions, as well as rebound widening of the colon after the contraction. Mirroring the ST maps of diameter, these maps show the contractions with intraluminal IVA starting in the middle, and radiating from there, with propagating relaxation instead of contractions at the proximal end for some anti-peristaltic waves.

To quantify where the contractions were occurring, the quantity of contractions over 1 mm were counted along the colon (Figure 33), and the centroid of the contractions calculated (Figure 34 A-B). A shift in the centroid of contractions from the proximal end to more distally in the IVA group quantifies the disappearance of the proximally contractions, and a shift back proximally when IVA is washed out. To show how much of the colon was experiencing contractions, the mean of contractions over 1 mm was calculated per colon, and the percent of that colon that experienced at least half the mean of those contractions calculated (Figure 34 C-D). From this it is apparent that a much shorter length of the colon with intraluminal IVA experienced contractions, and contractions lengthen when IVA is washed out. When comparing intraluminal pH 7.4 Krebs to pH 4.8 Krebs, these trends do not exist (Figure 34 A and C). Although lengths of the contraction were significantly smaller in the IVA group versus control, the number of any type of waves over a 20-minute period were not significantly different (Table 1). Full propagations from proximal to distal colon were uncommon with 50 mM IVA, with a

decrease in the average number of these propagating contractions from 7 to 3 over a 20 minute period (Table 2).

Figure 32) **DyDt Spatiotemporal mapping of mouse colons before and after 50 mM**

Intraluminal IVA. Images show change in colon diameter over 10 second period. Orange is no change, yellow is a decrease in diameter, red is an increase in diameter. Green arrows indicate approximately whether the contractions begin near the oral end (in the Krebs buffer groups) or in the middle (in 50 mM IVA). Arrows correlate to the same features in other ST Maps. In 50 mM IVA, contractions start near the middle, and waves propagate from there; some anti-peristaltic waves are relaxation-only.

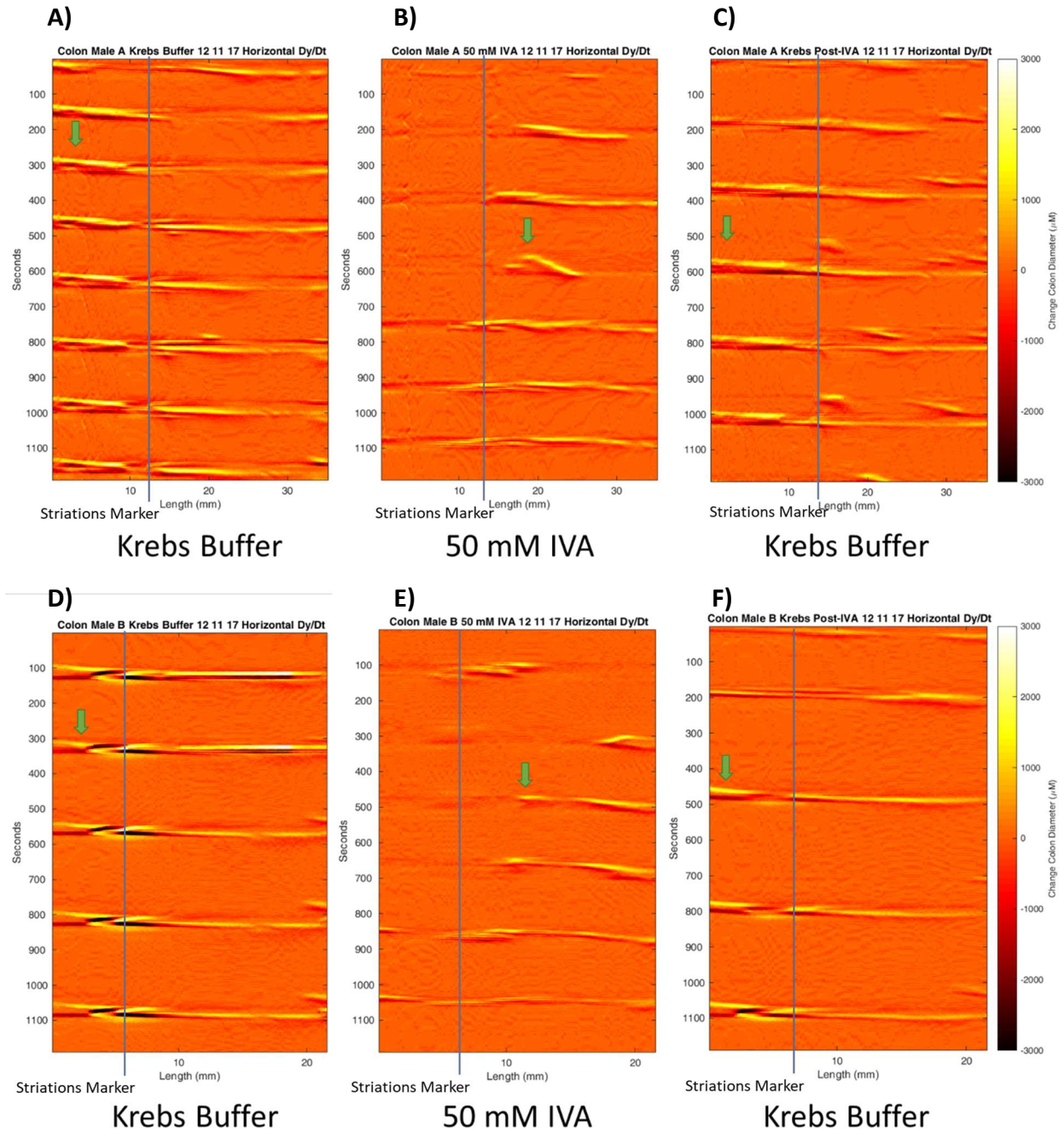


Figure 33) **Example measurement of contractions in ST Map.** Graphs below each figure show the number of frames of video (at 15 frames per second) of contractions over 1000 μm counted at that location. Graphs demonstrate a disappearance of contractions in the 50 mM IVA group, and the reappearance of those contractions once IVA was replaced intraluminally with Krebs buffer-only.

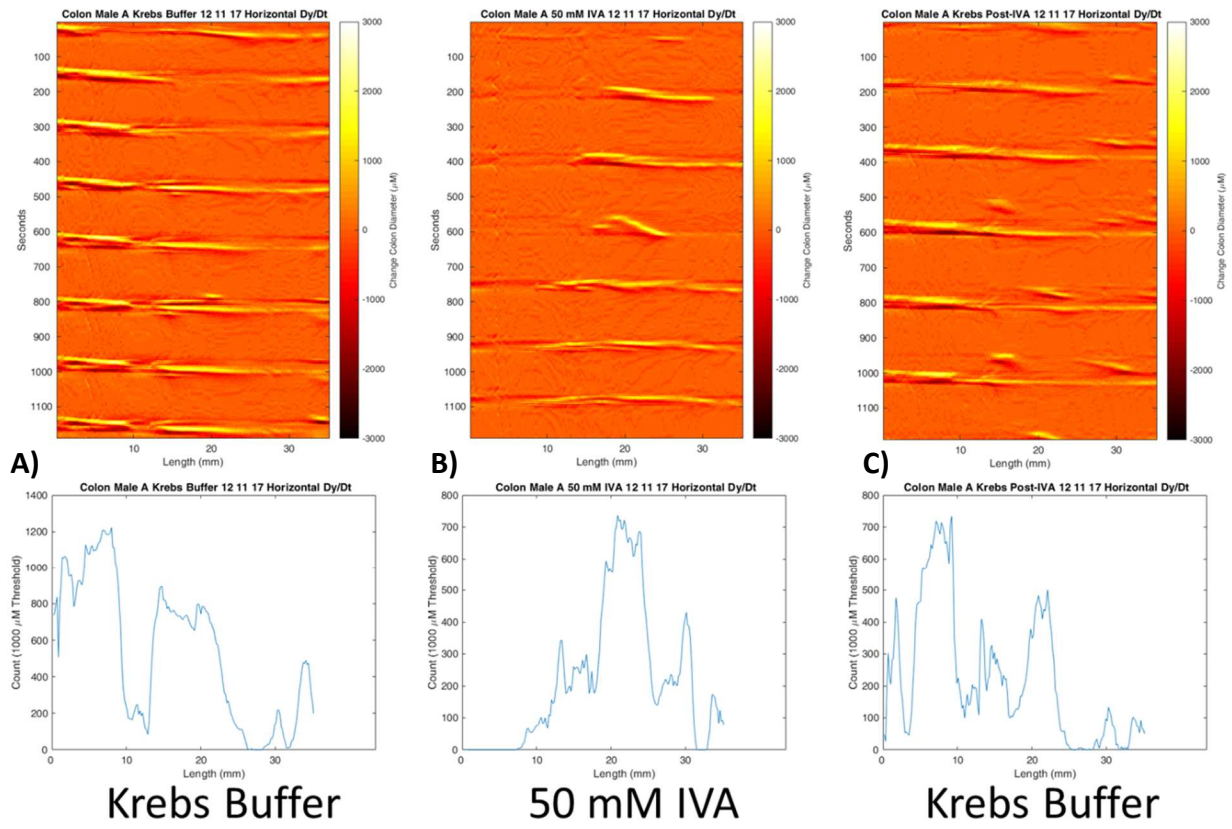


Figure 34) Length and Center of Contractions Along Colon Comparing Krebs Buffer vs 50 mM IVA, or Changes in pH. Contractions over 1000 μm along the length of the colon over 20 minutes were counted. A) The centroid of the contractions demonstrate a shift towards the distal end when 50 mM IVA in buffer is added to the lumen. The centroid shifts back proximally when the IVA is washed out by control Krebs buffer. One-Way ANOVA $F(2,14) = 11.37$ $p < 0.01$. Post-hoc Fisher's least significant difference * $p < 0.05$ vs. control, ++ $p < 0.001$ vs 50 mM IVA. $n=5$, # One outlier colon (centroid less than mean – 1.5*Inter-quartile Range) was removed; outlier value was caused by complete ablation of all contractions by IVA for most of measurement period followed by late recovery of small contractions at proximal end. B) Changes in intraluminal pH did not cause a significant shift in the centroid of contractions. C) The mean of the number of contractions over 100 μm was calculated per colon, and the length of the colon experiencing at least half the mean calculated. While approximately 70% of the colon meets this threshold for contraction in the control, less than 50% meets this with 50 mM IVA in the lumen. Washing out the IVA from the lumen recovers this to nearly 60%. $n=6$, One-Way ANOVA $F(2,17) = 6.76$ $p < 0.01$. Post-hoc Fisher's least significant difference ** $p < 0.01$ vs. control. Bars indicate standard deviation. D) Between colons with just the pH adjusted, there was not difference ($n=3$). Bars indicate standard deviation.

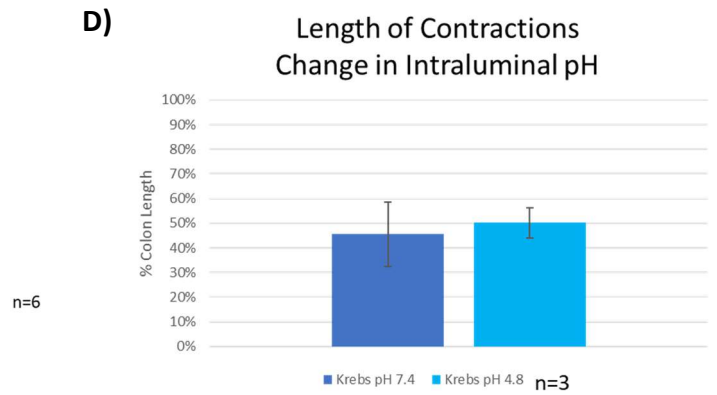
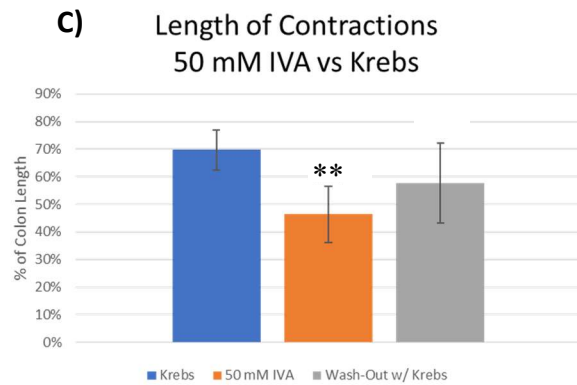
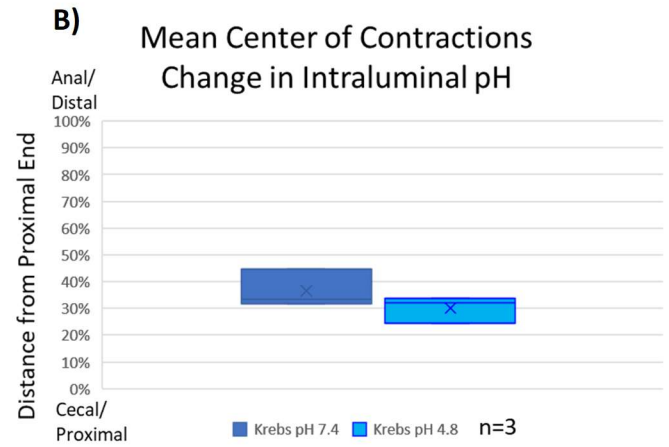
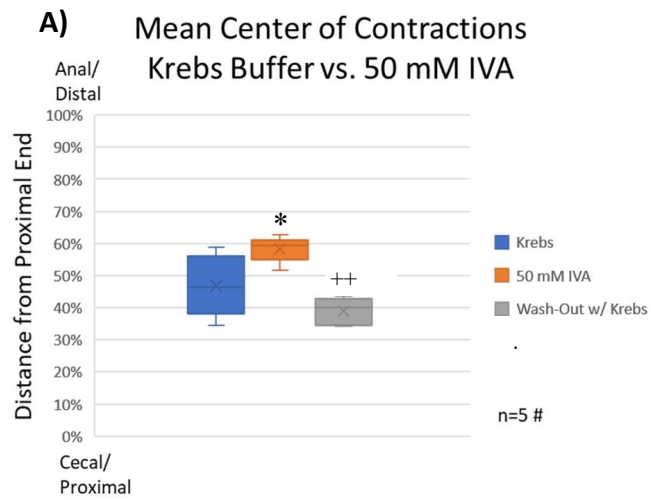


Table 1) **All Full Waves of Contraction and/or Relaxation Counted Over 20 Minutes.** ST
Change in Diameter Maps were counted for (anti-)peristaltic contractions and/or relaxations that
spanned the full width of the colon and had discernable relaxation between them before the next
wave started.

Total Counted Waves Over 20 Minutes				
	Sex	Pre IVA	IVA	Post IVA
1	M	8	7	6
2	M	5	6	4
3	M	12	9	10
4	M	7	6	3
5	F	8	8	8
6	F	7	8	7
	Average	7.833333	7.333333	6.333333
	St Dev	2.316607	1.21106	2.581989

Table 2) **All Proximal-to-Distal Contractile Propagations Counted Over 20 Minutes.** ST Change in Diameter Maps were counted for contractions that spanned from the proximal end to the distal end of the colon and had discernable relaxation between them. One-Way ANOVA $F(2,17) = 6.79$ $p < 0.01$. Post-hoc Fisher's least significant difference * $p < 0.05$, ** $p < 0.01$ vs. Pre-IVA control.

Full Contractile Propagations Reaching from Proximal to Distal End of Colon				
	Gender	Pre IVA	IVA	Post IVA
1	M	7	4	5
2	M	5	2	4
3	M	12	0	0
4	M	6	3	1
5	F	7	2	5
6	F	7	5	7
	Average	7.33333	** 2.66667	* 3.66667
	St Dev	2.42212	1.75119	2.65832

Luminal IVA Slows Proximal Colon Peristalsis

To quantify the (anti-)peristaltic wave velocity (without respect to whether it is a relaxation or contraction wave), the partial derivative of the change in diameter ST map with respect to length and time was taken (using the MATLAB “gradient” function) to show the relative difference in velocity of the peristaltic movements along the length of the colon. In the example ST wave velocity map (Figure 35), where green indicates peristaltic movement at that point and red indicates anti-peristaltic movement at that point, you can see a decrease in the amount of green on the proximal end going from Krebs to 50 mM IVA, and an increase in green going from IVA to the washout. The average relative wave velocity in the proximal region was greater for colon with luminal Krebs compared to 50 mM IVA, both at specific points and the regions in general (Figure 36). Washout of the IVA only recovered the velocity slightly in the proximal region. There was no noticeable change in velocity in the distal half of the colon.

Figure 35) **Example ST Wave Velocity Maps showing relative change of velocity of changes in diameter.** The ST Wave Velocity map shows general forward peristaltic movement (green), but a decrease in forward movement with 50 mM IVA in the lumen. Anti-peristaltic movement, denoted in red, appears to occur at the demarcation of the striations, and after the peristaltic wave in the Krebs buffer control A. Black is no velocity. Arrows correlate to the same features in other ST Maps.

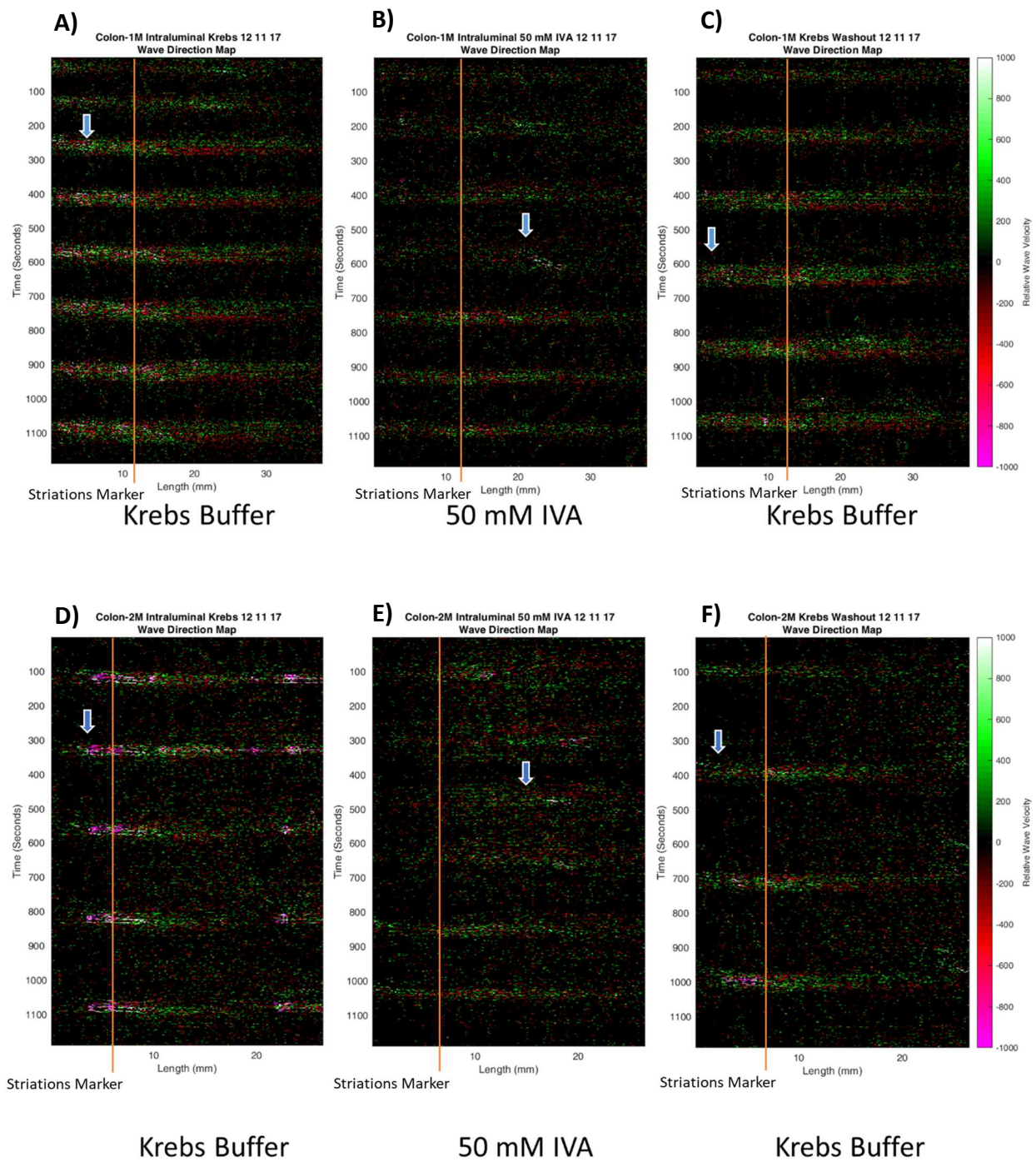
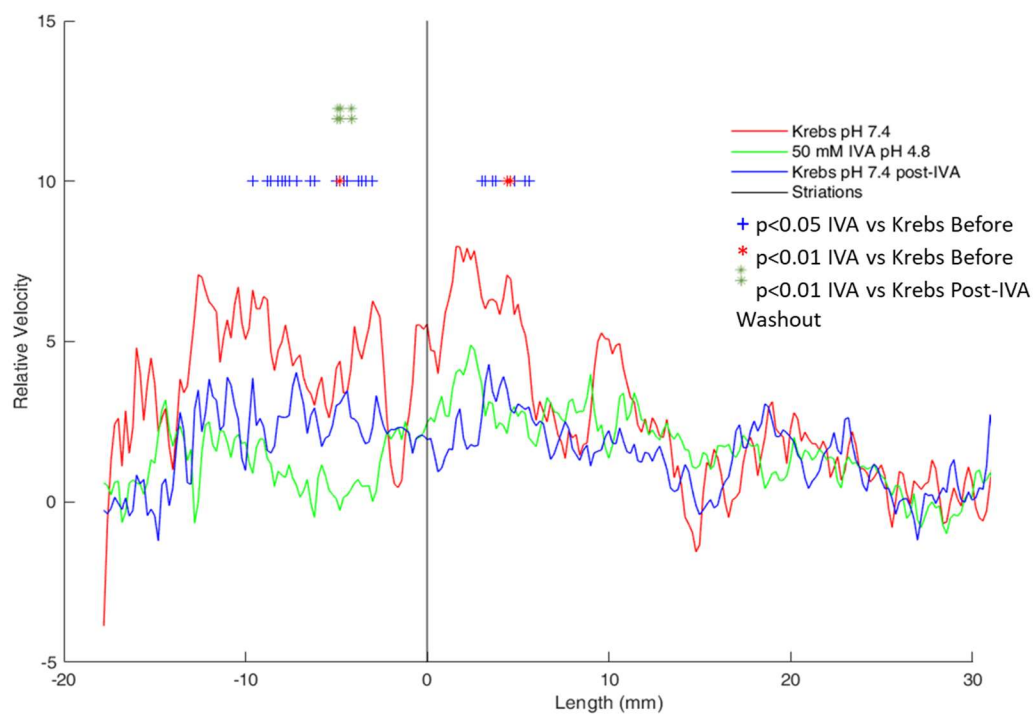


Figure 36) **Mean relative contraction wave velocity of contraction along colon over 20 minutes.** The average relative contraction wave velocity at intervals 0.2 mm from the striation mark was calculated and averaged together by treatment group. The 50 mM IVA group was significantly slower than Krebs buffer in the area of the striations. This proximal area of the colon was on average at a higher velocity than the distal portion in the control groups.

Mean Relative Velocity of Contractions Along Colon over 20 Minutes



Colonic Smooth Muscle, Enteroendocrine Cells Possess OLF Receptor

Murine Colon, Ileum, and Cultured STC-1 cells, Stain Positive for Olfr558

Tissue cryosections 10 μ M thick of mouse colon (Figure 37 A and C) and ileum (Figure 37 E) were cut perpendicular to the axis of the tube (creating rings of tissue, not long strips). Sections were then incubated overnight with 1:200 Thermo PA5-35298 OR51E1 Antibody in 5% normal goat serum at 4 °C. Sections stain positive for the olfactory receptor Olfr558 (murine analog to OR51E1), with the strongest staining on the outer longitudinal layer of muscle. Control slides prepared the same way but with the OR51E1 primary antibody not present (Figure 37 B,D,F) did not show evidence of OR51E1 staining. Tissue cultured STC-1 cells also stained positive for OR51E1 (Figure 38 A-B).

Figure 37) **40x Images of fluorescent staining of mouse Olfr558 (A,C,E) or Control (B,D,F) on 10 μ M cryosections of mouse colon (A-D) and ileum (E-F).** The outer smooth muscle layer of both colon and ileum stained positive for OR51E1 throughout. Some mild staining was in the circular muscle layer and in the mucosa. Primary antibody deletion from staining steps as a control did not demonstrate any staining for the protein.

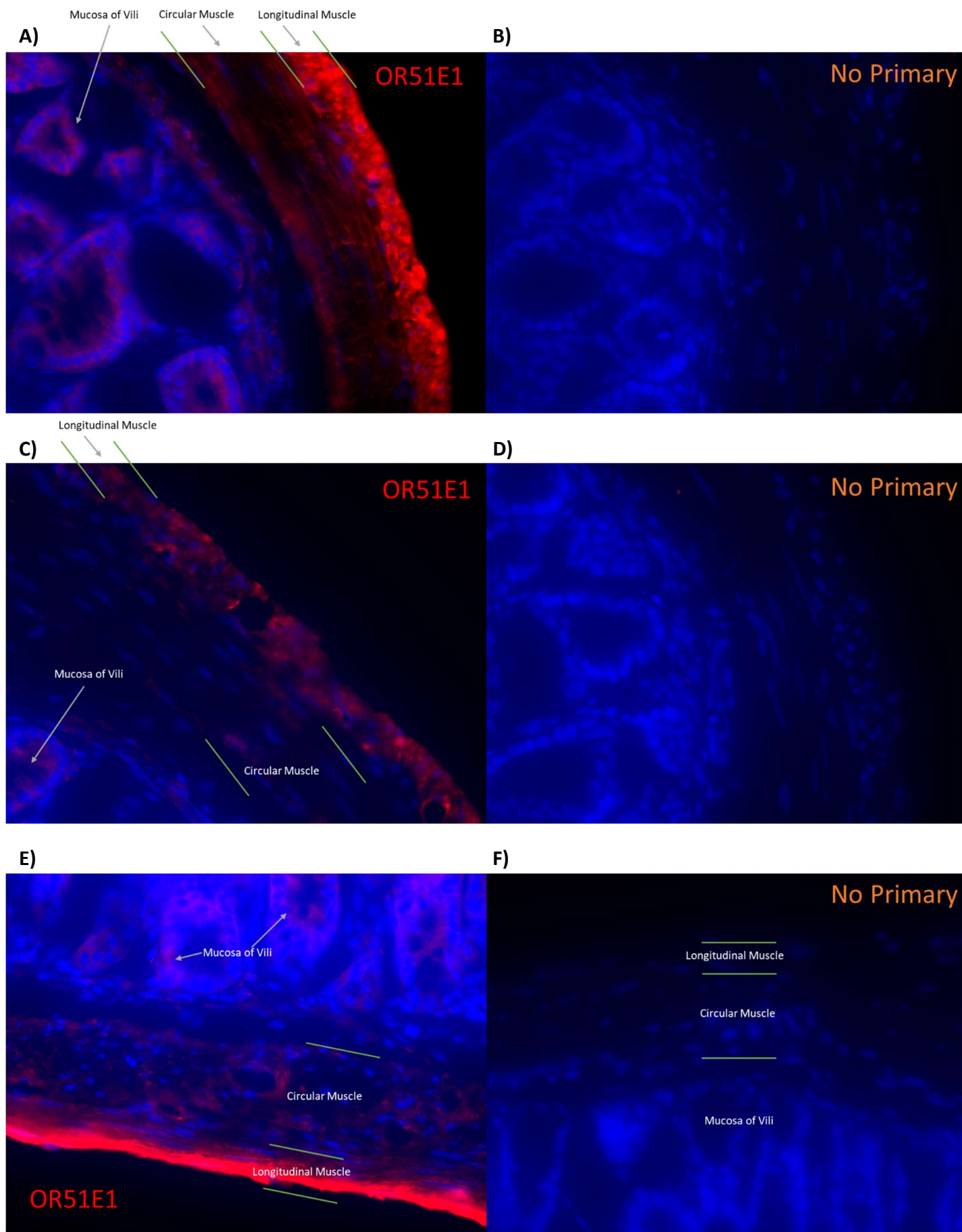
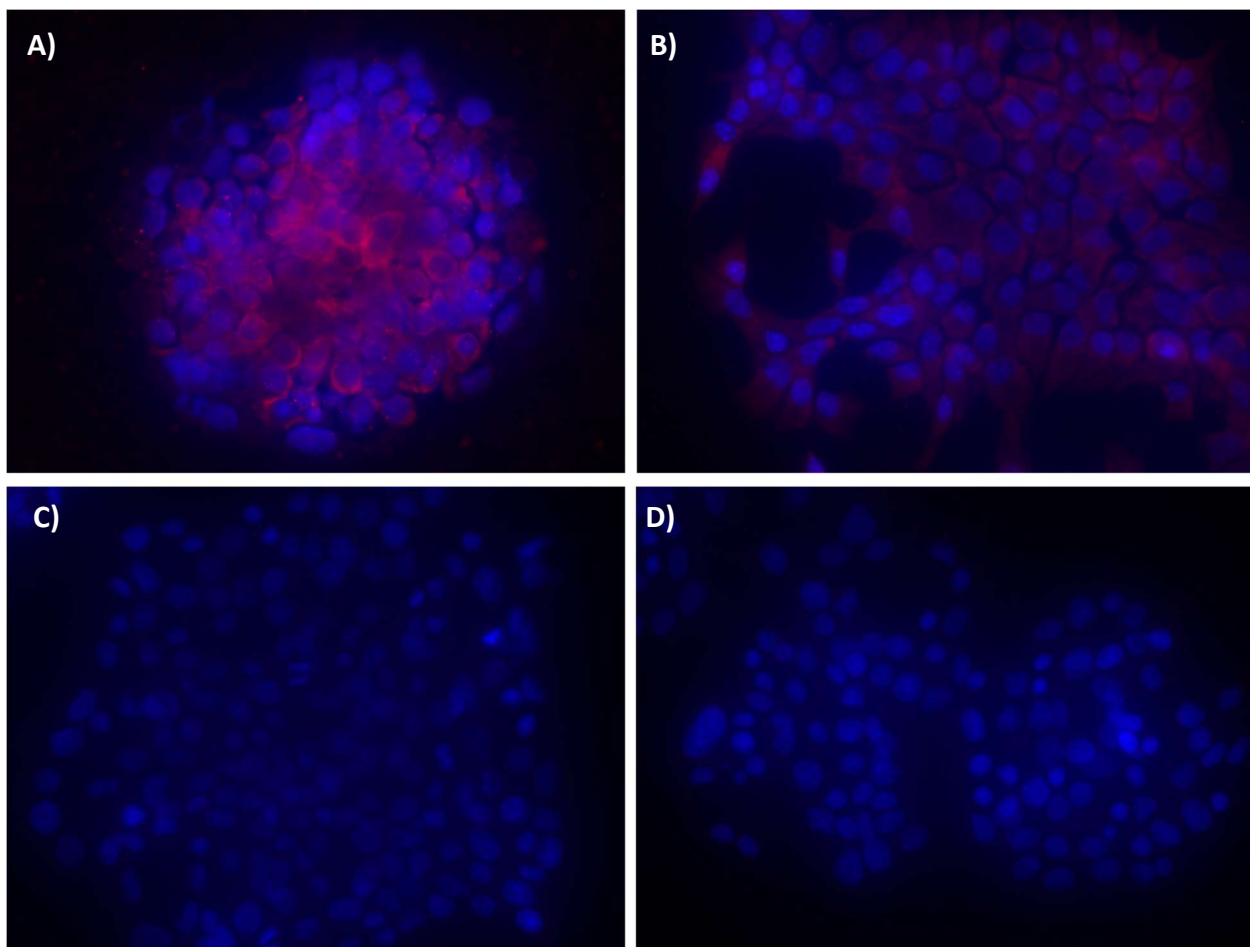


Figure 38) Cultured STC-1 cells stained with OR51E1 (A-B) or no Primary Antibody (C-D).

The enteroendocrine-derived mouse cell line stained positive for OR51E1 throughout the cell.

Deletion of the primary antibody step from staining showed no positive staining.



Discussion

Direct Signaling of Smooth Muscle by Fatty Acids

Response to IVA

The multitude of possible receptors, and the wide distribution of their expression, make pinpointing specific physiologically relevant targets tricky at the organ level. The response at the cellular level provides an idea of the potential physiological response at the tissue and organ level, but which cells are the gold standard for correlation to physiological organ response? There is no rule that if the smooth muscles respond to a molecule by relaxing, that neuro-epithelial mechanisms can't respond by trying to induce contraction. In fact, disparate responses are key to coordinating action in mechanical organs such as the colon.

At the cellular level, IVA concentrations between 1 μ M and 100 μ M at physiologically buffered pH cause individual colonic smooth muscle cells to relax from ACh-induced contraction in a dose-dependent manner. These IVA concentrations are physiologically relevant in human circulation for homeostatic patients⁴⁹ and for pathologic patients⁵¹; also, the relaxation response covers most of the possible range from minimal relaxation to 3/4ths of complete recovery. The relaxation is present in the short-term at 1 minute (Figure 14) and lasts at least 5 minutes (Figure 15). Thus, absent any external neurological or immune influences, the most likely response of smooth muscle to IVA is relaxation.

Relaxation of the longitudinal smooth muscle to IVA in a dose-response fashion (Figure 12, Figure 13) similar to the cellular response is the first piece of evidence that physiologically relevant BCFA signaling to the colon occurs directly to the smooth muscle. While IVA concentrations to elicit a response from the tissue are several magnitudes higher than in the

dispersed cells, the delivery to cells within tissue must account for diffusion to cells as opposed to something closer to direct delivery, which capillaries approximate. Also, the concentrations which elicit a response from whole tissue (around 10 mM to 50 mM), are close to physiological relevance in the lumen of the colon as concentration in stool⁵². Also of physiological relevance is the increased response to IVA when IVA is allowed to change the environmental pH (Figure 18). A relatively acidic pH of 6.7 is at the extreme end of possible human pathology for serum¹⁶⁶, but a reasonable pH to be found in the colon lumen²⁸. While changes in environmental pH itself will cause relaxation independent of the fatty acid¹⁶⁷, it is worth noting that fatty acids are the reason for the lower pH in the colon lumen and the cause for organic acidosis in several inherited pathologies, including isovaleric acidemia.

The second piece of evidence for direct BCFA signaling to smooth muscle is the tissue's response to IVA after TTx treatment, which inhibits the ability of neurons to elicit an action potential. At concentrations of TTx which elicit a response from the tissue, the colon segment's response to IVA is not changed relative to the vehicle control (Figure 21). The lack of change in response is even more evident when considering that only the response to ACh is decreased by TTx, not the relaxation induced by IVA.

The next piece of evidence is the lack of effect of the Nitric Oxide Synthase inhibitor L-NNA on IVA-induced relaxation (Figure 22). NOS signaling could be autocrine; however, it is also a potential signaling mechanism mediated by epithelial cells and neurons^{105,120}. Regardless, there was no significant decrease in IVA-induced relaxation. It could be argued that an increase in relative relaxation seen with L-NNA and IVA could be caused by inhibition of NOS (or of neurons by TTx) unmasking an example of NOS-induced contraction.¹⁶⁸ However, like TTx, the

effect of the NOS inhibitor was more to decrease ACh-induced contraction than to decrease IVA-induced relaxation.

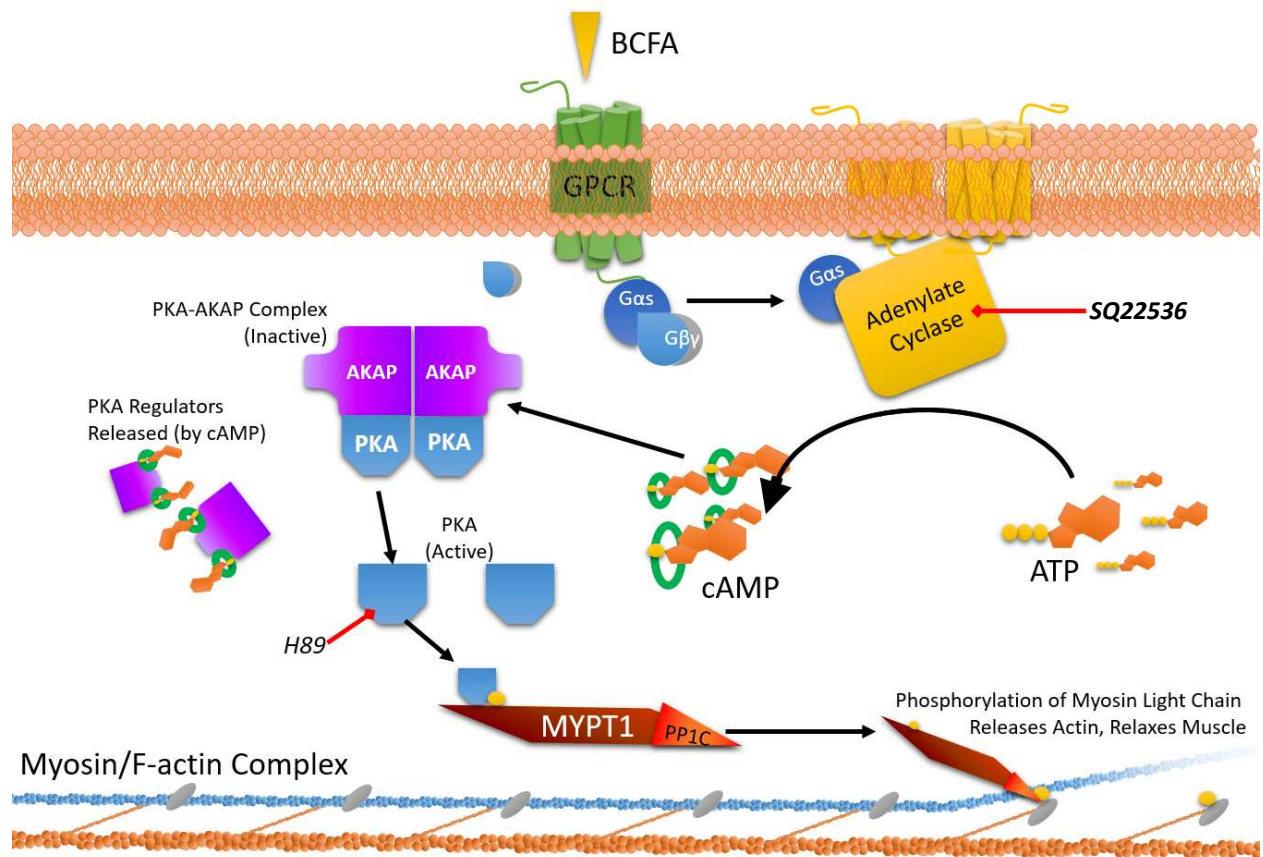
cAMP/PKA Pathway Signaling

Understanding the second-messenger system used by the signaling molecule provides crucial information about the potential upstream and downstream mechanisms. Evidence against Nitric Oxide's participation in the relaxation (Figure 22) is evidence against cGMP/PKG system pathways. Another key second messenger is cAMP, and the classical cAMP/PKA signaling pathway. The evidence at the cellular level that cAMP is a primary effector of IVA-induced relaxation is demonstrated by the strong inhibition of cell relaxation by SQ22536, an adenylate cyclase inhibitor (Figure 26 and Figure 27). The use of SQ22536 in colon segments to inhibit relaxation does not demonstrate as drastic an effect as seen with the individual cells; however, the decreased relaxation of the SQ22536 treated colon segments vs. the DMSO-only vehicle is present and statistically relevant (

Figure 25); more evidence of a physiological correlation to the cell data.

Inhibiting cAMP can affect multiple pathways such as EPac-related pathways^{146,147}, PKA¹⁴⁵, or cAMP-interacting domains of other proteins⁹². Relaxation of smooth muscle by cAMP via PKA is one of the most well-characterized pathways for smooth muscle relaxation. Almost complete reversal of IVA-induced relaxation via inhibition of PKA by treatment with H-89 in dispersed cells (Figure 26 and Figure 27) is a strong indication that this is the primary mechanism by which IVA induces relaxation in those cells. Combined with the evidence that the relaxation is not dependent on neuronal activity or uses a common paracrine signaling mechanism of generating NO, the evidence strongly upholds the hypothesis that IVA's relaxation effect is mediated directly by the smooth muscle cell, and that it is cAMP/PKA dependent (Figure 39).

Figure 39) **Diagram of a cAMP/PKA-Mediated Pathway for Smooth Muscle Relaxation.** A ligand, such as a GPCR, for a $G\alpha_s$ -linked GPCR, such as an olfactory receptor, can cause $G\alpha_s$ -mediated activation of adenylate cyclase (AC). AC mediates production of cAMP from ATP. cAMP acts as a messenger for numerous pathways, such as PKA, which can phosphorylate MYPT1. The kinase domain of MYPT1, PP1C, phosphorylates the myosin head of MLC, releasing the filamentous actin and causing relaxation. The compound SQ22536 inhibits AC, and H-89 inhibits PKA.



Presence of IVA Sensitive Receptors

The presence of a receptor capable of mediating the response seen is an important piece of evidence that a signaling molecule is in fact mediating that response. OR51E1 (and mouse analog Olfr558) is an enticing receptor for IVA to investigate as a mediator of BCFA fatty acid response because as a GPCR its action is mediated by $G\alpha_{olf}$ (similar in most ways to $G\alpha_s$) which activates adenylate cyclase III to produce the second messenger cAMP. The presence of a receptor for IVA on colonic smooth muscle which activates an adenylate cyclase fits the data showing that IVA-induced smooth muscle relaxation is adenylate cyclase-dependent. If the receptor mediating smooth muscle relaxation was FFAR3, a $G\alpha_i$ linked receptor, inhibition of adenylate cyclase would have been expected, causing an increase in contraction. Adenylate cyclase inhibitors such as SQ22536 would not have mediated $G\alpha_i$ linked receptor activity. If FFAR3 mediated this relaxation in longitudinal muscle by activating relaxation-inducing neurons, TTx would have inhibited the relaxation.

Immunofluorescence stains of mouse colon demonstrate positive staining for OR51E1/Olfr558, with the most prominent staining on the outer layers of the colon and ileum, where the longitudinal smooth muscle lies (Figure 37). Circular muscle and the mucosa also demonstrate moderate staining. Controls without the OR51E1-antibody did not stain for the secondary antibody. Positive staining of STC-1 cells (Figure 38), an immortalized cell line of mouse enteroendocrine cells, also confirms previously reported presence of IVA-sensitive OR51E1/Olfr558 in enteroendocrine cells of other GI tracts⁸⁸. Small molecule inhibitors for the numerous olfactory receptors are uncommon, which made the single report of 2-EHA as a negative modulator of OR51E1 interesting.⁸⁴ Unfortunately, the BCFA 2-EHA did not inhibit the

relaxation effect of IVA and instead appeared to act like IVA in terms of potency (Figure 23). Specific investigation in future study can definitively show whether OR51E1/Olfr558 mediates this relaxation effect; other receptors which activate adenylate cyclase could be the potential target mechanism by which IVA induces smooth muscle relaxation. The presence of a receptor like OR51E1/Olfr558 that fits the description of the required mechanisms for IVA-induced relaxation warrants further investigation.

SCFA and BCFA Response

The SCFA valeric acid was about 15% more potent a colonic longitudinal muscle relaxant than IVA (Figure 24) at one investigated concentration. This finding contradicts the assertion that BCFA are more relevant as signaling molecules than unbranched SCFA's which serve a role as nutrients; if BCFA were more important, one thought might be that receptors respond more for BCFA than the straight chain equivalents. Valeric Acid is about as prevalent as IVA in stool⁵², which is likely important for the mucosa in immediate contact, but, there is more than an order of magnitude more IVA in human blood serum⁴⁹. This could be because IVA can be derived from the amino acid leucine⁴⁷ whereas valeric acid does not have an immediate common molecular derivative, but could also be due to differences in how SCFA and BCFA are metabolized and transported which allows more BCFA to arrive to the smooth muscle. If the physiological purpose of colon peristalsis reacting to IVA is in response to protein in the GI tract being fermented, there may not have been enough selective pressure to differentiate the IVA response from response to valeric acid because valeric acid has a shorter biological half-life. Or, valeric acid may also occur in roughly the same dietary environments that produce IVA in the colon. Valeric acid (also known as C5:0 pentanoic acid) is a ligand of OR51E1⁸⁴; propionic and

acetic acid, which are the only other SCFA present in serum at a similar magnitude as IVA⁴⁹, are not OR51E1 ligands⁸⁴.

Regionally-Specific Inhibitions of Peristalsis

Differences in Colon Diameter

The physiological relevance of smooth muscle relaxation in the colon can go in opposite directions (metaphorically and literally). Relaxation distally-ahead of a bolus of nutrients opens the path for the bolus to move forward, while relaxation at the site of or behind the bolus would encourage stasis or even reversed direction. There is also some question whether different layers of smooth muscle (circular and longitudinal) relax and contract together or opposite of each other to achieve optimal peristalsis^{107–109}.

Observation of actual colonic peristalsis provides relevant information about how molecular mechanism plays into physiological function. It is mildly apparent from the still frames of colon intraluminally-filled with either plain Krebs buffer (Figure 28 A) or IVA (Figure 28 B) that the proximal end of the colon (behind the point where the striations ends) is slightly wider when equally filled with 50 mM IVA buffer than with control buffer. Looking at the ST map measuring the diameter of the colon over time (Figure 29) it is even clearer that the proximal end is wider after administration of IVA to the lumen (Figure 30).

While it is difficult to parse-out the individual mechanisms when looking at whole-organ, direct relaxation of smooth muscle, as seen in the experiments in individual cells and colon segments, would fit with the widening of the proximal end. But relaxation mediated by FFAR3 positive PYY-positive enteroendocrine cells⁷⁹ or neutrally mediated relaxation through FFAR3 positive neurons⁷⁸ would also fit. Regardless of mechanism, both findings of proximal

relaxation and distal constriction support the hypothesis that IVA inhibits forward movement of the luminal contents by normal peristalsis.

In the analysis of longitudinal relaxation by colon segments, the proximal end of male colons demonstrated a decreased response to IVA (Figure 16). While at first this doesn't fit the narrative of proximal-end relaxation, there are possible explanations. The arrangement of the circular muscle could cause a dampening of the measured response depending on their orientation, assuming the response for longitudinal and circular muscle is the same (but that is not a given), making that measured difference an artifact of the anatomy. Another reason could be differences in regional neuronal responses. What may not be apparent in the longitudinal muscle when testing colon segments, may be different when looking at the circular muscle. For example, another study showed that 10 μ M nicotine induced a cessation of proximal colon circular muscle rhythmic contraction for several minutes in rats (a net relaxation), and this effect is inhibited by FFAR3 specific agonists⁷⁸ (IVA is an FFAR3 agonist). In combination with anatomical arrangement differences, this difference may explain the decreased relative relaxation in proximal colon segments measured longitudinally but does not affect the net physiological result of increased luminal diameter in the proximal colon.

Differences in Peristaltic Waves

The most drastic difference manifested by intraluminal IVA was changes to the character of the peristaltic activity. The example maps showing the change in diameter over time show classical forward-moving peristaltic waves in the initial Krebs buffer-only control groups (Figure 32 A). In the 50 mM IVA group, most of the contractions at the first half of the length of the colon disappears. This is evidenced by the shift in the center of the contractions towards the distal end with IVA, and a shift proximally when IVA is removed (Figure 34). Relaxations

moving in an anti-peristaltic fashion (from mid-colon to the cecal end) are apparent (Figure 32 B). Removal of the IVA returns most of the proximal-sided contractions and there are fewer anti-peristaltic-appearing waves (Figure 32 C). Changing pH of intraluminal Krebs buffer from 7.4 to 4.8, without adding IVA, does not cause the same changes in the peristaltic wave activity, and proximal-sided contractions remain (Figure 34 B).

Finally, there is a quantifiable change in the velocity and direction of the (anti-)peristaltic waves. Wave direction ST maps, which show the relative velocity of the change in diameter at a point, demonstrate a decrease of peristaltic (i.e. forward) movements, and an increase in anti-peristaltic (i.e. backward) movements when going from Krebs-only to 50 mM IVA, and a recovery when the IVA is washed out (Figure 36). On average, the region around the cecal-ended striations of the proximal colon were close to standstill with intraluminal 50 mM IVA compared to the Krebs-only control before IVA. Differences were not apparent on the distal-half of the colon.

Surprisingly, there was no evidence of a change in the actual period of peristaltic waves (Table 1). Assuming the period of the waves is controlled by central pattern generating neurons in the ICC^{97,122}, the changes in peristalsis appears not to be with the timing of the wave generators, but where the waves begin. IVA-influenced peristaltic waves begin in the middle and have fewer contractions on the proximal end.

Differences in IVA sensitivity regionally could explain a change in where the peristaltic wave starts. This sensitivity could be mediated by differences in distribution of receptors on the smooth muscle cells, or by distribution of IVA-sensitive enteroendocrine cells. However, it is also likely that neurons of the myenteric plexus are activated by IVA-sensitive FFAR3 and inhibit peristalsis. This is supported by a previous study showing FFAR3 positive neurons in the

proximal colon which inhibit nicotinic activity by FFAR3 agonists, as well as decreased fecal pellet output with intraperitoneal FFAR3 agonists.⁷⁸ Direct action of IVA on smooth muscle is more likely to change non-periodic characteristics such colon diameter and the strength (and perhaps speed of propagation) of the contractions, whereas the period of contractions is more likely to be controlled by neuronal cell actions or the ICC.

Conclusions

The branched chain fatty acid isovaleric acid relaxes longitudinal colonic smooth muscle cells in a dose-dependent manner by direct interaction with those cells through a receptor activating an adenylate cyclase and activating PKA, and not mediated by neurons or enteroendocrine cells. This activity is part of an IVA-induced decrease in peristaltic activity and increase in luminal content retention due to an increase in proximal colon volume and a decrease in contractility and peristaltic velocity in the proximal end.

Physiological Applications

The interplay of nutritional and microbiome interactions for fatty acid signaling, particularly of BCFA signaling, makes this research particularly relevant not just for pharmacological applications but in everyday homeostasis.

The non-pathological primary source of IVA is bacterial fermentation of the amino acid leucine. Controlling the intake of leucine or controlling the microbiome's ability to produce IVA from leucine are two controllable mechanisms which can increase or decrease the physiological quantity of IVA. From this study, we know that IVA relaxes colonic smooth muscle and decreases forward peristaltic movement in the proximal end of the colon, increasing retention of

contents. Applications where increased retention is bad include surgical and pharmacological causes of constipation. Diseases causing diarrhea is where increased retention is desired.

There is also the opportunity for a feedback loop: increased retention time caused by BCFA mean increased opportunity for bacterial fermentation to occur, which means increased fatty acid production. While this study only addresses colonic motility caused by IVA, there is increasing awareness of digestive issues and the gastrointestinal microbiome being connected to psychological issues.⁵⁵ Also, fatty acid production and absorption's effect on adipose¹⁶⁹, inflammation¹⁷⁰, or oncogenesis^{19,171} is poorly understood. Whether to increase or decrease fatty acid concentration to treat a problem anywhere in a body starts in the gut.

This study also does not address long-term effects on colonic motility by branched chain amino acid fermentation. The production of ammonia by amino acid fermentation could oppose the effects of the BCFA. Increased retention of luminal contents could also increase the fermentation of carbohydrates and produce other SCFA opposing the effects of BCFA. Increased retention of colonic luminal contents could become increased evacuation of contents as the contents are changed by fermentation and the balance tilts in another direction.

Current pharmacological options for potential receptors of BCFA or their receptors are limited. FFAR3 agonists exist but not antagonists. 2-EHA was used as an inhibitor of OR51E1 mediated effects in one study⁸⁴, but if OR51E1 mediates IVA-induced relaxation the effect of 2-EHA appears to be like that of an agonist. The widespread expression of fatty acid sensitive receptors makes specific targeting difficult, but the role of the microbiome and diet is a non-pharmacological avenue for the development of a plan of action to modulate BCFA-mediated roles.

A possible pharmacological intervention to modulate the effect of BCFA that would not require the development of specific receptor-mediated inhibitors are enzymes that better utilize BCFA as substrates for oxidation. The enzymes of bacteria which can subsist entirely on branched chain fatty acids¹⁷² could serve as a template for treatments that decrease BCFA concentration for a desired result.

Directions for Further Study

There are a number of possible directions for future study, but there are specific immediate questions that could shed considerable light on the mechanism.

1. Does an olfactory receptor mediate IVA induced relaxation in smooth muscle? siRNA inhibition of olfactory-specific ADCY3 (adenylate cyclase III) or GNAL ($G\alpha_{olf}$) could narrow or eliminate olfactory receptors as the effector of BCFA-induced smooth muscle relaxation before specific olfactory receptors are targeted.
2. Are regional differences in effects a result of differences in IVA receptor distribution? The distribution of FFAR3, and olfactory receptors such as Olfr558/OR51E1 (or $G\alpha_{olf}$ for general olfactory receptor distribution) as determined by qualitative comparison of immunohistochemistry, qPCR, and western blotting could shed light on regional differences in response.
3. Are there gender differences in response to fatty acids? Data on the relaxation of colon segments hinted at the possibility of gender-specific differences, but the power in most experiments was not enough to definitively say so.
4. Are there more uniquely specific BCFA-induced relaxation mechanisms mediated by PKA? While PKA works to sequester and remove Ca^{2+} to induce relaxation, the activity of the BCFA valproic acid on TREK-1⁹⁴ hints at a possible ion channel involved in the

mechanism of smooth muscle relaxation⁹³. Better understanding this relationship could have applications in the tie between psychological issues, treatments, and the gastrointestinal system.

References

1. Brody, T. in *Nutritional Biochemistry* 311–378 (1999). doi:10.1016/B978-012134836-6/50009-3
2. Wang, T. Y., Liu, M., Portincasa, P. & Wang, D. Q.-H. New insights into the molecular mechanism of intestinal fatty acid absorption. *Eur. J. Clin. Invest.* **43**, 1203–23 (2013).
3. Ran-Ressler, R. R., Bae, S., Lawrence, P., Wang, D. H. & Brenna, J. T. Branched-chain fatty acid content of foods and estimated intake in the USA. *Br. J. Nutr.* **112**, 565–72 (2014).
4. Berg, J. M., Tymoczko, J. L. & Stryer, L. *Biochemistry*. (W H Freeman, 2002). at <<https://www.ncbi.nlm.nih.gov/books/NBK21173/>>
5. Houten, S. M. & Wanders, R. J. A. A general introduction to the biochemistry of mitochondrial fatty acid β -oxidation. *J. Inherit. Metab. Dis.* **33**, 469–477 (2010).
6. Nicolaides, N. & Ray, T. Skin lipids. III. Fatty chains in skin lipids. The use of *vernix caseosa* to differentiate between endogenous and exogenous components in human skin surface lipid. *J. Am. Oil Chem. Soc.* **42**, 702–707 (1965).
7. Ran-Ressler, R. R., Devapatla, S., Lawrence, P. & Brenna, J. T. Branched chain fatty acids are constituents of the normal healthy newborn gastrointestinal tract. *Pediatr. Res.* **64**, 605–9 (2008).
8. Cummings, J. H. Short chain fatty acids in the human colon. *Gut* **22**, 763–79 (1981).
9. Wong, J. M., de Souza, R., Kendall, C. W., Emam, A. & Jenkins, D. J. Colonic health:

- fermentation and short chain fatty acids. *J Clin Gastroenterol* **40**, 235–243 (2006).
10. Macfarlane, G. T. & Macfarlane, S. Bacteria, colonic fermentation, and gastrointestinal health. *J. AOAC Int.* **95**, 50–60 (2012).
 11. Bouillaut, L., Self, W. T. & Sonenshein, A. L. Proline-dependent regulation of *Clostridium difficile* Stickland metabolism. *J. Bacteriol.* **195**, 844–54 (2013).
 12. Elsdon, S. R. & Hilton, M. G. Volatile acid production from threonine, valine, leucine and isoleucine by clostridia. *Arch. Microbiol.* **117**, 165–172 (1978).
 13. Mander, L. & Liu, H. *Comprehensive Natural Products II: Chemistry and Biology*. (2010). at <<https://www.sciencedirect.com/science/referenceworks/9780080453828>>
 14. Nisman, B. The Stickland reaction. *Bacteriol. Rev.* **18**, 16–42 (1954).
 15. Nanninga, H. J. & Gottschal, J. C. Amino acid fermentation and hydrogen transfer in mixed cultures. *FEMS Microbiol. Lett.* **31**, 261–269 (1985).
 16. Topping, D. L. & Clifton, P. M. Short-chain fatty acids and human colonic function: roles of resistant starch and nonstarch polysaccharides. *Physiol Rev* **81**, 1031–1064 (2001).
 17. Macfarlane, G. T., Gibson, G. R. & Cummings, J. H. Comparison of fermentation reactions in different regions of the human colon. *J. Appl. Bacteriol.* **72**, 57–64 (1992).
 18. Ou, J., Carbonero, F., Zoetendal, E. G., DeLany, J. P., Wang, M., Newton, K., Gaskins, H. R. & O’Keefe, S. J. D. Diet, microbiota, and microbial metabolites in colon cancer risk in rural Africans and African Americans. *Am. J. Clin. Nutr.* **98**, 111–120 (2013).
 19. Weir, T. L., Manter, D. K., Sheflin, A. M., Barnett, B. A., Heuberger, A. L. & Ryan, E. P. Stool Microbiome and Metabolome Differences between Colorectal Cancer Patients and

- Healthy Adults. *PLoS One* **8**, e70803 (2013).
20. Kim, E., Coelho, D. & Blachier, F. Review of the association between meat consumption and risk of colorectal cancer. *Nutr. Res.* **33**, 983–994 (2013).
 21. Russell, W. R., Gratz, S. W., Duncan, S. H., Holtrop, G., Ince, J., Scobbie, L., Duncan, G., Johnstone, A. M., Lobley, G. E., Wallace, R. J., Duthie, G. G. & Flint, H. J. High-protein, reduced-carbohydrate weight-loss diets promote metabolite profiles likely to be detrimental to colonic health. *Am. J. Clin. Nutr.* **93**, 1062–1072 (2011).
 22. Herstad, K. M. V, Gajardo, K., Bakke, A. M., Moe, L., Ludvigsen, J., Rudi, K., Rud, I., Sekelja, M. & Skancke, E. A diet change from dry food to beef induces reversible changes on the faecal microbiota in healthy, adult client-owned dogs. *BMC Vet. Res.* **13**, 147 (2017).
 23. Yang, J., Martínez, I., Walter, J., Keshavarzian, A. & Rose, D. J. In vitro characterization of the impact of selected dietary fibers on fecal microbiota composition and short chain fatty acid production. *Anaerobe* **23**, 74–81 (2013).
 24. Wu, G. D., Chen, J., Hoffmann, C., Bittinger, K., Chen, Y.-Y., Keilbaugh, S. A., Bewtra, M., Knights, D., Walters, W. A., Knight, R., Sinha, R., Gilroy, E., Gupta, K., Baldassano, R., Nessel, L., Li, H., Bushman, F. D., Lewis, J. D., Seksik, P. & Langella, P. Linking long-term dietary patterns with gut microbial enterotypes. *Science* **334**, 105–8 (2011).
 25. Scott, K. P., Gratz, S. W., Sheridan, P. O., Flint, H. J. & Duncan, S. H. The influence of diet on the gut microbiota. *Pharmacological Research* **69**, 52–60 (2013).
 26. Kampf, J. P. & Kleinfeld, A. M. Is Membrane Transport of FFA Mediated by Lipid,

- Protein, or Both? *Physiology* **22**, 7–14 (2007).
27. Kortüm, G., Vogel, W. & Andrussow, K. *Dissociation constants of organic acids in aqueous solution*. (Butterworths, 1961). at
<<https://catalog.hathitrust.org/Record/009695003>>
 28. den Besten, G., van Eunen, K., Groen, A. K., Venema, K., Reijngoud, D.-J. & Bakker, B. M. The role of short-chain fatty acids in the interplay between diet, gut microbiota, and host energy metabolism. *J. Lipid Res.* **54**, 2325–40 (2013).
 29. Sellin, J. H. SCFAs: The Enigma of Weak Electrolyte Transport in the Colon. *Physiology* **14**, 58–64 (1999).
 30. Kirat, D. & Kato, S. Monocarboxylate transporter 1 (MCT1) mediates transport of short-chain fatty acids in bovine caecum. *Exp. Physiol.* **91**, 835–844 (2006).
 31. Ganapathy, V., Thangaraju, M., Prasad, P. D., Martin, P. M. & Singh, N. Transporters and receptors for short-chain fatty acids as the molecular link between colonic bacteria and the host. *Curr. Opin. Pharmacol.* **13**, 869–874 (2013).
 32. Ziegler, K., Kerimi, A., Poquet, L. & Williamson, G. Butyric acid increases transepithelial transport of ferulic acid through upregulation of the monocarboxylate transporters SLC16A1 (MCT1) and SLC16A3 (MCT4). *Arch. Biochem. Biophys.* **599**, 3–12 (2016).
 33. Reynolds, D. A., Rajendran, V. M. & Binder, H. J. Bicarbonate-stimulated [¹⁴C]butyrate uptake in basolateral membrane vesicles of rat distal colon. *Gastroenterology* **105**, 725–732 (1993).
 34. Charney, A. N., Micic, L. & Egnor, R. W. Nonionic diffusion of short-chain fatty acids

- across rat colon. *Am. J. Physiol. Liver Physiol.* **274**, G518–G524 (1998).
35. Harig, J. M., Soergel, K. H., Barry, J. A. & Ramaswamy, K. Transport of propionate by human ileal brush-border membrane vesicles. *Am. J. Physiol.* **260**, G776–82 (1991).
 36. Hamilton, J. A., Johnson, R. A., Corkey, B. & Kamp, F. Fatty Acid Transport: The Diffusion Mechanism in Model and Biological Membranes. *J. Mol. Neurosci.* **16**, 99–108 (2001).
 37. Clausen, M. R. & Mortensen, P. B. Kinetic studies on colonocyte metabolism of short chain fatty acids and glucose in ulcerative colitis. *Gut* **37**, 684–689 (1995).
 38. Honeyfield, D. C. & Froseth, J. A. Evaluation of Energy Sources with and without Carnitine in Newborn Pig Heart and Liver. *J. Nutr.* **121**, 1117–1122 (1991).
 39. Gregersen, N. Studies on the Effects of Saturated and Unsaturated Short-Chain Monocarboxylic Acids on the Energy Metabolism of Rat Liver Mitochondria. *Pediat. Res* **13**, 1227–1230 (1979).
 40. Veerkamp, J. H. H., van Moerkerk, H. T. B. T. B. & Wagenmakers, A. J. M. J. M. Interaction of short-chain and branched-chain fatty acids and their carnitine and CoA esters and of various metabolites and agents with branched-chain 2-oxo acid oxidation in rat muscle and liver mitochondria. *Int. J. Biochem.* **17**, 967–974 (1985).
 41. Hyun, S. A., Vahouny, V. & Treadwell, C. R. Portal absorption of fatty acids in lymph- and portal vein-cannulated rats. *Biochim. Biophys. Acta* **137**, 296–305 (1967).
 42. Kukis, A. in *Fat Digestion and Absorption* 163 (2000).
 43. Thierry, A., Maillard, M.-B. B. & Yvon, M. Conversion of L-leucine to isovaleric acid by

- Propionibacterium freudenreichii TL 34 and ITGP23. *Appl. Environ. Microbiol.* **68**, 608–615 (2002).
44. Steensels, J., Daenen, L., Malcorps, P., Derdelinckx, G., Verachtert, H. & Verstrepen, K. J. Brettanomyces yeasts - From spoilage organisms to valuable contributors to industrial fermentations. *International Journal of Food Microbiology* **206**, 24–38 (2015).
45. ‘The Good Scents Company’. isovaleric acid (3-methylbutyric acid). at <http://www.thegoodscentscompany.com/data/rw1056411.html>
46. Yvon, M., Chambellon, E., Bolotin, A. & Roudot-Algaron, F. Characterization and role of the branched-chain aminotransferase (BcaT) isolated from Lactococcus lactis subsp. cremoris NCDO 763. *Appl. Environ. Microbiol.* **66**, 571–577 (2000).
47. Mack, M., Schniegler-Mattox, U., Peters, V., Hoffmann, G. F., Liesert, M., Buckel, W. & Zschocke, J. Biochemical characterization of human 3-methylglutaconyl-CoA hydratase and its role in leucine metabolism. *FEBS J.* **273**, 2012–2022 (2006).
48. Vockley, J. & Ensenauer, R. Isovaleric acidemia: new aspects of genetic and phenotypic heterogeneity. *Am. J. Med. Genet. C. Semin. Med. Genet.* **142C**, 95–103 (2006).
49. Jakobsdottir, G., Bjerregaard, J. H., Skovbjerg, H. & Nyman, M. Fasting serum concentration of short-chain fatty acids in subjects with microscopic colitis and celiac disease: No difference compared with controls, but between genders. *Scand. J. Gastroenterol.* **48**, 696–701 (2013).
50. Ktsoyan, Z. A., Mkrtchyan, M. S., Zakharyan, M. K., Mnatsakanyan, A. A., Arakelova, K. A., Gevorgyan, Z. U., Sedrakyan, A. M., Hovhannisyan, A. I., Arakelyan, A. A. &

- Aminov, R. I. Systemic Concentrations of Short Chain Fatty Acids Are Elevated in Salmonellosis and Exacerbation of Familial Mediterranean Fever. *Front. Microbiol.* **7**, 776 (2016).
51. Shigematsu, Y., Sudo, M., Momoi, T., Inoue, Y., Suzuki, Y. & Kameyama, J. Changing plasma and urinary organic acid levels in a patient with isovaleric acidemia during an attack. *Pediatr. Res.* **16**, 771–5 (1982).
52. Høverstad, T., Fausa, O., Bjørneklett, A. & Bøhmer, T. Short-chain fatty acids in the normal human feces. *Scand J Gastroenterol* **19**, 375–381 (1984).
53. Heimann, E., Nyman, M., Pålbrink, A.-K., Lindkvist-Petersson, K. & Degerman, E. Branched short-chain fatty acids modulate glucose and lipid metabolism in primary adipocytes. *Adipocyte* **5**, 359–368 (2016).
54. Ackman, R. G. Birthweights in the Faroe Islands: possible role of isovaleric acid. *J Intern. Med* **225**, 73–75 (1989).
55. Szczesniak, O., Hestad, K. A., Hanssen, J. F. & Rudi, K. Isovaleric acid in stool correlates with human depression. *Nutr. Neurosci.* **18**, 1–12 (2016).
56. Ribeiro, C. A. J., Leipnitz, G., Amaral, A. U., de Bortoli, G., Seminotti, B. & Wajner, M. Creatine administration prevents Na⁺,K⁺-ATPase inhibition induced by intracerebroventricular administration of isovaleric acid in cerebral cortex of young rats. *Brain Res.* **1262**, 81–88 (2009).
57. Eadie, M. J. Could Valerian have been the first anticonvulsant? *Epilepsia* **45**, 1338–1343 (2004).

58. Mayers, J. R., Wu, C., Clish, C. B., Kraft, P., Torrence, M. E., Fiske, B. P., Yuan, C., Bao, Y., Townsend, M. K., Tworoger, S. S., Davidson, S. M., Papagiannakopoulos, T., Yang, A., Dayton, T. L., Ogino, S., Stampfer, M. J., Giovannucci, E. L., Qian, Z. R., Robinson, D. A., Ma, J., Sesso, H. D., Gaziano, J. M., Cochrane, B. B., Liu, S., Wactawski-Wende, J., Manson, J. E., Pollak, M. N., Kimmelman, A. C., Souza, A., Pierce, K., Wang, T. J., Gerszten, R. E., Fuchs, C. S., Vander Heiden, M. G. & Wolpin, B. M. Elevation of circulating branched-chain amino acids is an early event in human pancreatic adenocarcinoma development. *Nat. Med.* **20**, 1193–1198 (2014).
59. Liaw, C. W. & Connolly, D. T. Sequence polymorphisms provide a common consensus sequence for GPR41 and GPR42. *DNA Cell Biol.* **28**, 555–560 (2009).
60. Miyauchi, S., Hirasawa, A., Ichimura, A., Hara, T. & Tsujimoto, G. New Frontiers in Gut Nutrient Sensor Research: Free Fatty Acid Sensing in the Gastrointestinal Tract. *J. Pharmacol. Sci.* **112**, 19–24 (2010).
61. Hirasawa, A., Tsumaya, K., Awaji, T., Katsuma, S., Adachi, T., Yamada, M., Sugimoto, Y., Miyazaki, S. & Tsujimoto, G. Free fatty acids regulate gut incretin glucagon-like peptide-1 secretion through GPR120. *Nat. Med.* **11**, 90–94 (2005).
62. Briscoe, C. P., Tadayyon, M., Andrews, J. L., Benson, W. G., Chambers, J. K., Eilert, M. M., Ellis, C., Elshourbagy, N. A., Goetz, A. S., Minnick, D. T., Murdock, P. R., Sauls, H. R., Shabon, U., Spinage, L. D., Strum, J. C., Szekeres, P. G., Tan, K. B., Way, J. M., Ignar, D. M., Wilson, S. & Muir, A. I. The orphan G protein-coupled receptor GPR40 is activated by medium and long chain fatty acids. *J. Biol. Chem.* **278**, 11303–11 (2003).
63. Stewart, G., Hira, T., Higgins, A., Smith, C. P. & McLaughlin, J. T. Mouse GPR40

- heterologously expressed in *Xenopus* oocytes is activated by short-, medium-, and long-chain fatty acids. *Am. J. Physiol. Physiol.* **290**, C785–C792 (2006).
64. Hara, T., Hirasawa, A., Sun, Q., Sadakane, K., Itsubo, C., Iga, T., Adachi, T., Koshimizu, T., Hashimoto, T., Asakawa, Y. & Tsujimoto, G. Novel selective ligands for free fatty acid receptors GPR120 and GPR40. *Naunyn. Schmiedebergs. Arch. Pharmacol.* **380**, 247–255 (2009).
65. Mizuta, K., Zhang, Y., Mizuta, F., Hoshijima, H., Shiga, T., Masaki, E. & Emala, C. W. Novel identification of the free fatty acid receptor FFAR1 that promotes contraction in airway smooth muscle. *Am. J. Physiol. - Lung Cell. Mol. Physiol.* **309**, L970–L982 (2015).
66. Matoba, A., Matsuyama, N., Shibata, S., Masaki, E., Emala, C. W. & Mizuta, K. The free fatty acid receptor 1 promotes airway smooth muscle cell proliferation through MEK/ERK and PI3K/Akt signaling pathways. *Am. J. Physiol. Cell. Mol. Physiol.* **314**, L333–L348 (2018).
67. Brown, A. J., Goldsworthy, S. M., Barnes, A. A., Eilert, M. M., Tcheang, L., Daniels, D., Muir, A. I., Wigglesworth, M. J., Kinghorn, I., Fraser, N. J., Pike, N. B., Strum, J. C., Steplewski, K. M., Murdock, P. R., Holder, J. C., Marshall, F. H., Szekeres, P. G., Wilson, S., Ignar, D. M., Foord, S. M., Wise, A. & Dowell, S. J. The orphan G protein-coupled receptors GPR41 and GPR43 are activated by propionate and other short chain carboxylic acids. *J. Biol. Chem.* **278**, 11312–11319 (2003).
68. Le Poul, E., Loison, C., Struyf, S., Springael, J.-Y., Lannoy, V., Decobecq, M.-E., Brezillon, S., Dupriez, V., Vassart, G., Van Damme, J., Parmentier, M. & Detheux, M. Functional characterization of human receptors for short chain fatty acids and their role in

- polymorphonuclear cell activation. *J. Biol. Chem.* **278**, 25481–9 (2003).
69. Ang, Z. & Ding, J. L. GPR41 and GPR43 in obesity and inflammation - Protective or causative? *Frontiers in Immunology* **7**, (2016).
70. Kaji, I., Karaki, S.-I., Tanaka, R. & Kuwahara, A. Density distribution of free fatty acid receptor 2 (FFA2)-expressing and GLP-1-producing enteroendocrine L cells in human and rat lower intestine, and increased cell numbers after ingestion of fructo-oligosaccharide. *J. Mol. Histol.* **42**, 27–38 (2011).
71. Schmidt, J., Smith, N. J., Christiansen, E., Tikhonova, I. G., Grundmann, M., Hudson, B. D., Ward, R. J., Drewke, C., Milligan, G., Kostenis, E. & Ulven, T. Selective orthosteric free fatty acid receptor 2 (FFA2) agonists: Identification of the structural and chemical requirements for selective activation of FFA2 versus FFA3. *J. Biol. Chem.* **286**, 10628–10640 (2011).
72. Lee, T., Schwandner, R., Swaminath, G., Weiszmann, J., Cardozo, M., Greenberg, J., Jaeckel, P., Ge, H., Wang, Y., Jiao, X., Liu, J., Kayser, F., Tian, H. & Li, Y. Identification and Functional Characterization of Allosteric Agonists for the G Protein-Coupled Receptor FFA2. *Mol Pharmacol* **74**, 1599–1609 (2008).
73. Namour, F., Galien, R., Van Kaem, T., Van der Aa, A., Vanhoutte, F., Beetens, J. & Van't Klooster, G. Safety, pharmacokinetics and pharmacodynamics of GLPG0974, a potent and selective FFA2 antagonist, in healthy male subjects. *Br. J. Clin. Pharmacol.* **82**, 139–48 (2016).
74. Sergeev, E., Hansen, A. H., Bolognini, D., Kawakami, K., Kishi, T., Aoki, J., Ulven, T., Inoue, A., Hudson, B. D. & Milligan, G. A single extracellular amino acid in Free Fatty

- Acid Receptor 2 defines antagonist species selectivity and G protein selection bias. *Sci. Rep.* **7**, 13741 (2017).
75. Stoddart, L. A., Smith, N. J., Jenkins, L., Brown, A. J. & Milligan, G. Conserved polar residues in transmembrane domains V, VI, and VII of free fatty acid receptor 2 and free fatty acid receptor 3 are required for the binding and function of short chain fatty acids. *J. Biol. Chem.* **283**, 32913–24 (2008).
76. Puhl III, H. L., Won, Y.-J., Lu, V. B. & Ikeda, S. R. Human GPR42 is a transcribed multisite variant that exhibits copy number polymorphism and is functional when heterologously expressed. *Sci. Rep.* **5**, 12880 (2015).
77. Kaji, I., Akiba, Y., Konno, K., Watanabe, M., Kimura, S., Iwanaga, T., Kuri, A., Iwamoto, K.-I., Kuwahara, A. & Kaunitz, J. D. Neural FFA3 activation inversely regulates anion secretion evoked by nicotinic ACh receptor activation in rat proximal colon. *J. Physiol.* **594**, 3339–52 (2016).
78. Kaji, I., Akiba, Y., Furuyama, T., Adelson, D. W., Iwamoto, K., Watanabe, M., Kuwahara, A. & Kaunitz, J. D. Free fatty acid receptor 3 activation suppresses neurogenic motility in rat proximal colon. *Neurogastroenterol. Motil.* **30**, e13157 (2018).
79. Tazoe, H., Otomo, Y., Karaki, S., Kato, I., Fukami, Y., Terasaki, M. & Kuwahara, A. Expression of short-chain fatty acid receptor GPR41 in the human colon. *Biomed. Res.* **30**, 149–156 (2009).
80. Ang, Z., Xiong, D., Wu, M. & Ding, J. L. FFAR2-FFAR3 receptor heteromerization modulates short-chain fatty acid sensing. *FASEB J.* **32**, 289–303 (2018).

81. Kang, N., Kim, H., Jae, Y., Lee, N., Ku, C. R., Margolis, F., Lee, E. J., Bahk, Y. Y., Kim, M.-S. & Koo, J. Olfactory marker protein expression is an indicator of olfactory receptor-associated events in non-olfactory tissues. *PLoS One* **10**, e0116097 (2015).
82. Reisert, J., Yau, K.-W. & Margolis, F. L. Olfactory marker protein modulates the cAMP kinetics of the odour-induced response in cilia of mouse olfactory receptor neurons. *J. Physiol.* **585**, 731–40 (2007).
83. Menashe, I., Abaffy, T., Hasin, Y., Goshen, S., Yahalom, V., Luetje, C. W. & Lancet, D. Genetic elucidation of human hyperosmia to isovaleric acid. *PLoS Biol.* **5**, 2462–2468 (2007).
84. Jovancevic, N., Dendorfer, A., Matzkies, M., Kovarova, M., Heckmann, J. C., Osterloh, M., Boehm, M., Weber, L., Nguemo, F., Semmler, J., Hescheler, J., Milting, H., Schleicher, E., Gelis, L. & Hatt, H. Medium-chain fatty acids modulate myocardial function via a cardiac odorant receptor. *Basic Res. Cardiol.* **112**, 13 (2017).
85. Kalbe, B., Schlimm, M., Wojcik, S., Philippou, S., Maßberg, D., Jansen, F., Scholz, P., Luebbert, H., Ubrig, B., Osterloh, S. & Hatt, H. Olfactory signaling components and olfactory receptors are expressed in tubule cells of the human kidney. *Arch. Biochem. Biophys.* **610**, 8–15 (2016).
86. Priori, D., Colombo, M., Clavenzani, P., Jansman, A. J. M., Lallès, J. P., Trevisi, P. & Bosi, P. The olfactory receptor OR51E1 is present along the gastrointestinal tract of pigs, co-localizes with enteroendocrine cells and is modulated by intestinal microbiota. *PLoS One* **10**, e0129501 (2015).
87. Pronin, A., Levay, K., Velmeshev, D., Faghihi, M., Shestopalov, V. I. & Slepak, V. Z.

- Expression of olfactory signaling genes in the eye. *PLoS One* **9**, e96435 (2014).
88. Bellono, N. W., Bayrer, J. R., Leitch, D. B., Brierley, S. M., Ingraham, H. A., Julius, D., Bellono, N. W., Bayrer, J. R., Leitch, D. B., Castro, J., Zhang, C. & Donnell, T. A. O. Enterochromaffin Cells Are Gut Chemosensors that Couple to Sensory Neural Pathways Article Enterochromaffin Cells Are Gut Chemosensors that Couple to Sensory Neural Pathways. *Cell* **170**, 1–14 (2017).
 89. Maingret, F., Patel, A. J., Lesage, F., Lazdunski, M. & Honoré, E. Lysophospholipids open the two-pore domain mechano-gated K(+) channels TREK-1 and TRAAK. *J. Biol. Chem.* **275**, 10128–33 (2000).
 90. Murthy, K. S. SIGNALING FOR CONTRACTION AND RELAXATION IN SMOOTH MUSCLE OF THE GUT. *Annu. Rev. Physiol.* **68**, 345–374 (2006).
 91. Liu, H., Enyeart, J. A. & Enyeart, J. J. ACTH inhibits bTREK-1 K⁺ channels through multiple cAMP-dependent signaling pathways. *J. Gen. Physiol.* **132**, 279–94 (2008).
 92. Brand, T., Poon, K. L., Simrick, S. & Schindler, R. F. R. The Popeye Domain Containing Genes and cAMP Signaling. *J. Cardiovasc. Dev. Dis.* **1**, 121–133 (2014).
 93. Ma, R., Seifi, M., Papanikolaou, M., Brown, J. F., Swinny, J. D. & Lewis, A. TREK-1 Channel Expression in Smooth Muscle as a Target for Regulating Murine Intestinal Contractility: Therapeutic Implications for Motility Disorders. *Front. Physiol.* **9**, 157 (2018).
 94. Kim, E.-J., Lee, D. K., Hong, S.-G., Han, J. & Kang, D. Activation of TREK-1, but Not TREK-2, Channel by Mood Stabilizers. *Int. J. Mol. Sci.* **18**, (2017).

95. Kristev, A., Peichev, L., Zaprianov, G. & Lukanov, J. Effect of sodium valproate on the spontaneous contractile and bioelectric activity of smooth muscle fibres isolated from experimental animals. *Folia Med. (Plovdiv)*. **36**, 11–9 (1994).
96. Barrett, K. E. & Raybould, H. E. in *Berne and Levy physiology* (eds. Koeppen, B. M. & Stanton, B. A.) (Elsevier, 2018).
97. Bayguinov, P. O., Hennig, G. W. & Smith, T. K. Calcium activity in different classes of myenteric neurons underlying the migrating motor complex in the murine colon. *J. Physiol.* **588**, 399–421 (2010).
98. Hennig, G. W., Gould, T. W., Koh, S. D., Corrigan, R. D., Heredia, D. J., Shonnard, M. C. & Smith, T. K. Use of Genetically Encoded Calcium Indicators (GECIs) Combined with Advanced Motion Tracking Techniques to Examine the Behavior of Neurons and Glia in the Enteric Nervous System of the Intact Murine Colon. *Front. Cell. Neurosci.* **9**, 436 (2015).
99. Bornstein, J. C., Costa, M. & Grider, J. R. Enteric motor and interneuronal circuits controlling motility. in *Neurogastroenterology and Motility* **16**, 34–38 (2004).
100. Koeppen, B. M. & Stanton, B. A. in *Berne and Levy physiology* (eds. Koeppen, B. M. & Stanton, B. A.) (Elsevier, 2018).
101. Holzer, P., Schluet, W. & Maggi, C. A. Ascending enteric reflex contraction: roles of acetylcholine and tachykinins in relation to distension and propagation of excitation. *J. Pharmacol. Exp. Ther.* **264**, (1993).
102. Costa, M., Furness, J. B. & Humphreys, C. M. S. Apamin distinguishes two types of

- relaxation mediated by enteric nerves in the guinea-pig gastrointestinal tract. *Naunyn. Schmiedebergs. Arch. Pharmacol.* **332**, 79–88 (1986).
103. Lecci, A., Santicioli, P. & Maggi, C. A. Pharmacology of transmission to gastrointestinal muscle. *Curr. Opin. Pharmacol.* **2**, 630–641 (2002).
 104. Barthó, L., Lénárd Jr., L. & Szigeti, R. Nitric oxide and ATP co-mediate the NANC relaxant response in the guinea-pig taenia caeci. *Naunyn. Schmiedebergs. Arch. Pharmacol.* **358**, 496–499 (1998).
 105. Nalli, A. D., Bhattacharya, S., Wang, H., Kendig, D. M., Grider, J. R. & Murthy, K. S. Augmentation of cGMP/PKG pathway and colonic motility by hydrogen sulfide. *Am. J. Physiol. Gastrointest. Liver Physiol.* **313**, G330–G341 (2017).
 106. Nalli, A. D., Wang, H., Bhattacharya, S., Blakeney, B. A. & Murthy, K. S. Inhibition of RhoA/Rho kinase pathway and smooth muscle contraction by hydrogen sulfide. *Pharmacol. Res. Perspect.* **5**, (2017).
 107. Spencer, N. J. & Smith, T. K. Simultaneous intracellular recordings from longitudinal and circular muscle during the peristaltic reflex in guinea-pig distal colon. *J. Physiol.* **533**, 787–99 (2001).
 108. Smith, T. K., Oliver, G. R., Hennig, G. W., O'Shea, D. M., Vanden Berghe, P., Kang, S. H. & Spencer, N. J. A smooth muscle tone-dependent stretch-activated migrating motor pattern in isolated guinea-pig distal colon. *J. Physiol.* **551**, 955–69 (2003).
 109. Grider, J. R. Reciprocal activity of longitudinal and circular muscle during intestinal peristaltic reflex. *Am. J. Physiol. Liver Physiol.* **284**, G768–G775 (2003).

110. Buffa, R., Capella, C., Fontana, P., Usellini, L. & Solcia, E. Types of endocrine cells in the human colon and rectum. *Cell Tissue Res.* **192**, 227–240 (1978).
111. Gunawardene, A. R., Corfe, B. M. & Staton, C. A. Classification and functions of enteroendocrine cells of the lower gastrointestinal tract. *Int. J. Exp. Pathol.* **92**, 219–31 (2011).
112. Kim, M., Cooke, H. J., Javed, N. H., Carey, H. V., Christofi, F. & Raybould, H. E. D-glucose releases 5-hydroxytryptamine from human BON cells as a model of enterochromaffin cells. *Gastroenterology* **121**, 1400–1406 (2001).
113. Grider, J. R. & Piland, B. E. The peristaltic reflex induced by short-chain fatty acids is mediated by sequential release of 5-HT and neuronal CGRP but not BDNF. *Am. J. Physiol. Gastrointest. Liver Physiol.* **292**, G429-37 (2006).
114. Cells, S.-, Qian, J., Mummalaneni, S. K., Alkahtani, R. M., Mahavadi, S., Murthy, S., Grider, J. R. & Lyall, V. Nicotine-Induced Effects on Nicotinic Acetylcholine Receptors (nAChRs), Ca²⁺ and Brain-Derived Neurotrophic Factor (BDNF) in. *PLoS One* **11**, 1–24 (2016).
115. Linan-Rico, A., Ochoa-Cortes, F., Beyder, A., Soghomonyan, S., Zuleta-Alarcon, A., Coppola, V. & Christofi, F. L. Mechanosensory Signaling in Enterochromaffin Cells and 5-HT Release: Potential Implications for Gut Inflammation. *Front. Neurosci.* **10**, 564 (2016).
116. Grider, J. R. CGRP as a transmitter in the sensory pathway mediating peristaltic reflex. *Am. J. Physiol.* **266**, G1139–G1145 (1994).

117. Grider, J. R., Foxx-Orenstein, A. E. & Jin, J. G. 5-Hydroxytryptamine₄receptor agonists initiate the peristaltic reflex in human, rat, and guinea pig intestine. *Gastroenterology* **115**, 370–380 (1998).
118. Grider, J. R., Kuemmerle, J. F. & Jin, J. G. 5-HT released by mucosal stimuli initiates peristalsis by activating 5-HT₄/5-HT_{1p} receptors on sensory CGRP neurons. *Am. J. Physiol.* **270**, G778-82 (1996).
119. Plujà, L., Albertí, E., Fernández, E., Mikkelsen, H. B., Thuneberg, L. & Jiménez, M. Evidence supporting presence of two pacemakers in rat colon. *Am. J. Physiol. Liver Physiol.* **281**, G255–G266 (2001).
120. Smith, T. K. & Koh, S. D. A model of the enteric neural circuitry underlying the generation of rhythmic motor patterns in the colon: the role of serotonin. *Am. J. Physiol. - Gastrointest. Liver Physiol.* **312**, G1–G14 (2017).
121. Dinning, P. G., Szczesniak, M. & Cook, i. j. Removal of tonic nitrergic inhibition is a potent stimulus for human proximal colonic propagating sequences. *Neurogastroenterol. Motil.* **18**, 37–44 (2006).
122. Smith, T. K., Park, K. J. & Hennig, G. W. Colonic migrating motor complexes, high amplitude propagating contractions, neural reflexes and the importance of neuronal and mucosal serotonin. *J. Neurogastroenterol. Motil.* **20**, 423–46 (2014).
123. Dickson, E. J., Heredia, D. J., McCann, C. J., Hennig, G. W. & Smith, T. K. The mechanisms underlying the generation of the colonic migrating motor complex in both wild-type and nNOS knockout mice. *Am. J. Physiol. Gastrointest. Liver Physiol.* **298**, G222-32 (2010).

124. Heredia, D. J., Dickson, E. J., Bayguinov, P. O., Hennig, G. W. & Smith, T. K. Localized release of serotonin (5-hydroxytryptamine) by a fecal pellet regulates migrating motor complexes in murine colon. *Gastroenterology* **136**, 1328–38 (2009).
125. Gershon, M. D., Dreyfus, C. F., Pickel, V. M., Joh, T. H. & Reis, D. J. Serotonergic neurons in the peripheral nervous system: Identification in gut by immunohistochemical localization of tryptophan hydroxylase (myenteric plexus/serotonin/monoamines/tissue culture/neurotransmission). *Poc. Naal Acad. scE. MSA Neurobiol.* **74**, (1977).
126. Costa, M., Furness, J. B., Cuello, A. C., Verhofstad, A. A. J., Steinbusch, H. W. J. & Elde, R. P. Neurons with 5-hydroxytryptamine-like immunoreactivity in the enteric nervous system: Their visualization and reactions to drug treatment. *Neuroscience* **7**, 351–363 (1982).
127. Dickson, E. J., Heredia, D. J. & Smith, T. K. Critical role of 5-HT_{1A}, 5-HT₃, and 5-HT₇ receptor subtypes in the initiation, generation, and propagation of the murine colonic migrating motor complex. *Am. J. Physiol. Gastrointest. Liver Physiol.* **299**, G144-57 (2010).
128. Okamoto, T., Barton, M. J., Hennig, G. W., Birch, G. C., Grainger, N., Corrigan, R. D., Koh, S. D., Sanders, K. M. & Smith, T. K. Extensive projections of myenteric serotonergic neurons suggest they comprise the central processing unit in the colon. *Neurogastroenterol. Motil.* **26**, 556–570 (2014).
129. Lyster, D. J. K., Bywater, R. A. R. & Taylor, G. S. Neurogenic control of myoelectric complexes in the mouse isolated colon. *Gastroenterology* **108**, 1371–1378 (1995).
130. Murthy, K. S., Zhou, H., Grider, J. R., Brautigan, D. L., Eto, M. & Makhlouf, G. M.

- Differential signalling by muscarinic receptors in smooth muscle: m2-mediated inactivation of myosin light chain kinase via Gi3, Cdc42/Rac1 and p21-activated kinase 1 pathway, and m3-mediated MLC20 (20 kDa regulatory light chain of myosin II) phosphorylat. *Biochem. J.* **374**, 145–55 (2003).
131. Murthy, K. S. & Makhlouf, G. M. Differential coupling of muscarinic m2 and m3 receptors to adenylyl cyclases V/VI in smooth muscle. Concurrent M2-mediated inhibition via Galphai3 and m3-mediated stimulation via Gbetagammaq. *J. Biol. Chem.* **272**, 21317–24 (1997).
 132. Jenco, J. M., Becker, K. P. & Morris, A. J. Membrane-binding properties of phospholipase C-beta1 and phospholipaseC-beta2: role of the C-terminus and effects of polyphosphoinositides, G-proteins and Ca²⁺. *Biochem. J.* **327 (Pt 2)**, 431–7 (1997).
 133. Murthy, K. S. & Makhlouf, G. M. Phosphoinositide metabolism in intestinal smooth muscle: preferential production of Ins(1,4,5)P3 in circular muscle cells. *Am. J. Physiol.* **261**, G945-51 (1991).
 134. Murthy, K. S. & Zhou, H. Selective phosphorylation of the IP₃ R-I in vivo by cGMP-dependent protein kinase in smooth muscle. *Am. J. Physiol. Liver Physiol.* **284**, G221–G230 (2003).
 135. Murthy, K. S., Grider, J. R. & Makhlouf, G. M. InsP3-dependent Ca²⁺ mobilization in circular but not longitudinal muscle cells of intestine. *Am. J. Physiol.* **261**, G937-44 (1991).
 136. Clapper, D. L. & Lee, H. C. Inositol triphosphate induces calcium release from nonmitochondrial stores in sea urchin egg homogenates. *Journal of Biological Chemistry*

- 260**, 13947–13954 (1985).
137. Murthy, K. S., Kuemmerle, J. F. & Makhlouf, G. M. Agonist-mediated activation of PLA2 initiates Ca^{2+} mobilization in intestinal longitudinal smooth muscle. *Am J Physiol* **269**, G93--102 (1995).
138. Wang, X. B., Osugi, T. & Uchida, S. Muscarinic Receptors Stimulate Ca^{2+} Influx via Phospholipase A2 Pathway in Ileal Smooth Muscles. *Biochem. Biophys. Res. Commun.* **193**, 483–489 (1993).
139. Murthy, K. S., Coy, D. H. & Makhlouf, G. M. Somatostatin receptor-mediated signaling in smooth muscle. Activation of phospholipase C- β 3 by Gbetagamma and inhibition of adenylyl cyclase by G α hi1 and G α ho. *J. Biol. Chem.* **271**, 23458–63 (1996).
140. Murthy, K. S., Teng, B., Jin, J. & Makhlouf, G. M. G protein-dependent activation of smooth muscle eNOS via natriuretic peptide clearance receptor. *Am. J. Physiol.* **275**, C1409-16 (1998).
141. Nalli, A. D., Kumar, D. P., Al-Shboul, O., Mahavadi, S., Kuemmerle, J. F., Grider, J. R. & Murthy, K. S. Regulation of G β γ i-dependent PLC- β 3 activity in smooth muscle: inhibitory phosphorylation of PLC- β 3 by PKA and PKG and stimulatory phosphorylation of G α i-GTPase-activating protein RGS2 by PKG. *Cell Biochem. Biophys.* **70**, 867–80 (2014).
142. Murthy, K. S. & Makhlouf, G. M. Heterologous desensitization mediated by G protein-specific binding to caveolin. *J. Biol. Chem.* **275**, 30211–9 (2000).
143. Bhattacharya, S., Mahavadi, S., Al-Shboul, O., Rajagopal, S., Grider, J. R. & Murthy, K.

- S. Differential regulation of muscarinic M2 and M3 receptor signaling in gastrointestinal smooth muscle by caveolin-1. *Am. J. Physiol. Cell Physiol.* **305**, C334-47 (2013).
144. Ferguson, S. S. G. Evolving Concepts in G Protein-Coupled Receptor Endocytosis: The Role in Receptor Desensitization and Signaling. *Pharmacol. Rev.* **53**, (2001).
 145. Murthy, K. S., Jin, J. G., Grider, J. R. & Makhoulf, G. M. Characterization of PACAP receptors and signaling pathways in rabbit gastric muscle cells. *Am. J. Physiol.* **272**, G1391-9 (1997).
 146. Roscioni, S. S., Maarsingh, H., Elzinga, C. R. S., Schuur, J., Menzen, M., Halayko, A. J., Meurs, H. & Schmidt, M. Epac as a novel effector of airway smooth muscle relaxation. *J. Cell. Mol. Med.* **15**, 1551–63 (2011).
 147. Schmidt, M., Dekker, F. J. & Maarsingh, H. Exchange protein directly activated by cAMP (epac): a multidomain cAMP mediator in the regulation of diverse biological functions. *Pharmacol. Rev.* **65**, 670–709 (2013).
 148. Tanaka, Y., Horinouchi, T. & Koike, K. NEW INSIGHTS INTO β -ADRENOCEPTORS IN SMOOTH MUSCLE: DISTRIBUTION OF RECEPTOR SUBTYPES and MOLECULAR MECHANISMS TRIGGERING MUSCLE RELAXATION. *Clin. Exp. Pharmacol. Physiol.* **32**, 503–514 (2005).
 149. Nelson, M. T. & Quayle, J. M. Physiological roles and properties of potassium channels in arterial smooth muscle. *Am. J. Physiol.* **268**, C799-822 (1995).
 150. Horinouchi, T., Tanaka, Y. & Koike, K. Evidence for the primary role for 4-aminopyridine-sensitive Kv channels in β 3-adrenoceptor-mediated, cyclic AMP-

- independent relaxations of guinea-pig gastrointestinal smooth muscles. *Naunyn. Schmiedebergs. Arch. Pharmacol.* **367**, 193–203 (2003).
151. Tanaka, Y., Yamashita, Y., Yamaki, F., Horinouchi, T., Shigenobu, K. & Koike, K. Evidence for a significant role of a G_s-triggered mechanism unrelated to the activation of adenylyl cyclase in the cyclic AMP-independent relaxant response of guinea-pig tracheal smooth muscle. *Naunyn. Schmiedebergs. Arch. Pharmacol.* **368**, 437–441 (2003).
 152. Gagelmann, M. & Güth, K. Force generated by non-cycling crossbridges at low ionic strength in skinned smooth muscle from *Taenia coli*. *Pflügers Arch. Eur. J. Physiol.* **403**, 210–214 (1985).
 153. Hagerty, L., Weitzel, D. H., Chambers, J., Fortner, C. N., Brush, M. H., Loiselle, D., Hosoya, H. & Haystead, T. A. J. ROCK1 phosphorylates and activates zipper-interacting protein kinase. *J. Biol. Chem.* **282**, 4884–93 (2007).
 154. Huang, J., Mahavadi, S., Sriwai, W., Hu, W. & Murthy, K. S. Gi-coupled receptors mediate phosphorylation of CPI-17 and MLC20 via preferential activation of the PI3K/ILK pathway. *Biochem. J.* **396**, 193–200 (2006).
 155. Hurst, N. R., Kendig, D. M., Murthy, K. S. & Grider, J. R. The short chain fatty acids, butyrate and propionate, have differential effects on the motility of the guinea pig colon. *Neurogastroenterol. Motil.* **26**, 1586–1596 (2014).
 156. Masselli, G. & Gualdi, G. CT and MR enterography in evaluating small bowel diseases: when to use which modality? *Abdom. Imaging* **38**, 249–259 (2013).
 157. Froehlich, J. M., Waldherr, C., Stoupis, C., Erturk, S. M. & Patak, M. A. MR motility

- imaging in Crohn's disease improves lesion detection compared with standard MR imaging. *Eur. Radiol.* **20**, 1945–1951 (2010).
158. Smolinski, S., George, M., Dredar, A., Hayes, C. & Rakita, D. Magnetic resonance enterography in evaluation and management of children with crohn's disease. *Semin. Ultrasound, CT MRI* **35**, 331–348 (2014).
 159. Eliakim, R. Video capsule endoscopy of the small bowel. *Current Opinion in Gastroenterology* **26**, 129–133 (2010).
 160. Dinning, P. G., Wiklendt, L., Gibbins, I., Patton, V., Bampton, P., Lubowski, D. Z., Cook, I. J. & Arkwright, J. W. Low-resolution colonic manometry leads to a gross misinterpretation of the frequency and polarity of propagating sequences: Initial results from fiber-optic high-resolution manometry studies. *Neurogastroenterol. Motil.* **25**, n/a-n/a (2013).
 161. Bayliss, W. M. & Starling, E. H. The movements and innervation of the small intestine. *J. Physiol.* **24**, 99–143 (1899).
 162. Hennig, G. W. in 31–42 (Springer, Cham, 2016). doi:10.1007/978-3-319-27592-5_4
 163. Costa, M., Wiklendt, L., Arkwright, J. W., Spencer, N. J., Omari, T., Brookes, S. J. H. & Dinning, P. G. An experimental method to identify neurogenic and myogenic active mechanical states of intestinal motility. *Front. Syst. Neurosci.* **7**, 7 (2013).
 164. Rueden, C. T., Schindelin, J., Hiner, M. C., DeZonia, B. E., Walter, A. E., Arena, E. T. & Eliceiri, K. W. ImageJ2: ImageJ for the next generation of scientific image data. *BMC Bioinformatics* **18**, 529 (2017).

165. Schindelin, J., Arganda-Carreras, I., Frise, E., Kaynig, V., Longair, M., Pietzsch, T., Preibisch, S., Rueden, C., Saalfeld, S., Schmid, B., Tinevez, J.-Y., White, D. J., Hartenstein, V., Eliceiri, K., Tomancak, P. & Cardona, A. Fiji: an open-source platform for biological-image analysis. *Nat. Methods* **9**, 676–82 (2012).
166. Di Rollo, N., Caesar, D., Ferenbach, D. A. & Dunn, M. J. G. Survival from profound metabolic acidosis due to hypovolaemic shock. A world record? *BMJ Case Rep.* **2013**, (2013).
167. Wray, S. & Smith, R. D. Mechanisms of action of pH-induced effects on vascular smooth muscle. *Mol. Cell. Biochem.* **263**, 163–172 (2004).
168. Zhang, Y. & Paterson, W. G. Nitric oxide contracts longitudinal smooth muscle of opossum oesophagus via excitation-contraction coupling. *J. Physiol.* **536**, 133–140 (2001).
169. Layden, B. T., Angueira, A. R., Brodsky, M., Durai, V. & Lowe, W. L. Short chain fatty acids and their receptors: new metabolic targets. *Transl. Res.* **161**, 131–140 (2013).
170. Ang, Z., Er, J. Z., Tan, N. S., Lu, J., Liou, Y. C., Grosse, J. & Ding, J. L. Human and mouse monocytes display distinct signalling and cytokine profiles upon stimulation with FFAR2/FFAR3 short-chain fatty acid receptor agonists. *Sci. Rep.* **6**, 34145 (2016).
171. Heerdt, B. G., Houston, M. A. & Augenlicht, L. H. Potentiation by specific short-chain fatty acids of differentiation and apoptosis in human colonic carcinoma cell lines. *Cancer Res.* **54**, 3288–93 (1994).
172. Kazakov, A. E., Rodionov, D. A., Alm, E., Arkin, A. P., Dubchak, I. & Gelfand, M. S. Comparative genomics of regulation of fatty acid and branched-chain amino acid

- utilization in proteobacteria. *J. Bacteriol.* **191**, 52–64 (2009).
173. Arthur, K. & Hommes, F. A. Simple isotope dilution assay for propionic acid and isovaleric acid. *J. Chromatogr. B. Biomed. Appl.* **673**, 132–5 (1995).
174. Evans, D., Claiborne, J. B. & Currie, S. *The physiology of fishes*. (2014).

Vita

Bryan Adam Blakeney was born November 14, 1986 in Gulfport, Mississippi, where his family still resides. Adam graduated from the Mississippi School for Mathematics and Science in Columbus, Mississippi in 2005, where his interest in research began. After several years as an undergraduate research assistant at the University of Alabama at Birmingham, where his work resulted in a first-author publication and a patent, he earned his Bachelors of Science in Biomedical Engineering in 2010. He joined Virginia Commonwealth University in 2011 to pursue a Medical Degree and a Doctor of Philosophy Degree, and has been a student in the Department of Physiology and Biophysics since 2013. Adam is incredibly grateful for the encouragement to pursue academic interests and support during his formative years from his father, and the experiences and guidance from teachers and mentors in academia.